LOCALIZATION AND DYNAMICS OF DISULFIDE REDUCTION AND THEIR KEY REGULATORS DURING INTERNALIZATION IN ENDOLYSOSOMAL COMPARTMENTS

by

Juhee Lee

A dissertation submitted in partial fulfillment
of the requirements for the degree of
Doctor of Philosophy
(Pharmaceutical Sciences)
in The University of Michigan
2012

Doctoral Committee:

Professor Kyung-Dall Lee, Chair
Professor Gordon L. Amidon
Professor Joel A. Swanson
Associate Professor Gus R. Rosania

To my Lord, my God

And

To my husband

ACKNOWLEDGEMENTS

First, I would like to express my deep and sincere gratitude to my advisor, Dr. Kyung-Dall Lee for his dedicated advise, supervision and support throughout my Ph.D. study. His expertise, insight and guidance improved my knowledge, scientific thinking process and provided me with invaluable preparation for future challenges.

I would like to thank my doctoral committee members, Dr. Joel Swanson, Dr. Gus Rosania and Dr. Gordon Amidon for their patient guidance with kind and pertinent discussions. I sincerely thank Dr. Joel Swanson and his research team for allowing me to have an enjoyable research environment, especially Dr. Samuel Straight for his expert training and assistance in Center for Live Cell Imaging (CLCI). I thank Dr. Gus Rosania, my temporary advisor for the first year, for his suggestions in my project as well as helpful advice for being confident. I would also like to thank Dr. Gordon Amidon for his guidance on developing my public speaking skills.

Special thanks to all past and present Lee lab members for making it a memorable journey, especially to Dr. Zachary Walls and Dr. Chester Provoda for their valuable time and instrumental help. This work would not have been possible without their guidance. I also would like to thank Dr. Emily Rabinsky, Dr. Chasity Andrews, Dr. Hiro Tsume,

Kefeng Sun, Oluseyi Adeniyi and Alison Matyas for their friendship. I always enjoyed our conversations and birthday lunches.

I would especially like to thank my classmates, Dr. Shu-Pei Wu, Dr. Jason Baik, Dr. Cara Hartz Nelson, Chinmay Maheshwari, Lindsey White, and Dr. Nan Zheng for their continuous motivation. I'll miss our lunches and coffee breaks.

I would like to thank all the KPCAA members for their support and prayers. I am grateful to Dr. Na Hyung Kim, Dr. Suna Choi, and Dr. Young Min Kwon for their emotional support. I'd also like to thank Hanna Song, Yea-min Huh, and Dr. Jin Hyun Kim for their friendship. I'll never forget many wonderful and fun activities we've done together.

Finally, I'd like to thank my family. I love my parents and in-laws for all the support and prayers that they gave. I want to express my gratitude to my sister, brother-in-law and sister-in-law for their prayers and encouragement. Special thanks to my aunts and cousins for giving me wonderful, family-filled holidays. Last but not least, I want to thank my dear husband, Woong Hee, literally "The giving tree" for me. He gave, and continues to give unconditional love, and just being happy by doing so at every stage. I thank God for him the Lord has given to me to share this amazing journey and I hope to continue all my work within God's eternal blessings.

TABLE OF CONTENTS

LIST OF FIGURES

LIST OF ABBREVIATIONS

APC	Antigen presenting cell
BMDC	Bone marrow dendritic cell
BMM	Bone marrow-derived macrophage
BoNT	Botulinum Toxin
CD	Cathepsin D
CDC	Cholesterol-dependent cytolysin
CHO	Chinese hamster ovary
CTL	Cytotoxic T lymphocytes
Cys	Cysteine
Cyss	Cystine
DC	Dendritic cell
DT	Diphtheria toxin
DTT	Dithiothreitol
DTNB	5,5'-dithiobis(2-nitro-benzoic acid)
ER	Endoplasmic reticulum
FITC	Fluorescein isothiocyanate
FRET	Fluorescence resonance energy transfer
GILT	Gamma interferon-inducible lysosomal thiol reductase
GSH	Glutathione

GSSG	Oxidized glutathione
HC	Heavy chain
hRPE	Human retinal pigment epithelial
HSD	Honestly significant difference
kD	Kilodalton
LC	Light chain
LLO	Listeriolysin O
LPS	Lipopolysaccharide
mCit	Monomeric Citrine
mECFP	Monomeric enhanced cyan fluorescent protein
MHC	Major histocompatibility complex
OVA	Ovalbumin
PCR	Polymerase chain reaction
PDI	Protein disulfide isomerase
PN	Protamine
RNI	Reactive nitrogen intermediate
roGFP	Redox-sensitive green fluorescent protein
ROS	Reactive oxygen species
rxYFP	Redox-sensitive yellow fluorescent protein
SH	Sulfhydryl
SOD2	Superoxide dismutase 2
SS	Disulfide bond
TCEP	tris 2-carboxyethyl phosphine

TRD	Texas red dextran
Trx	Thioredoxin
YFP	Yellow fluorescent protein

ABSTRACT

Subcellular differences in redox potential are essential for intracellular protein dynamics, cellular entry by many viruses and intracellular pathogens, and the targeted delivery of macromolecular therapeutics. This study focuses on evaluation of disulfide reduction in the endocytic pathway in the context of macromolecules internalized as particles. Recently, bioconjugation employing disulfide reduction has been exploited in drug delivery and those conjugates are being used more frequently in protein and oligonucleotide systems. Disulfide-based macromolecular therapeutic agents are membrane-impermeant, thus typically internalized into cells via endocytosis, and apparently reduced at some point in endocytic compartments en route to the lysosomal compartments. However, little is known about the spatiotemporal dynamics of disulfide bond reduction at the subcellular level, especially within endolysosomal compartments. Direct analysis of intracellular redox conditions is limited by current redox indicators, which either lack the necessary sensitivity or perturb the normal subcellular physiology. The probe in this study was designed to address some of these challenges. A genetically engineered redox-sensitive fusion protein, consisting of monomeric enhanced cyan fluorescent protein (mECFP) and monomeric Citrine (mCit), joined by an intervening disulfide-bonded and protease-sensitive linker, were expressed and characterized *in vitro*

and used to measure redox potential following endocytosis by living cells. FRET microscopy revealed that disulfide bond reduction began in the early endosome and continued throughout endolysosomal maturation. Phagocytic oxidase activity slowed reduction, while expression of gamma-interferon inducible lysosomal thiol reductase (GILT) accelerated reduction, indicating at least one mechanism of regulation of reduction in endocytic compartments. The information obtained from this study demonstrated not only the potential utility of this reporter for the design of targeted delivery systems, but also for studying cell type-dependent variations in the disufide reduction mechanism of endocytosed macromolecules and cellular factors modulating the reduction processes. There were differential rates of disulfide reduction by BMDCs, fibroblasts, cancer cells and BMMs, suggesting that further investigation in other cell types in various states will provide critical information that can be used to investigate the impact of novel treatments, as well as informing the design of targeted pharmaceutical agents that rely on disulfide bonds.

CHAPTER I

REDUCTION OF DISULFIDE BONDS IN THE ENDOCYTIC COMPARTMENT AND IMPLICATIONS FOR DRUG DELIVERY SYSTEMS

INTRODUCTION

The overall intracellular redox status exerts a profound influence on the normal cellular processes of protein folding, gene expression, enzyme activity, metabolism, cell cycle proliferation and apoptosis [1-3]. Therefore, measuring the status of intracellular redox potentials is important for understanding and manipulating homeostatic cellular processes as potential tools within the biomedical arena [4, 5]. Currently the disulfide bond is one of the most popular linkers, while in a parallel research concerning redox biochemistry is increasingly recognized as an integral component within the cellular signaling [6]. Disulfide bonds play an important role in many biological processes contributing to the controlled cleavage in the reducing space, thereby releasing reduced species as a redox switch [7]. Accordingly, disulfide bonds have been exploited in drug delivery for bioconjugation of macromolecules such as peptides, proteins and oligonucleotides, all of which are typically internalized into cells via endocytosis [8-10]. Therefore, characterizing and understanding the redox potential within the endocytic pathway is an essential component of this type of macromolecular delivery system;

however, surprisingly little is known about the dynamics of disulfide bond reduction at the subcellular level, especially in the endolysosomal compartment [11]. To this end, designing reporters to monitor disulfide redox status in the endocytic pathway is essential for disulfide conjugation-based delivery strategies; once native processes are understood, drug delivery systems that use disulfide bonds can be more appropriately designed.

This chapter mainly focuses on the mechanism(s) of disulfide bond reduction especially in the endocytic pathway after the cellular uptake to define redox control and identify sites of reduction, and on the related disulfide conjugation-based delivery strategies for macromolecules. In particular we concentrate on cellular redox mechanisms, from indirect evidence in the form of disulfide reduction in pathogenesis to direct evidence with redox biosensors that report disulfide reduction in subcellular compartments.

BACKGROUND

Disulfide bond as a redox switch

A disulfide bond (SS) is a single covalent bond derived from the coupling of sulfhydryl (SH) groups. It is chemically formed from thiol-containing compounds or, in the case of proteins, may be spontaneously oxidized from thiol groups of cysteine residues or mediated by enzymes. Disulfide linkages are readily reversible in reducing environments, resulting in the linkage being converted to thiols; however, they are relatively stable even in acidic environments [12]. Disulfide bonds contribute to the folding, structure, and stability of many proteins in both prokaryotes and eukaryotes. In prokaryotes, structural disulfide bonds are mostly formed in the periplasmic space after being translocated across the cytoplasmic membrane [7]. In eukaryotic cells, disulfide bonds are generally formed in the lumen of the rough endoplasmic reticulum (ER) which is oxidative [13]. However, the main pathway that catalyzes disulfide bond formation is strikingly similar between prokaryotes and eukaryotes, and is based on thiol-disulfide exchange reactions [14]. The disulfide bond is reversibly cleaved in the cytosol, due to the presence of glutathione that is primarily responsible for maintaining protein thiols [15]. The reversibility between thiol and disulfide is a key feature in living systems, although functional evidence for the cellular mechanistic details of disulfide bond reduction is still lacking, not only where and how reduction occurs but also what conditions are required for reduction in subcellular compartments.

Cellular reducing activities via intracellular redox agents/enzymes

Regulation of thiol-disulfide redox in various subcellular compartments is critical to the maintenance and function of many cellular processes [16]. The intracellular distribution of glutathione in its reduced form (GSH) vs. its oxidized form (GSSG) contributes to the generation of different redox potentials in various subcellular compartments. Involvement of diverse redox enzymes also contributes to redox compartmentalization in cells (Fig 1.1) [17].

Glutathione (GSH)

GSH, the most abundant thiol-source in mammalian cells, functions in cellular processes such as synthesis of proteins and DNA, amino acid transport, enzyme activity, metabolism, and protection of cells [18]. As depicted in Fig 1.1, the ratio of GSH to GSSG contributes to the generation of different redox potentials in various subcellular compartments. Usually, the concentration of glutathione in the cell is rather high (5-10 mM), but the ratio between GSH and GSSG differs among cellular compartments. While the cytosol exhibits a GSH:GSSG ratio of up to 100, the ER, where disulfides are introduced into proteins, is more oxidizing with a ratio of 1~3 [19]. Mitochondria, the organelles with the greatest reducing potential, have the highest rates of electron transfer and are highly sensitive to oxidation [20]. Extracellular compartments are stably maintained at oxidizing potentials principally by cysteine/cystine (Cys/CySS) [21]. However, there is not much information about the endosomal compartments, even though

previous studies suggest evidence (will be discussed later) for reductive activity within the endocytic pathway.

Thioredoxin (Trx)

Another important redox enzyme is Trx, a 12 kD oxidoreductase containing a dithiol-disulfide active site [3]. It is ubiquitous and found in many organisms from plants and bacteria to mammals [22]. It facilitates the refolding of disulfide-containing proteins and reduces several transcription factors therefore it regulates the DNA binding activity and gene expression [23]. While the GSH/GSSG couple provides a major cellular redox buffer, Trx serves a more specific function as hydrogen donors for ribonucleotide reductase in regulating redox-sensitive proteins by changing the reduced/oxidized thioredoxin ratio [24]. However, the redox equilibrium both in Trx and GSH is driven by NADPH-dependent reaction; thus, they are thermodynamically connected to each other [2, 25]. The majority of these enzymes are functional at neutral or slightly alkaline conditions, they have similar three-dimensional structures, and all feature a highly conserved active site loop containing two cysteines in the sequence -CGPC- [26]. GILT is a unique and unusual member of the thiol reductase family because its optimal enzymatic activity is at a low pH and has an atypical active site (-CGAC-) [27]. However, the active site, determined by mutagenesis, still consists of a pair of cysteine residues separated by two amino acids, similar to other enzymes of the thioredoxin family [28].

Protein disulfide isomerase (PDI)

PDI was initially characterized by Christian Anfinsen in the 1960's as an enzyme that catalyzes the refolding of ribonuclease A [29]. It is a unique thiol-disulfide oxidoreductase that catalyzes substrate proteins via the active-site cysteines, facilitating protein folding in the lumen of the ER and disulfide bond formation, and also ironically catalyzing disulfide reduction. PDI reduces disulfide bonds in the cytosol, endosomes, and at the plasma membrane as a consequence of the more reducing environments through expressed on cell surface or secreted by cells (Fig 1.2) [11]. Cell-surface PDI has been implicated in reduction of the disulfide-linked diphtheria toxin heterodimer [29], and also controls the redox state of cell-surface protein thiols/disulfides [30].

Taken together, these redox enzymes and redox agents, which are capable of reducing disulfide bonds, exist at different intracellular locations within a cell. GILT is a unique member with its optimal enzymatic activity at pH 4.5–5.5, as described in detail later.

Indirect evidence for reductive activity in the endocytic pathway: disulfide reduction in pathogenesis

A specific subset of toxins consist of an active subunit (A) that has enzymatic activity linked to a binding subunit (B) through a disulfide bridge that confers specificity to a particular mechanism of toxin entry (Fig 1.3) [31]. The mechanism of bacterial toxins has contributed to the understanding of important cellular pathways including cytosolic delivery of a catalytic domain linked to a receptor binding domain via a

disulfide bond through plasma membrane permeabilization [32]. Since some bacterial or plant toxins have a disulfide bond between two subunits, they take advantage of its reversible thiol-disulfide interchange reactions. For example, when cholera toxin binds to the cell surface and transports to the ER, PDI dissociates the disulfide bond between A and B subunits before translocation into the cytosol [33]. Similarly, diphtheria toxin and botulinum toxin are cytotoxic only after reduction of the disulfide bond to release the A subunit from the endosome into the cytosol [34, 35]. Reversible cleavage of the disulfide bond and controlled release of reduced components in the process of translocation are essential mechanisms that toxins employ for cell entry. Therefore, the study of transport pathways in pathogenesis plays an important role in understanding of disulfide bond reduction in the intracellular redox environment.

Diphtheria toxin (DT)

DT, secreted by the bacteria *Corynebacterium diphtheriae,* is an exotoxin that functions to terminate host cell functions [35]. DT is composed of two subunits; subunit A has the catalytic domain which is responsible for inhibiting protein synthesis, and subunit B has the receptor binding region and the translocation region for getting the toxin into the cytoplasm [36]. Subunit B is separated into two domains, the transmembrane (T) domain and the receptor-binding (R) domain. After proteolytic cleavage of DT, the T domain promotes the formation of a channel and then releases the A domain into the cytoplasm after reduction of the disulfide bond (Fig. 1.4) [35, 37]. The physiological dynamics of DT support the hypothesis that reduction occurs within

endocytic compartments. Following endocytosis, reduction of the disulfide bond allows one of the subunits to penetrate the endosomal membrane and inhibit protein translation [38].

Botulinum Toxin (BoNT)

BoNT is one of the most potent substances expressed by Clostridium botulinum, a Gram positive aerobic bacterium composed of disulfide linked heavy chain (HC) and light chain (LC) (Fig 1.5) [34]. There are two main steps for BoNT action, one is transcytosis across the transport cell and the other is receptor-mediated endocytosis into the target cell. First, BoNT binds to the lumen of the gut, and then escapes by transcytosis to the interstitial fluid where it reaches the general circulation. During the second step, BoNT penetrates the cell membrane of peripheral cholinergic nerve endings at the neuromuscular junction by receptor-mediated endocytosis [39]. Aside from the initial binding event of both steps, the toxin's behavior in gut cells and target cells is fundamentally different. In gut cells, the toxin is transported in an unmodified form from one cell surface to the other, where it is released to the cell exterior. In target cells, the toxin is transported to the interior of the nerve ending, where it undergoes pH-induced translocation to reach the cytosol. At some point in this migration, the interchain disulfide bond of the toxin is reduced so that the enzymatic LC becomes fully active [40]. Fischer et al. demonstrated that replacement of a disulfide bond by a peptide linkage between LC and HC resulted in nonproductive LC translocation, indicating that the disulfide bond is critical for the outcome of translocation [41]. BoNT activity in which BoNT have

cytotoxicity only after reduction of the disulfide bond to release the A subunit from the endosome into the cytosol appears the possibility that reduction of the disulfide bond involves within the endosome. Within the peripheral nerve endings the light chain prevents the release of acetylcholine, leading to neuromuscular paralysis [42]. Most cases of botulism originate from ingestion, and thus BoNT is able to escape the lumen of the gut due to its transcytosis transport system [43]. Therefore, BoNT may serve as a delivery vehicle because native BoNT can survive the harsh conditions of the gastrointestinal system [44]. The translocation domain of BoNT is known to participate in the pH-dependent translocation of the enzymatic LC across the endosomal membrane; however, its mechanism of action and whether cellular redox proteins are required for this process remain unknown.

Listeriolysin O (LLO)

LLO is a sulfhydryl-activated pore-forming protein of the cholesterol-dependent cytolysin (CDC) family from the Gram-positive facultative intracellular bacteria, *Listeria monocytogenes (L. monocytogenes)* [45]. Once *L. monocytogenes* is phagocytosed, it secretes LLO into the endosomal compartment where LLO exhibits optimal activity at pH 5.5 - 5.9. LLO forms pores to breach the endosomal membrane to escape into the cytosol where cytosolic delivery of macromolecules using LLO can be achieved without severe cytotoxicity since its activity gets attenuated at pH ~7.2 [45, 46].

The hemolytic activity of LLO has been shown to be abolished upon modification of the unique cysteine residue by oxidation of the sulfhydryl group [9]. This interesting

feature allows one to regulate the hemolytic activity of LLO as well as to reversibly conjugate LLO with lipids or polymers through a disulfide bridge without affecting its pore-forming ability. Although it is known to be pH-dependent and requires reduction for activation, the molecular mechanism of its reduction is not clearly understood; specifically, the temporal and spatial reduction of the unique single cysteine is not clear.

Direct evidence for reductive activity in the endocytic pathway

Previous studies to explore the reductive process in the endocytic pathway

Shen et al. used poly (D-lysine) linked to methotrexate through a disulfide linker to show that reduction of endocytosed ligand to release methotrexate from the disulfide spacer occurs in a prelysosomal intracellular compartment in Chinese hamster ovary (CHO) cells [47]. A similar study was performed by Feener et al. [48] using a disulfide conjugate between poly (D-lysine) and [^{125}I]-tyramine. Disulfide reduction started immediately and continued over 6 hr in CHO cells, indicating that reduction takes place after uptake via endocytosis. Further evidence and potential mechanisms for the reduction are proposed through antigen presentation. For many antigens, the rate-limiting step in unfolding may involve reduction of disulfide bonds in antigen presenting cells [49]. Collins et al. showed disulfide reducing activity for lysosomes in the processing of antigen presentation to T cells using conjugation of [^{125}I]-tyrosine to [^{131}I]-α_2-macroglobulin through disulfide spacer by primary cultures of mouse peritoneal macrophages [50]. To directly monitor disulfide reduction during endocytosis, a 4,4-difluoro-5,7-dimethyl-4-bora-3a,4a-diaza-s-indacene-3-propionic acid (BODIPY)

fluorescent ($488_{ex}/520_{em}$ nm), which is linked to folate via an amide bond, disulfide linked to tetraethyl rhodamine ($545_{ex}/595_{em}$ nm) (BODIPY folate-SS-rhodamine) was designed and characterized to demonstrate fluorescence changes from red to green upon reduction after receptor-mediated endocytosis [51].

Gamma interferon-inducible lysosomal thiol reductase (GILT)

GILT is the first identified and characterized redox enzyme in endosomes and lysosomes. It is synthesized as a 35 kDa soluble glycoprotein precursor and processed into the mature form (30 kDa), therefore initially named IP-30, by proteolytic removal of N- and C-terminal peptides [52]. The lysosomal thiol reductase is a soluble glycoprotein that is synthesized as a precursor. After delivery into the endosomal/lysosomal system by the mannose 6-phosphate receptor, N- and C-terminal prosequences are removed [53]. The enzyme is expressed constitutively in antigen-presenting cells and induced by IFN-γ in other cell types, suggesting a potentially important role in antigen processing [54]. GILT is an enzyme involved in facilitating MHC class II-restricted antigen processing, which generates cell surface MHC class II-peptide complexes essential for the activation of CD4+ T cells; GILT catalyzes initial unfolding of antigenic protein that becomes more accessible for further processing through proteolysis to initiate the adaptive immune response [55, 75]. GILT can also facilitate the transfer of disulfide-containing antigens into the cytosol, enhancing their cross-presentation, the processing of exogenous antigens for presentation by MHC class I molecules to CD8+ T cells [56]. GILT is constitutively expressed in T cells, involved in the regulation of T cell activation, indicating that GILT has a more fundamental role in cellular processes [76]. Recently, GILT has been found to regulate the cellular redox state, regulating the expression of superoxide dismutase 2

(SOD2), a mitochondrial enzyme responsible for the conversion of superoxide radical into hydrogen peroxide [57]. Finally, GILT has been shown to be a critical host factor that facilitates the activity of bacterial hemolysins such as LLO and streptolysin O [58]. The use of GILT-/- mice will be explored further in Chapter III.

Limitations of reduction studies

Given that the study of redox processes in biological systems is a very broad field, it is not surprising that a variety of redox probes have been developed. Direct analysis of intracellular redox conditions, however, is limited by current redox indicators, which either lack the necessary sensitivity or perturb the normal subcellular physiology induced by the process of imaging itself.

Redox biosensors

Historically, measurements of GSH or Trx concentration by use of enzymatic assays, HPLC, and gel mobility have the advantage of high specificity; however, these cannot deliver information about the redox state, typically pursued by subcellular fractionation by cell homogenization and gradient separation, which results in the loss of cellular integrity. Conventional methodologies using the redox-active fluorescent dyes have also encountered difficulty when used to measure oxidative stress due to the formation of reactive oxygen species (ROS) [59]. One of the most promising methods for investigating intracellular redox conditions involves the use of disulfide bonds engineered into the GFP β-barrel, redox-sensitive yellow fluorescent proteins (rxYFP) and redox-sensitive green fluorescent proteins (roGFPs) [60, 61]. These genetically encoded probes have advantages over more traditional methods and have contributed greatly to the

understanding of structural and chemical aspects of cellular functions that depend upon thiol/disulfide exchange elements. The endoplasmic reticulum (ER) is indeed more oxidizing than cytosol as determined using roGFP variants [62]. Moreover, the fusion of human glutaredoxin to roGFP was demonstrated to increase the sensitivity of probes on a scale of time and redox changes to directly overcome some limitations [63]. Despite the information gained by studies detailing redox conditions for certain subcellular compartments, a well-defined picture of reduction-oxidation dynamics and kinetics for the endocytic pathway remains elusive.

Drug delivery strategy utilizing disulfide bonds

Recent discoveries regarding the disulfide reduction in the endocytic pathway have exploited these attributes of disulfide bonds for bioconjugation purposes. Recently, the use of disulfide bonds for target-specific release of macromolecular drugs has emerged as an important contributor to anti-cancer drug delivery systems as exemplified by the development of the immunoconjugate gemtuzumab ozogamicin (GO; Mylotarg^{TM}) to target acute myelogenous leukemia [64]. Also captopril, an orally active inhibitor of the angiotensin-converting enzyme (ACE) for the treatment of hypertension and congestive heart failure, was converted into prodrugs by conjugating via disulfide to polyethylene glycol (captopril-SS-PEG), which did not inhibit ACE activity but regained this ability after reduction [81], or to lysozyme for specific targeting to kidney [82]. The disulfide linkage was used to release drugs under specific conditions and cleavage was triggered by the mildly reducing environment found in intracellular fluids [65]. Disulfide cross-linked copolymer was also used for intracellular drug delivery [66-68]. Bacterial toxins have contributed to the discovery of important pathways in cellular processes and some

of them have been approved in drug delivery systems. They take advantage using their intrinsic disulfide bond by virtue of its reversible nature in cellular redox systems [32]. Bade et al. explored the full-length BoNT as a potential carrier for targeted delivery of biomolecules [69]. Recent studies have altered the BoNT by mutation or deletion of the LC such that it retains the capabilities to bind and transcytose across gut, still utilizing the disulfide bridge [70]. The general concept for use of a modified BoNT, genetically engineered HC without LC subunit, maintains its capability of transcytosis through epithelial cells but is nontoxic. The study of intracellular transport pathways of toxins plays an important role in understanding of disulfide bond reduction in the intracellular redox environment. LLO, another sulfhydryl-mediated bacterial protein, has been considered for its possible use in drug delivery when encapsulated with a drug and taken up by the cell via endocytosis. Previously, LLO-containing liposomes efficiently delivered model antigen, ovalbumin (OVA) to the cytosol *in vitro*, as measured by OVA-specific MHC class I-restricted antigen presentation [71]. Dramatic enhancement of gene delivery was observed with disulfide-linked LLO and protamine (PN) condensed DNA complexes without apparent cytotoxicity [9]. Similarly, Choi et al. demonstrated high levels of gene transfection efficiency but low cell toxicity using polyethylenimine disulfide conjugated with LLO [8]. More recently, LLO has been reported as an efficient delivery carrier in *in vivo* reporter gene transfections using LLO-containing pH-sensitive anionic liposomes [72]. The mechanism to escape the endocytic compartment can be used to deliver macromolecules, such as antigens, to the cytosol of cells. LLO can also be co-encapsulated with antigens in pH-sensitive liposomes to enhance the efficiency of

cytosolic delivery by demonstrating an enhanced cellular immune response compared to pH-sensitive liposomes without LLO [73, 74].

CONCLUSIONS

The presence of subcellular redox differences makes the disulfide bond attractive as a potential delivery tool. Recently, bioconjugation employing disulfide reduction has been exploited in drug delivery in protein and oligonucleotide system [77-79], typically internalized by endocytosis by cells. Although controversial [80], a reductive activity has been evidenced in the endocytic pathway. As the reduction of disulfide bonds in the endocytic pathway is prerequisite in many cases of pathogenesis and drug delivery systems, characterizing and understanding the endolysosomal redox potential is extremely important. The primary goal of this research is to develop a redox-sensitive reporter that is able to monitor reducing environments to define redox mechanisms and identify spatiotemporal disulfide reduction, particularly in the endosomal compartments. Recent development of redox biosensors and study of redox enzymes localized in the endosomal compartments have generated more excitement for our approach. With the recognition of reductive activity in the endocytic pathway, we then evaluate disulfide reduction in the endocytic pathway to investigate key cellular factors modulating the redox potential, likely dependent on cell types, demonstrating the potential utility of this reporter for the design of drug delivery systems utilizing disulfide bonds.

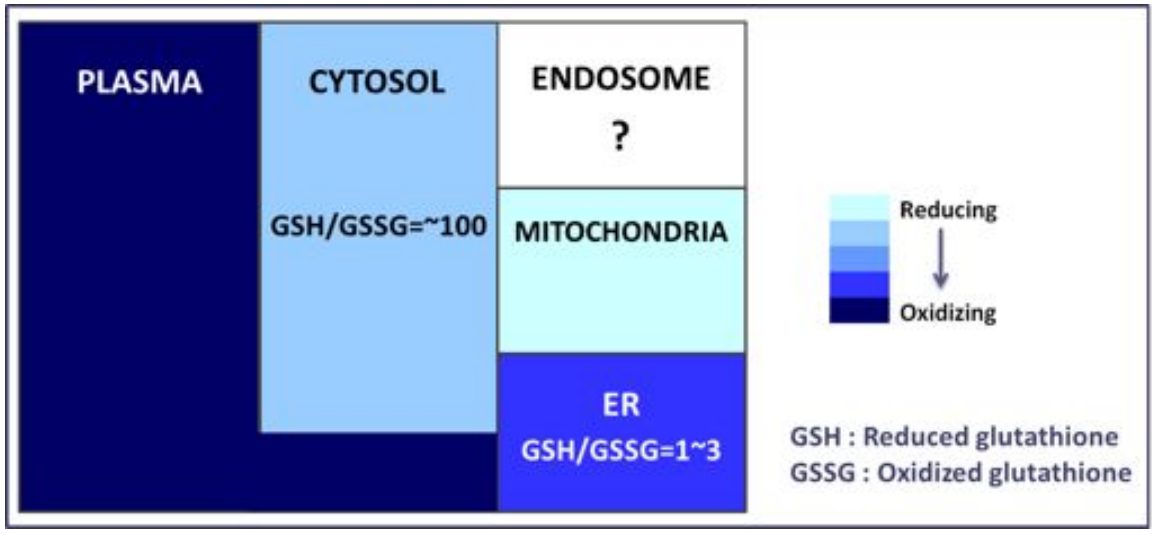

Figure 1.1 Redox compartmentalization according to the ratio of GSH to GSSG.

Maintaining redox potentials in the cell is regulated by the ratio of GSH/GSSG. The gradient indicating redox potentials starts from light color, most reducing and as it gets darker, it becomes more oxidizing. The redox potential in a subcellular compartment plays an important role in how it functions, and has been found to be variant in different subcellular compartments. Figure modified from Kemp et al [17].

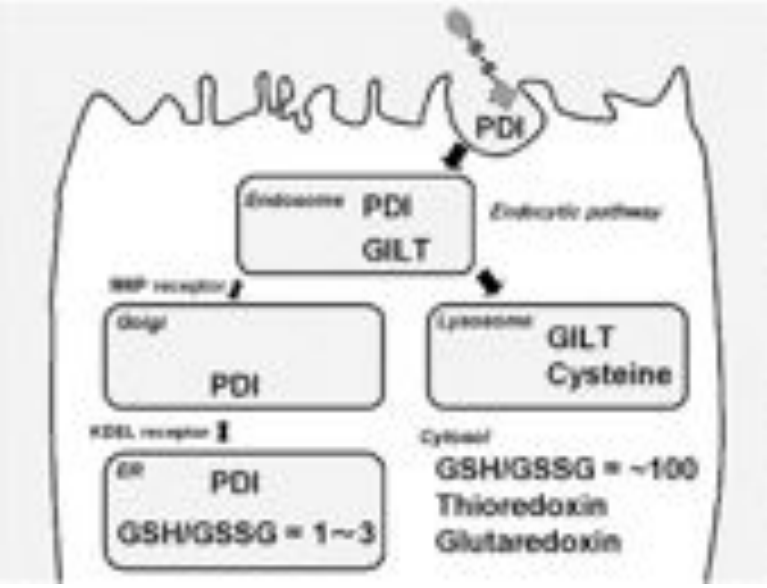

Figure 1.2 Various cellular redox enzymes and redox agents at different sites.

The endocytosed macromolecules contact various redox enzymes and redox agents such as protein disulfide isomerase (PDI), gamma interferon-inducible lysosomal thiol reductase (GILT), and cysteine. These cellular redox enzymes/agents and various ratios of glutathione and oxidized glutathione (GSH/GSSG) are localized at different subcellular locations. Figure adapted from Saito et al. [11]

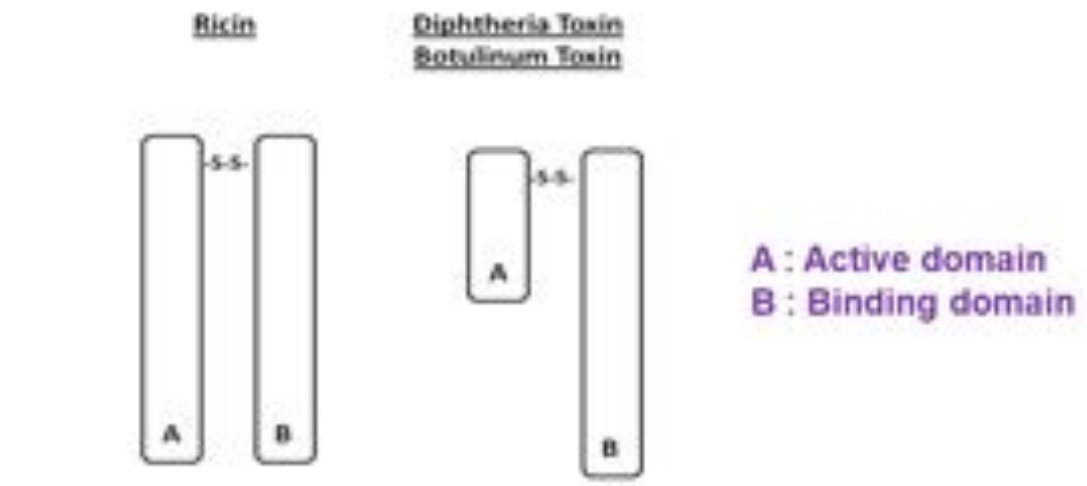

Figure 1.3 Schematic structures of protein toxins with their disulfide bond between the A and B moieties.

Toxins have several common characteristics with the active domain (A) and binding domain (B) linked by a disulfide bond. They utilize the disulfide bridge in their pathogenesis process by disulfide cleavage and controlled release of reduced components. Reduction of the disulfide bond is required for optimal enzymatic activity of these toxins. Figure modified from Sandvig et al. [31]

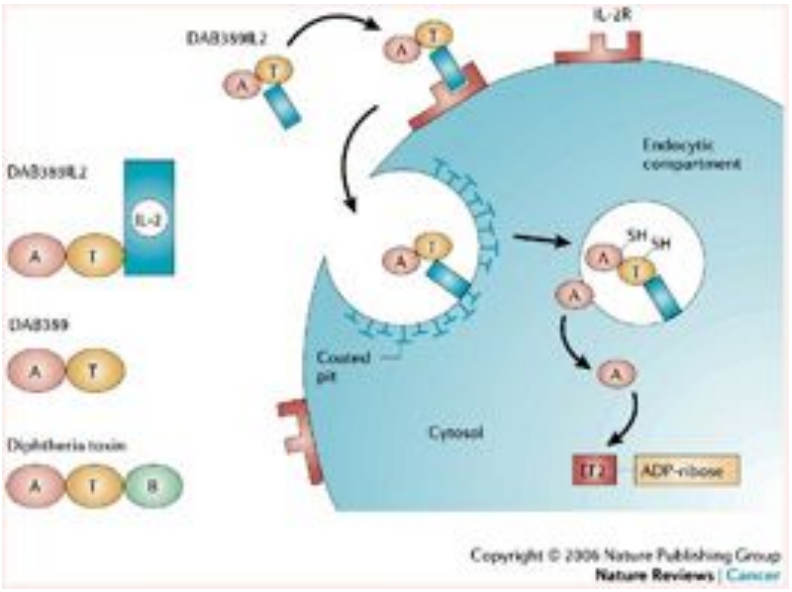

Figure 1.4 Chimeric toxin molecules made by replacing the B domain of DT with an antibody by recombinant DNA techniques.

DAB389IL2 (denileukin diftitox) is composed of the A and T domains of DT fused to human interleukin 2 (IL2). Denileukin diftitox binds with cell-surface receptors and then enters cells through endocytosis. The acidic pH in the endocytic compartment causes a conformational change that enables the translocation of the A chain of DT to the cytosol. Figure adapted from Pastan et al. [37]

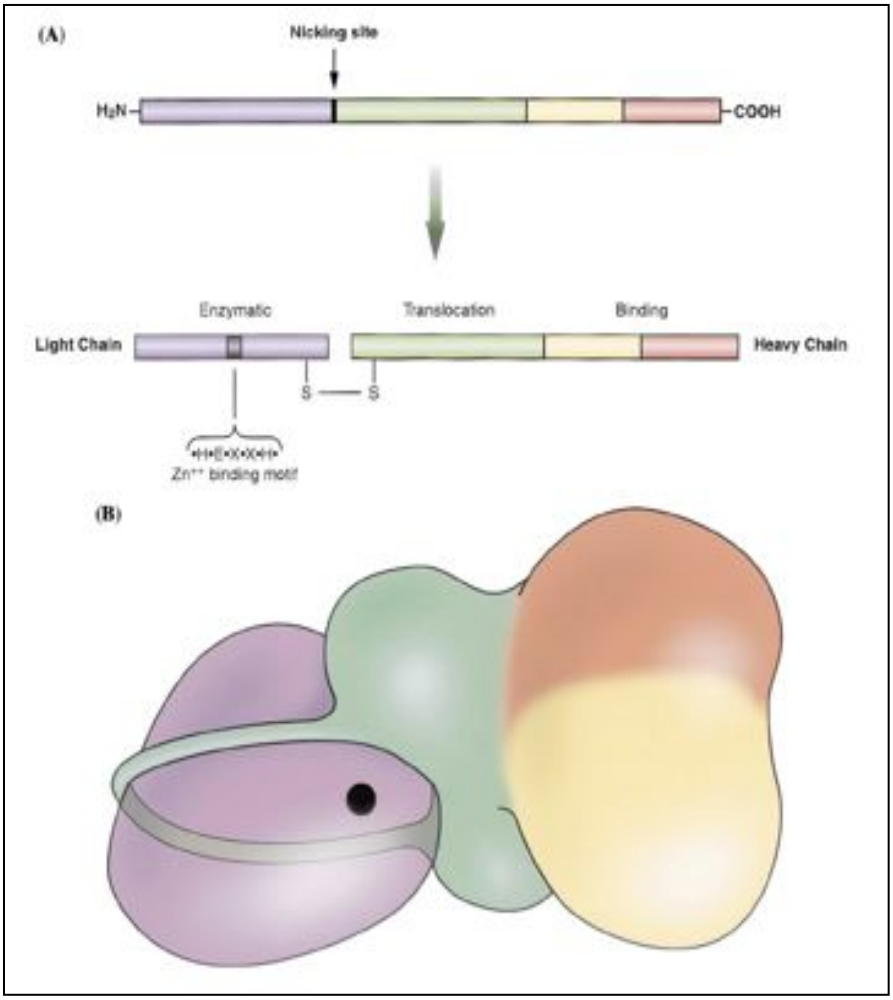

Figure 1.5 Schematic representation in linear structure (A) and three-dimensional structure (B) of botulinum toxin.

The purple region indicates the LC with an enzymatic domain with a zinc molecule (black sphere). The green portion represents the translocation domain with its belt-like encirclement of the LC, whereas the yellow and the orange regions show, respectively, the N-terminal and C-terminal portions of the binding domain within the HC. Figure adapted from Simpson et al. [34].

REFERENCES

1. Schafer, F.Q. and G.R. Buettner, *Redox environment of the cell as viewed through the redox state of the glutathione disulfide/glutathione couple.* Free Radic Biol Med, 2001. **30**(11): p. 1191-212.
2. Trotter, E.W. and C.M. Grant, *Non-reciprocal regulation of the redox state of the glutathione-glutaredoxin and thioredoxin systems.* EMBO Rep, 2003. **4**(2): p. 184-8.
3. Matsuo, Y., et al., *Redox Regulation by Thioredoxin and its Related Molecules.* Drug News Perspect, 2002. **15**(9): p. 575-580.
4. Ostergaard, H., et al., *Shedding light on disulfide bond formation: engineering a redox switch in green fluorescent protein.* Embo J, 2001. **20**(21): p. 5853-62.
5. Cannon, M.B. and S. James Remington, *Redox-sensitive green fluorescent protein: probes for dynamic intracellular redox responses. A review.* Methods Mol Biol, 2009. **476**: p. 50-64.
6. Chen, X., et al., *Design of an in vivo cleavable disulfide linker in recombinant fusion proteins.* Biotechniques. **49**(1): p. 513-8.
7. Depuydt, M., J. Messens, and J.F. Collet, *How proteins form disulfide bonds.* Antioxid Redox Signal. **15**(1): p. 49-66.
8. Choi, S. and K.D. Lee, *Enhanced gene delivery using disulfide-crosslinked low molecular weight polyethylenimine with listeriolysin o-polyethylenimine disulfide conjugate.* J Control Release, 2008. **131**(1): p. 70-6.
9. Saito, G., G.L. Amidon, and K.D. Lee, *Enhanced cytosolic delivery of plasmid DNA by a sulfhydryl-activatable listeriolysin O/protamine conjugate utilizing cellular reducing potential.* Gene Ther, 2003. **10**(1): p. 72-83.
10. Bauhuber, S., et al., *Delivery of nucleic acids via disulfide-based carrier systems.* Adv Mater, 2009. **21**(32-33): p. 3286-306.
11. Saito, G., J.A. Swanson, and K.D. Lee, *Drug delivery strategy utilizing conjugation via reversible disulfide linkages: role and site of cellular reducing activities.* Adv Drug Deliv Rev, 2003. **55**(2): p. 199-215.
12. Roberts, M.J., M.D. Bentley, and J.M. Harris, *Chemistry for peptide and protein PEGylation.* Adv Drug Deliv Rev, 2002. **54**(4): p. 459-76.
13. Riemer, J., N. Bulleid, and J.M. Herrmann, *Disulfide formation in the ER and mitochondria: two solutions to a common process.* Science, 2009. **324**(5932): p. 1284-7.
14. Sevier, C.S. and C.A. Kaiser, *Formation and transfer of disulphide bonds in living cells.* Nat Rev Mol Cell Biol, 2002. **3**(11): p. 836-47.
15. Go, Y.M. and D.P. Jones, *Redox compartmentalization in eukaryotic cells.* Biochim Biophys Acta, 2008. **1780**(11): p. 1273-90.
16. Smith, C.V., *Compartmentalization of redox regulation of cell response.* Toxicol Sci, 2005. **83**(1): p. 1-3.
17. Kemp, M., Y.M. Go, and D.P. Jones, *Nonequilibrium thermodynamics of thiol/disulfide redox systems: a perspective on redox systems biology.* Free Radic Biol Med, 2008. **44**(6): p. 921-37.
18. Pastore, A., et al., *Analysis of glutathione: implication in redox and detoxification.* Clin Chim Acta, 2003. **333**(1): p. 19-39.

19. Hwang, C., A.J. Sinskey, and H.F. Lodish, *Oxidized redox state of glutathione in the endoplasmic reticulum.* Science, 1992. **257**(5076): p. 1496-502.

20. Jezek, P. and L. Plecita-Hlavata, *Mitochondrial reticulum network dynamics in relation to oxidative stress, redox regulation, and hypoxia.* Int J Biochem Cell Biol, 2009. **41**(10): p. 1790-804.

21. Moriarty-Craige, S.E. and D.P. Jones, *Extracellular thiols and thiol/disulfide redox in metabolism.* Annu Rev Nutr, 2004. **24**: p. 481-509.

22. Hirota, K., et al., *Thioredoxin superfamily and thioredoxin-inducing agents.* Ann N Y Acad Sci, 2002. **957**: p. 189-99.

23. Arrigo, A.P., *Gene expression and the thiol redox state.* Free Radic Biol Med, 1999. **27**(9-10): p. 936-44.

24. Nakamura, H., *Thioredoxin and its related molecules: update 2005.* Antioxid Redox Signal, 2005. **7**(5-6): p. 823-8.

25. Nkabyo, Y.S., et al., *Glutathione and thioredoxin redox during differentiation in human colon epithelial (Caco-2) cells.* Am J Physiol Gastrointest Liver Physiol, 2002. **283**(6): p. G1352-9.

26. Meyer, Y., et al., *Thioredoxins and glutaredoxins: unifying elements in redox biology.* Annu Rev Genet, 2009. **43**: p. 335-67.

27. Arunachalam, B., et al., *Enzymatic reduction of disulfide bonds in lysosomes: characterization of a gamma-interferon-inducible lysosomal thiol reductase (GILT).* Proc Natl Acad Sci U S A, 2000. **97**(2): p. 745-50.

28. Phan, U.T., B. Arunachalam, and P. Cresswell, *Gamma-interferon-inducible lysosomal thiol reductase (GILT). Maturation, activity, and mechanism of action.* J Biol Chem, 2000. **275**(34): p. 25907-14.

29. Mandel, R., et al., *Inhibition of a reductive function of the plasma membrane by bacitracin and antibodies against protein disulfide-isomerase.* Proc Natl Acad Sci U S A, 1993. **90**(9): p. 4112-6.

30. Jiang, X.M., et al., *Redox control of exofacial protein thiols/disulfides by protein disulfide isomerase.* J Biol Chem, 1999. **274**(4): p. 2416-23.

31. Sandvig, K. and B. van Deurs, *Entry of ricin and Shiga toxin into cells: molecular mechanisms and medical perspectives.* EMBO J, 2000. **19**(22): p. 5943-50.

32. Schiavo, G. and F.G. van der Goot, *The bacterial toxin toolkit.* Nat Rev Mol Cell Biol, 2001. **2**(7): p. 530-7.

33. Fujinaga, Y., *Transport of bacterial toxins into target cells: pathways followed by cholera toxin and botulinum progenitor toxin.* J Biochem, 2006. **140**(2): p. 155-60.

34. Simpson, L.L., A.B. Maksymowych, and N. Kiyatkin, *Botulinum toxin as a carrier for oral vaccines.* Cell Mol Life Sci, 1999. **56**(1-2): p. 47-61.

35. Duncan, J.L. and N.B. Groman, *Activity of diphtheria toxin. II. Early events in the intoxication of HeLa cells.* J Bacteriol, 1969. **98**(3): p. 963-9.

36. Madshus, I.H., et al., *Entry of diphtheria toxin-protein A chimeras into cells.* J Biol Chem, 1991. **266**(26): p. 17446-53.

37. Pastan, I., et al., *Immunotoxin therapy of cancer.* Nat Rev Cancer, 2006. **6**(7): p. 559-65.

38. Falnes, P.O. and S. Olsnes, *Cell-mediated reduction and incomplete membrane translocation of diphtheria toxin mutants with internal disulfides in the A fragment.* J Biol Chem, 1995. **270**(35): p. 20787-93.

39. Simpson, L.L., *Botulinum toxin: potent poison, potent medicine.* Hosp Pract (Minneap), 1999. **34**(4): p. 87-91; quiz 163.

40. Simpson, L.L., et al., *The role of the interchain disulfide bond in governing the pharmacological actions of botulinum toxin.* J Pharmacol Exp Ther, 2004. **308**(3): p. 857-64.

41. Fischer, A. and M. Montal, *Crucial role of the disulfide bridge between botulinum neurotoxin light and heavy chains in protease translocation across membranes.* J Biol Chem, 2007. **282**(40): p. 29604-11.

42. Ahsan, C.R., et al., *Visualization of binding and transcytosis of botulinum toxin by human intestinal epithelial cells.* J Pharmacol Exp Ther, 2005. **315**(3): p. 1028-35.

43. Simpson, L.L., *Identification of the major steps in botulinum toxin action.* Annu Rev Pharmacol Toxicol, 2004. **44**: p. 167-93.

44. Simpson, L.L., *Identification of the characteristics that underlie botulinum toxin potency: implications for designing novel drugs.* Biochimie, 2000. **82**(9-10): p. 943-53.

45. Portnoy, D.A. and S. Jones, *The cell biology of Listeria monocytogenes infection (escape from a vacuole).* Ann N Y Acad Sci, 1994. **730**: p. 15-25.

46. Schnupf, P. and D.A. Portnoy, *Listeriolysin O: a phagosome-specific lysin.* Microbes Infect, 2007. **9**(10): p. 1176-87.

47. Shen, W.C., H.J. Ryser, and L. LaManna, *Disulfide spacer between methotrexate and poly(D-lysine). A probe for exploring the reductive process in endocytosis.* J Biol Chem, 1985. **260**(20): p. 10905-8.

48. Feener, E.P., W.C. Shen, and H.J. Ryser, *Cleavage of disulfide bonds in endocytosed macromolecules. A processing not associated with lysosomes or endosomes.* J Biol Chem, 1990. **265**(31): p. 18780-5.

49. Jensen, P.E., *Antigen unfolding and disulfide reduction in antigen presenting cells.* Semin Immunol, 1995. **7**(6): p. 347-53.

50. Collins, D.S., E.R. Unanue, and C.V. Harding, *Reduction of disulfide bonds within lysosomes is a key step in antigen processing.* J Immunol, 1991. **147**(12): p. 4054-9.

51. Yang, J., et al., *Evaluation of disulfide reduction during receptor-mediated endocytosis by using FRET imaging.* Proc Natl Acad Sci U S A, 2006. **103**(37): p. 13872-7.

52. Luster, A.D., et al., *Molecular and biochemical characterization of a novel gamma-interferon-inducible protein.* J Biol Chem, 1988. **263**(24): p. 12036-43.

53. Phan, U.T., R.L. Lackman, and P. Cresswell, *Role of the C-terminal propeptide in the activity and maturation of gamma -interferon-inducible lysosomal thiol reductase (GILT).* Proc Natl Acad Sci U S A, 2002. **99**(19): p. 12298-303.

54. Hastings, K.T. and P. Cresswell, *Disulfide reduction in the endocytic pathway: immunological functions of gamma-interferon-inducible lysosomal thiol reductase.* Antioxid Redox Signal. **15**(3): p. 657-68.

55. Maric, M., et al., *Defective antigen processing in GILT-free mice.* Science, 2001. **294**(5545): p. 1361-5.

56. Singh, R. and P. Cresswell, *Defective cross-presentation of viral antigens in GILT-free mice.* Science. **328**(5984): p. 1394-8.

57. Bogunovic, B., et al., *An unexpected functional link between lysosomal thiol reductase and mitochondrial manganese superoxide dismutase.* J Biol Chem, 2008. **283**(14): p. 8855-62.

58. Singh, R., A. Jamieson, and P. Cresswell, *GILT is a critical host factor for Listeria monocytogenes infection.* Nature, 2008. **455**(7217): p. 1244-7.

59. Rota, C., Y.C. Fann, and R.P. Mason, *Phenoxyl free radical formation during the oxidation of the fluorescent dye 2',7'-dichlorofluorescein by horseradish*

peroxidase. Possible consequences for oxidative stress measurements. J Biol Chem, 1999. **274**(40): p. 28161-8.

60. Meyer, A.J. and T.P. Dick, *Fluorescent protein-based redox probes.* Antioxid Redox Signal. **13**(5): p. 621-50.

61. Bjornberg, O., H. Ostergaard, and J.R. Winther, *Measuring intracellular redox conditions using GFP-based sensors.* Antioxid Redox Signal, 2006. **8**(3-4): p. 354-61.

62. Delic, M., D. Mattanovich, and B. Gasser, *Monitoring intracellular redox conditions in the endoplasmic reticulum of living yeasts.* FEMS Microbiol Lett. **306**(1): p. 61-6.

63. Gutscher, M., et al., *Real-time imaging of the intracellular glutathione redox potential.* Nat Methods, 2008. **5**(6): p. 553-9.

64. Niculescu-Duvaz, I., *Technology evaluation: gemtuzumab ozogamicin, Celltech Group.* Curr Opin Mol Ther, 2000. **2**(6): p. 691-6.

65. Neidle, S. and D.E. Thurston, *Chemical approaches to the discovery and development of cancer therapies.* Nat Rev Cancer, 2005. **5**(4): p. 285-96.

66. Cerritelli, S., D. Velluto, and J.A. Hubbell, *PEG-SS-PPS: reduction-sensitive disulfide block copolymer vesicles for intracellular drug delivery.* Biomacromolecules, 2007. **8**(6): p. 1966-72.

67. Koo, A.N., et al., *Disulfide-cross-linked PEG-poly(amino acid)s copolymer micelles for glutathione-mediated intracellular drug delivery.* Chem Commun (Camb), 2008(48): p. 6570-2.

68. Zhang, L., et al., *Degradable disulfide core-cross-linked micelles as a drug delivery system prepared from vinyl functionalized nucleosides via the RAFT process.* Biomacromolecules, 2008. **9**(11): p. 3321-31.

69. Bade, S., et al., *Botulinum neurotoxin type D enables cytosolic delivery of enzymatically active cargo proteins to neurones via unfolded translocation intermediates.* J Neurochem, 2004. **91**(6): p. 1461-72.

70. Zhang, P., et al., *An efficient drug delivery vehicle for botulism countermeasure.* BMC Pharmacol, 2009. **9**: p. 12.

71. Lee, K.D., et al., *Delivery of macromolecules into cytosol using liposomes containing hemolysin from Listeria monocytogenes.* J Biol Chem, 1996. **271**(13): p. 7249-52.

72. Sun, X., C. Provoda, and K.D. Lee, *Enhanced in vivo gene expression mediated by listeriolysin O incorporated anionic LPDII: Its utility in cytotoxic T lymphocyte-inducing DNA vaccine.* J Control Release. **148**(2): p. 219-25.

73. Mandal, M. and K.D. Lee, *Listeriolysin O-liposome-mediated cytosolic delivery of macromolecule antigen in vivo: enhancement of antigen-specific cytotoxic T lymphocyte frequency, activity, and tumor protection.* Biochim Biophys Acta, 2002. **1563**(1-2): p. 7-17.

74. Mandal, M., et al., *Cytosolic delivery of viral nucleoprotein by listeriolysin O-liposome induces enhanced specific cytotoxic T lymphocyte response and protective immunity.* Mol Pharm, 2004. **1**(1): p. 2-8.

75. Phan, U.T., M. Maric, and P. Cresswell, *Disulfide reduction in major histocompatibility complex class II-restricted antigen processing by interferon-gamma-inducible lysosomal thiol reductase.* Methods Enzymol, 2002. 348: p. 43-8.

76. Barjaktarevic, I., et al., *Inhibitory role of IFN-gamma-inducible lysosomal thiol reductase in T cell activation.* J Immunol, 2006. 177(7): p. 4369-75.

77. Weecharangsan, W., et al., *Disulfide-linked liposomes: effective delivery vehicle for Bcl-2 antisense oligodeoxyribonucleotide G3139.* Anticancer Res. 30(1): p. 31-7.

78. Heffernan, M.J. and N. Murthy, *Disulfide-crosslinked polyion micelles for delivery of protein therapeutics.* Ann Biomed Eng, 2009. 37(10): p. 1993-2002.

79. Hirosue, S., et al., *Antigen delivery to dendritic cells by poly(propylene sulfide) nanoparticles with disulfide conjugated peptides: Cross-presentation and T cell activation.* Vaccine. 28(50): p. 7897-906.

80. Austin, C.D., et al., *Oxidizing potential of endosomes and lysosomes limits intracellular cleavage of disulfide-based antibody-drug conjugates.* Proc Natl Acad Sci U S A, 2005. 102(50): p. 17987-92.

81. Vincentelli, J., et al., *Poly(ethylene glycol) derivatized prodrugs through mixed disulfide bond formation: preliminary report on captopril.* Int J Pharm, 1996. **134**: p. 147-155.

82. Kok, R.J., et al., *Specific delivery of captopril to the kidney with the prodrug captopril-lysozyme.* J Pharmacol Exp Ther, 1999. **288**(1): p. 281-5.

CHAPTER II

DESIGN AND EXPRESS OF RECOMBINANT REDOX-SENSITIVE FRET REPORTER

SUMMARY

A genetically engineered redox-sensitive probe, composed of a thrombin-cleavable monomeric enhanced cyan fluorescent protein (mECFP) and monomeric Citrine (mCit) fusion protein, was generated through modified constructs and successfully expressed in bacteria. When incubated with DTT and thrombin, the single polypeptide was specifically cleaved at the thrombin recognition sequence bordered on both sides by cysteine and produced a dynamic change of up to 5-fold in the ratio of fluorescence emission upon disulfide reduction. Liposome-encapsulated probes were successfully monitored for sensitivity to redox changes without significant sensitivity to changes in pH. The recombinant fusion protein between mECFP and mCit shows great promise for the determination of redox status *in vitro* as well as the possibility for live-cell imaging.

INTRODUCTION

Direct analysis of intracellular redox potential, the ability of a given protein or molecule to gain or donate electrons [1], exerts a profound influence on the design and interactions of disulfide-conjugated macromolecular drug delivery [2]. The ability to sense the redox potential in live cells has far-reaching implications for understanding and manipulating drug delivery systems that underlie complex biomedical problems [2, 3]. Therefore, development of genetically encoded biosensors that enable real-time and extended assessment of alterations in intracellular metabolism without cellular disruption is essential [4]. One of the most promising applications involves the use of GFP [5], with major advantages being efficient fluorescence properties and resistance to proteases [6]. GFP possesses excellent targeting performance to specific organelles as GFP-fusion proteins in tagging applications [7], and can also be modulated as an indicator by mutagenesis [8]. One method for making biochemically sensitive GFPs exploits fluorescence resonance energy transfer (FRET) between variants of GFP [9, 10]; however, currently available redox biosensors mostly employ single GFP variants in non-FRET-based applications [11-14]. A FRET-based approach can be implemented to achieve maximum sensitivity within the physiological redox range based on dynamic ratiometric measurements. FRET is a quantum mechanical process whereby the excited state energy of a fluorescent donor molecule is transferred to a ground state acceptor molecule [15]. There are three requirements for FRET: (i) donor and acceptor molecules must be in close proximity, typically 10–100 Å, (ii) the absorption spectrum of the acceptor must overlap the fluorescence emission spectrum of the donor, and (iii) donor and acceptor transition dipole orientations must be approximately parallel. Although the orientation of

the dipole alignment should be appropriate to create an efficient energy transfer, the wavelength and distance are the only factors that can be controlled [16, 17].

In this study, we explored the use of FRET-based biosensors consisting of the common FRET-compatible pair of GFP variants, mECFP and mCit, a variant of yellow fluorescent protein (YFP) with reduced pH sensitivity [18]. We hypothesized that this fusion protein can be incorporated into the endolysosomal compartments in order to monitor redox environments with a detectable change in FRET efficiency as measured by changes in the redox profiles *in vitro* as well as in living cells. The redox-sensitive fusion protein was developed and expressed as a His-tagged polypeptide in *E. coli* and its ability to sense redox changes was characterized biochemically through its response to reduction with various ratios of oxidized and reduced forms of dithiothreitol (DTT).

MATERIALS AND METHODS

Expression and purification of mECFP-Th-mCit fusion protein

mECFP was transferred from Bluescript cloning vector (Bsk, Stratagene) to bacterial expression vector pET-29b (Novagen) using the XbaI and BamHI restriction sites and ligated to GDPCLVPRGSC-mCit by BamHI and XhoI resctriction sites using polymerase chain reaction (PCR). The expression construct was transformed into *E. coli* strain BL21 (DE3) RIPL (Stratagene, Santa Clara, CA). A starting culture from a single colony was grown in 50 mL LB media at 37°C overnight with 30 μg/mL kanamycin. The culture was diluted 1:50 into 2 L LB media, and then incubated at 37°C until the absorbance at 600 nm reached ~0.7. The culture was induced at 30°C for 10 h with 1 mM IPTG, and then centrifuged at 7,000 × g for 10 min at 4°C. The bacterial pellet was resuspended in wash buffer (50 mM sodium phosphate, 300 mM NaCl, 20 mM imidazole, pH 8.0) and incubated on ice for 30 min with 1 mg/mL lysozyme and lysed using a French press (Thermo Spectronic) or a micro ultrasonic cell disrupter (Kontes). The lysate was centrifuged at 10,000 × g for 30 min followed by binding to nickel-nitrilotriacetic acid (Ni-NTA) agarose (Qiagen, Valencia, CA) up to 3 h. The Ni-NTA agarose was washed with a total of 500 mL wash buffer containing 0.03% hydrogen peroxide (H_2O_2, Fisher Scientific) by gravity-flow, and then eluted with wash buffer containing 250 mM imidazole (elution buffer, EB). The purified recombinant proteins were buffer-exchanged into HBS (20 mM HEPES, 150 mM NaCl, pH 7.4) using PD10 desalting columns (Amersham Biosciences).

Expression and purification of mECFP-G_4STh-mCit fusion protein

Separating the coding domains of the two proteins was the sequence GDPCGGGGSLVPRGSC, of which GDP resulted from the vector backbone (in order to retain the BamHI site), while CLVPRGSC was inserted by overlap extension PCR, and GGGGS was subsequently inserted by Site-directed, Ligase-Independent Mutagenesis (SLIM) PCR [19, 20]. SLIM PCR was also used to replace the S-Tag affinity sequence in pET-29b with the Strep-tag II affinity sequence (WSHPQFEK). The construct was expressed in *E. coli* BL21 (DE3) as a single polypeptide and purified via Ni-NTA and hexahistidine affinity chromatography.

Thrombin cleavage

Proteolytic cleavage experiments were performed in the cleavage buffer (50 mM Tris, 150 mM NaCl, 2.5 mM $CaCl_2$ and 0.1% β-mercaptoethanol, pH 8.0) according to Zhang [21]. To determine optimal conditions for proteolysis by thrombin, different amounts of thrombin (0, 0.1, 0.25 and 0.5 U/ug) were incubated with the fusion protein at room temperature. Each aliquot was taken out at various time points (0, 3, 6, 9, 12, 24 hr) and frozen until analysis by sodium dodecyl sulfate-polyacrylamide gel electrophoresis (SDS-PAGE) and imperial protein stain (Thermo Scientific). Gels were digitally recorded using a KODAK Digital Sciences Electrophoresis Documentation and Analysis System.

Ellman's assay

Ellman's assay is a sulfhydryl assay using the specificity for free thiol groups of Ellman's reagent (5,5'-Dithio-bis-(2-nitrobenzoic acid), DTNB, Pierce) at neutral pH with short reaction time. For quantification of sulfhydryl groups, a cysteine standard was made by serial dilution in the reaction buffer (0.1 M sodium phosphate, pH 8.0, containing 1 mM EDTA) and 4 mg Ellman′s reagent was dissolved in 1 ml of reaction buffer to make a reagent solution. Each test sample was prepared with 50 µl of Ellman′s reagent solution, 2.5 ml of reaction buffer and 250 µl of each standard or unknown. After incubation at room temperature for 15 minutes, the absorbance was measured at 412 nm using an Emax microplate reader (Molecular Devices). The experimental sample concentrations were determined from the cysteine standard curve.

Liposome preparation

For liposome preparation, probes were encapsulated inside pH-sensitive liposomes composed of phosphatidylethanolamine (PE, Avanti, Alabaster, AL) and cholesteryl hemisuccinate (CHEMS, Sigma-Aldrich, St. Louis, MO) in a 2:1 molar ratio, respectively, by a thin lipid film hydration and freeze/thaw method [22]. Liposomes were extruded through 0.4 µm Whatman Nuclepore polycarbonate filters (GE Healthcare) and unencapsulated probes were removed from liposomes by size-exclusion chromatography using a 1 x 25 cm Sepharose CL-4B column (GE Healthcare). Concentrations of encapsulated unnicked or nicked probes were analyzed by measuring fluorescence intensities using standard curve based on known concentrations of the proteins with the

bicinchoninic acid assay (BCA, Thermo Scientific) using bovine serum albumin as a standard.

Redox buffer preparation

The oxidized fusion protein (0.5 μM) was incubated in reaction buffer consisting of sodium phosphate, pH 7.4 or 5.5, to which varying concentrations of DTT_{red} and DTT_{ox} were added. Mixed forms of DTT were reciprocally varied from 0:0.5 to 0.5:0 mM in 0.1 mM increments, where total concentration was kept 0.5 mM.

Redox titration and Nernst equation

Titration of FRET-reporters in redox buffers was performed to generate a standard curve to determine the redox potential according to fluorescence changes by fluorescence spectroscopy (Jobin Yvon-Spex Instruments SA., NJ). R_{FRET} is defined by dividing the intensity of mCit emission (525 nm) by mECFP emission (475 nm) at 435 nm CFP excitation. To determine the probe's sensitivity to redox and pH changes, the probe was incubated in redox buffers containing mixtures of oxidized and reduced DTT at room temperature for 15 min. The redox potential of a protein is most often expressed as an electrochemical potential in units of volts using the following Nernst equation: $E = E^{0'}_{DTT} - \frac{RT}{nF}\ln\frac{[DTT_{red}]}{[DTT_{ox}]}$ [12], where $E^{0'}_{DTT}$ is the standard potential of the DTT_{red}/DTT_{ox} couple (-323 mV at pH 7 and 30°C [23]), R is the gas constant (8.315 J K^{-1}

mol^{-1}), T is the absolute temperature (303.15 K), n is the number of transferred electrons, and F is the Faraday constant (9.649×10^4 C mol^{-1}).

RESULTS

Genetic coupling: mECFP-Th-mCit

mECFP and mCit were cloned into pET-29b using canonical methods [24]. After verification by DNA sequencing, mECFP-Th-mCit fusion proteins were expressed in *E. coli* BL21(DE3) (Stratagene), and purified using Ni-NTA agarose with an average yield of 6 mg/L. The peptide sequence is shown in Fig 2.1. Fluorescence spectroscopy and SDS-PAGE were used to characterize the probe. A linker containing a redox switch and a proteolytic recognition site was inserted between the FRET pair consisting of mECFP and mCit (unnicked, Fig 2.2). When incubated with thrombin, the single polypeptide is specifically cleaved at the thrombin recognition sequence (nicked), yet still produces FRET at a similar efficiency due to the disulfide bond between two cysteines. However, a dramatic change in the fluorescence emission ratio results upon disulfide reduction after incubation with DTT (reduced). The fusion protein mECFP-Th-mCit had a high level of FRET efficiency and the linker had thrombin specificity and redox sensitivity. A significant change in the fluorescence emission ratio resulted upon disulfide reduction and consequent separation of the FRET pair proteins (Fig. 2.3a), as independently confirmed by non-reducing SDS-PAGE (Fig. 2.3b). The fusion protein was expressed as a single polypeptide (lane I), and treatment with DTT or thrombin alone resulted in barely detectable cleavage (lanes II and III, respectively), and both DTT and thrombin produced the cleavage products of mECFP and mCit as shown in lane IV. The last lane (V) contains thrombin alone, MW 45 kDa. The graded response of the fluorescence emission spectra is ratiometric with an isosbestic point separating the two peaks at 510

nm, consistent with two molecular species in redox equilibrium and validation that the change in R_{FRET} was dependent exclusively on redox changes.

Optimization of thrombin cleavage

Optimization of proteolytic cleavage experiments was performed according to Zhang [21]. The single peptide of mECFP-Th-mCit started to be specifically cleaved after application of various amounts of thrombin (Fig. 2.4), more efficiently cleaved at the higher concentrations and longer incubation of proteolytic reaction. To confirm the stability of fusion proteins throughout the incubation, the reaction mixtures were resolved in SDS-PAGE at the indicated times. Compared to control (0 U/ug thrombin), no significant amounts of non-specific cleavage products were observed. These results indicated that the fusion proteins could be cleaved specifically by thrombin, and also that the activity of thrombin is most efficient at 0.5 U/ug for 24 h in thrombin cleavage buffer at room temperature.

Improvements by conformational modification : mECFP-G_4STh-mCit

Briefly, the construct was modified by SLIM PCR to insert a polypeptide spacer (GGGGS) between cysteine and the thrombin recognition sequence, and to replace the S-Tag with the Strep-tag II affinity sequence (Fig. 2.5). Through consecutively modified sequence, the single polypeptide is predicted to become more flexible so that the fluorescent proteins remained tethered by a disulfide bond with a greater chance of

disulfide bonds following cleavage in the linker region that is easily accessible to thrombin by reducing steric hindrance. The recombinant fusion protein has extraneous amino acids (aa) on either side of each protein; upstream of mECFP is a Strep-tag II (8 aa) plus 8 aa from the vector backbone, and downstream is the C-GGGGSLVPR using SLIM PCR plus 3 aa from the vector backbone. Upstream of mCit is GSC that we cloned in and downstream is the His-tag plus 2 aa from the vector backbone. The recombinant form of mECFP is 18 aa longer than mCit which results in a larger apparent MW in SDS-PAGE and hence two bands (Fig 2.6). With the same ratio of thrombin to protein, construct modification resulted in more efficient cleavage to save the amount of thrombin. Following thrombin proteolysis, nicked probes carrying both His-tag and Strep-tag II were purified sequentially in Ni-NTA agarose and Strep-Tactin sepharose columns (IBA) to remove the untethered mECFP and mCit that would otherwise have contributed to an elevated fluorescence background signal.

Fluorescence emission analysis of probes against DTT redox buffer

Fluorescence spectroscopy was used to characterize the new structure through specific cleavage after proteolysis and disulfide reduction. Even though the construct was modified, R_{FRET} was identical based on the degree of disulfide reduction as determined by the ratio of the two fluorescent intensities ($mCit_{em}/mECFP_{em} = F_{525}/F_{475}$). In Fig. 2.7, a graded response of the fluorescence emission spectra was observed in the presence of various ratios of redox buffers. At the highest concentration of DTT_{red}, the disulfide bond between the two fluorescent proteins is reduced, leading to a loss in FRET as indicated by

an increase in the 475 nm emission peak (mECFP donor) and a decrease in the 525 nm emission peak (mCit acceptor). The emission spectra are ratiometric, thus minimizing measurement errors and allowing convenient calculation of R_{FRET} by dividing the $mCit_{em}$ by $mECFP_{em}$. An increase in the amount of DTT_{red} led to a decrease in FRET signal, suggesting that the R_{FRET} of the probe was indicative of the reducing environment.

Liposomes

The next step was preparation of pH-sensitive liposomes composed of PE:CHEMS in a 2:1 molar ratio to encapsulate probes. Average encapsulation efficiency of probes was 14~17 %. To investigate the redox-sensing properties of liposomes, fluorescence kinetics of disulfide reduction and pH effects were tested (Fig. 2.8). In Fig. 2.8a, R_{FRET} was plotted as a function of time; in the presence of DTT, the FRET ratio decreased rapidly and reached steady state within 10 min. Although fluorescence emission was scanned at 435 nm (CFP excitation) immediately after adding reducing agent, reduction had already begun as indicated by the lower level of R_{FRET} at time 0, an aspect of probes' fast response (Fig. 2.8a). To investigate the effect of pH on redox measurement when the probe is internalized from the cell surface (pH 7.4) along the endocytic pathway to acidic lysosomes (pH ≤ 5.5), R_{FRET} was measured as a function of redox potential at two different pHs using liposome-encapsulated nicked or unnicked probes (Fig. 2.8b). The R_{FRET} of unnicked (control) probes remained constant regardless of the redox potential, while the R_{FRET} of nicked probes decreased with increasing reduction potential. Using the Nernst equation and nonlinear regression to calculate redox

potential (Fig. 2.9), it was determined that the probe was sensitive to small changes in redox potential between -350 mV and -280 mV, a slightly lower range within physiologically relevant redox potential values between -320 mV and -240 mV, which offers advantageous use in reducing compartments [25]. This standard curve generated by observing FRET signal in different redox buffers can be used to directly investigate redox potentials in the subcellular compartments without destructive sampling and chemical analysis [26].

DISCUSSION

The goal of this study was to develop a probe to report the redox potential. A redox-sensitive FRET reporter was designed as a disulfide bond-containing recombinant fusion protein and encapsulated in liposomes. To this end we designed and successfully expressed a genetically engineered redox-sensitive fusion protein in *E. coli* consisting of the FRET pair, mECFP and mCit, joined by an intervening disulfide-bonded and protease-sensitive linker. The single polypeptide included cysteine residues immediately bordering a thrombin-specific linker, which allowed the fluorescent proteins remained tethered by a disulfide bond following cleavage in the linker region. This conjugation conferred the necessary proximity of donor and acceptor molecules in order for FRET to occur, and a significant change in the fluorescence emission ratio was indeed observed. However, we realized that the amount of thrombin used was much larger than unit definition (one unit of enzyme cleaves > 90% of 100 μg of a test GST fusion protein when incubated in 1X PBS at 22°C for 16 h) during optimization of thrombin cleavage. One possibility is that the relatively short linker resulted in insufficient enzyme access; due to the bulky substrate components, either thrombin activity or the efficiency of disulfide bond formation might be reduced. With improving the yield of disulfide formation and decreasing the ratios of thrombin to proteins, site-specific modification was shown to be successful without any significant change in the FRET ratio. Using the Ellman's assay (Fig. 2.10), we quantified free thiol concentrations before and after modification, also tested mECFP-G4STh-mCit transformed into Origami competent cells (DE3, Novagen), which have mutations in both the thioredoxin reductase and glutathione reduactase genes to greatly enhance disulfide bond formation in the *E. coli* cytoplasm,

therefore providing an oxidizing environment conducive to disulfide formation [27]. Based on the assumption that cysteines bordered on the side of linker are completely oxidized, the theoretical concentration of free thiol was 18 μM. The oxidizing *E. coli* did not significantly improve disulfide formation, although a 40% decrease in free thiols revealed that there was some improvement after construct modification. The difference between the theoretical and experimental values may be explained by the possibility that either mECFP or mCit formed intramolecular disulfide bonds between conserved cysteines (one is buried and one is surface-located) [28]. In addition to linker flexibility, SLIM PCR was used to replace the S-Tag with a Strep-tag II affinity sequence. Through high-affinity binding of Strep-Tactin sepharose, nicked probes were prepared with > 99% exclusively disulfide-mediated protein cross-linking. Furthermore, Ni-NTA agarose resin was exposed to hydrogen peroxide during protein purification in order to promote disulfide bond formation between cysteine residues. These methods ensured that the change in FRET signal was not caused by mechanisms other than disulfide reduction of the nicked probes. A significant change in the fluorescence emission ratio resulted upon disulfide reduction, while that of unnicked probes remained constant regardless of the redox potential, independently confirmed by SDS-PAGE. An isosbestic point separating the two peaks is observed at 510 nm, consistent with two molecular species in redox equilibrium and validation that the change in R_{FRET} is exclusively dependent on redox changes.

To compare redox buffer capacities between DTT and other cellular reducing agents, GSH, β-merceptoethanol and cysteine were tested in the various concentrations and the FRET ratios were measured by fluorescence spectroscopy (Fig. 2.11). Probes

reacted readily with more strongly reducing agents, so they will primarily reflect the potential of the most strongly reducing redox buffers. There are membrane-permeant reducing agents such as DTT, β-mercaptoethanol and dihydrolipoic acid, while cysteine, tris (2-carboxyethyl) phosphine (TCEP), and GSH are membrane-impermeant reducing agents [12]. DTT was chosen for redox buffers not only by almost complete reduction but also by membrane permeability.

Initially we sought to compare two different formulations of liposomes: one has protein encapsulated inside liposomes and in the other one protein is immobilized on the liposome surface using Ni-chelating lipid to characterize both species in terms of specific activity. Since the probe has a His-tag on the C-terminus of mCit, it could be immobilized on lipid film by mixing 2-5mol% 1,2-di-(9Z-octadecenoyl)-sn-glycero-3-[(N-(5-amino-1-carboxypentyl)iminodiacetic acid)succinyl] (nickel salt) (DGS-NTA-Ni, Avanti) with 2:1 molar ratio of PE:CHEMS. However, we found that surface-conjugated probes were not efficiently taken up by cells compared to liposome-encapsulated probes (Fig. 2.12). Though the different efficiency may be at least partly explained by reducing non-specific binding, inconsistent data from pH study due to protonated His-tags competing off with the Ni ion [29] leads us to use liposome encapsulation.

Taken together, the FRET reporter was designed as a disulfide bond-containing recombinant fusion protein encapsulated into liposomes and characterized. When incubated with DTT and thrombin, the single polypeptide was more specifically cleaved at the thrombin recognition sequence after sequence modification and produced a fluorescence dynamic range between the fully oxidized and fully reduced forms of the probe corresponding to a 5-fold change in the ratiometric spectroscopic signal, which led

to better discrimination of the redox states in complex biological specimens. Liposome-encapsulated probes were shown to be well-suited for measuring redox conditions by successfully monitored for sensitivity to redox changes *in vitro* without significant sensitivity to changes in pH, suggested the potential for utility in for cell imaging. Furthermore, using the Nernst equation and nonlinear regression, the midpoint redox potential was estimated to be as low as -315 mV vs the apparent midpoint potential of roGFPs that were found to be in the more oxidizing range of -270 to -290 mV [12]. Taken together, these characteristics make our FRET-based probe very promising for monitoring redox changes in environments that are relatively acidic and reducing.

Figure 2.1 Peptide sequcence of mECFP-Th-mCit

Amino acids in bold characters correspond to expressed part of cloning vector backbone pET-29b, underlined amino acids to protein tag, S-tag and His-tag, and dotted underline to a linker containing thrombin recognition sequence and two cysteines.

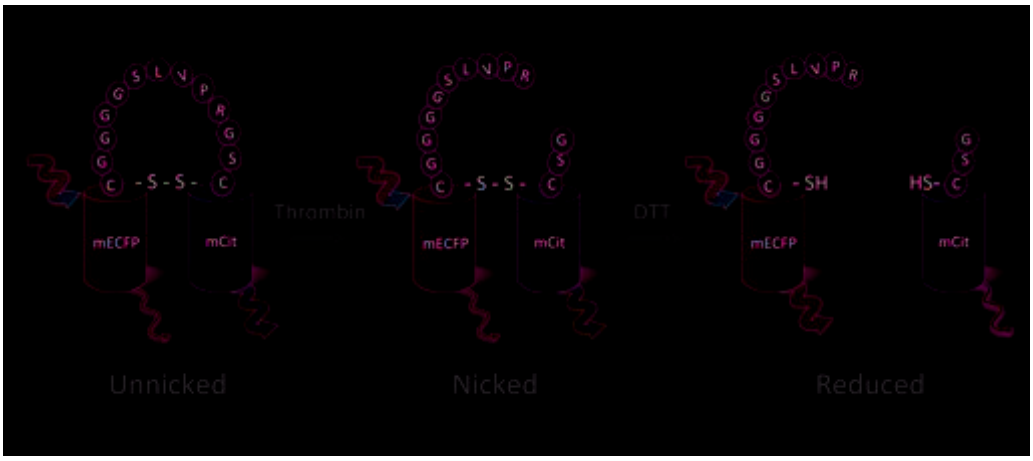

Figure 2.2 Schematic representation of the redox-sensitive FRET reporter.

A single polypeptide was designed such that the donor and acceptor are linked by both a thrombin-cleavable peptide and a reducible disulfide bond for efficient intramolecular energy transfer (unnicked). When incubated with thrombin, the single polypeptide is specifically cleaved at the thrombin recognition sequence (nicked), yet still produces FRET at a similar efficiency due to the disulfide bond between two cysteines. However, a dramatic change in the fluorescence emission ratio results upon disulfide reduction after incubation with DTT (reduced).

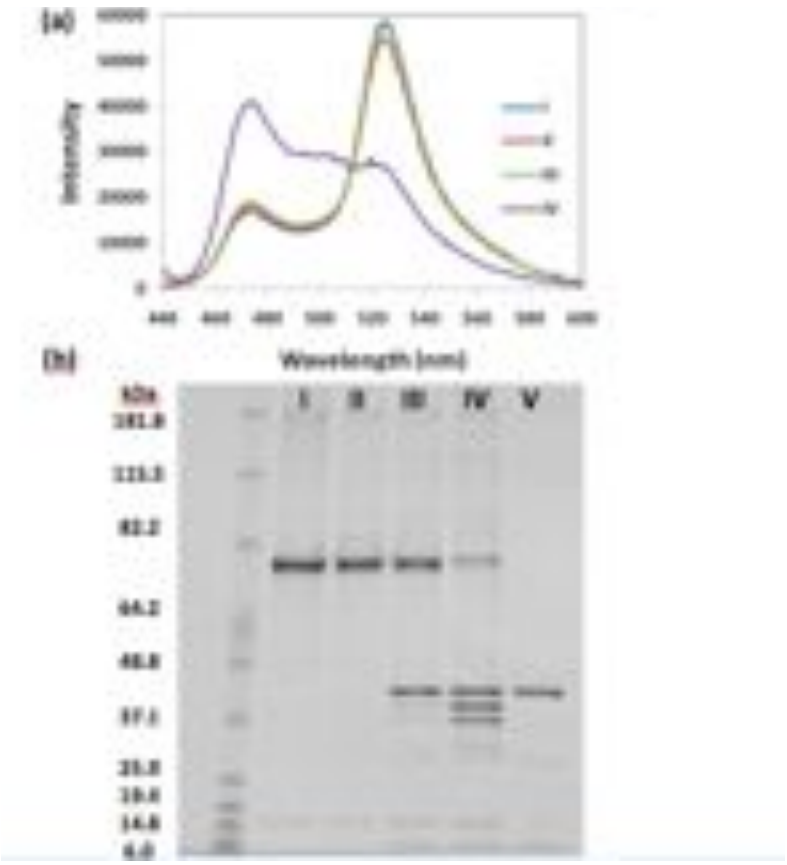

Figure 2.3 Fluorescence emission analysis (a) and SDS-PAGE analysis (b) of the mECFP-Th-mCit.

Each fluorescence emission spectrum (I~IV) corresponds to each of SDS-PAGE lane. I, mECFP-Th-mCit; II, mECFP-Th-mCit w/ DTT; III, mECFP-Th-mCit w/ Thrombin; IV, mECFP-Th-mCit w/ DTT+Thrombin; V, Thrombin.

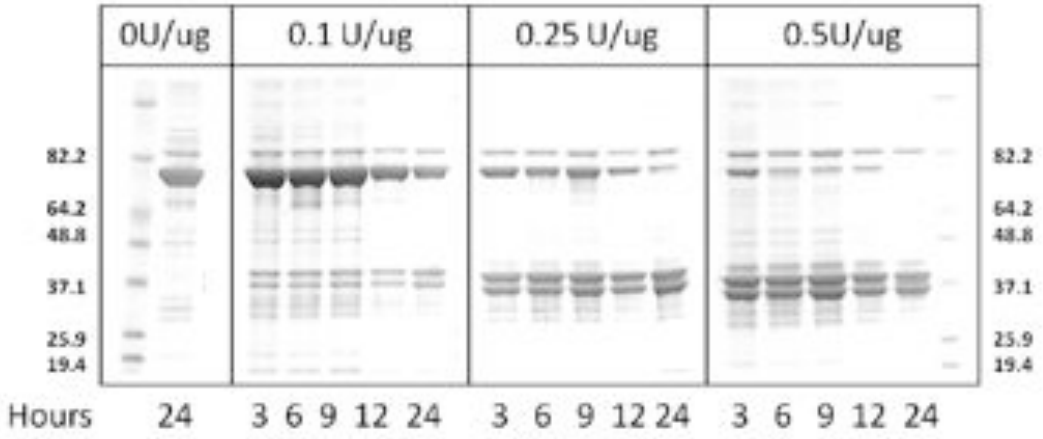

Figure 2.4 Proteolytic analysis of mECFP-Th-mCit fusion protein to thrombin.

Various amounts of thrombin were added to samples containing 30 μg of fusion proteins in thrombin cleavage buffer. At times indicated in the figure, aliquots of the reaction mixture were removed and frozen at -80°C until analysis by SDS-PAGE.

Figure 2.5 Modified peptide sequence of mECFP-G4STh-mCit

Amino acids in bold characters correspond to expressed part of cloning vector backbone pET-29b, underlined amino acids to protein tag, Strep-tag and His-tag, and dotted underline to a linker containing thrombin recognition sequence and two cysteines plus spacer.

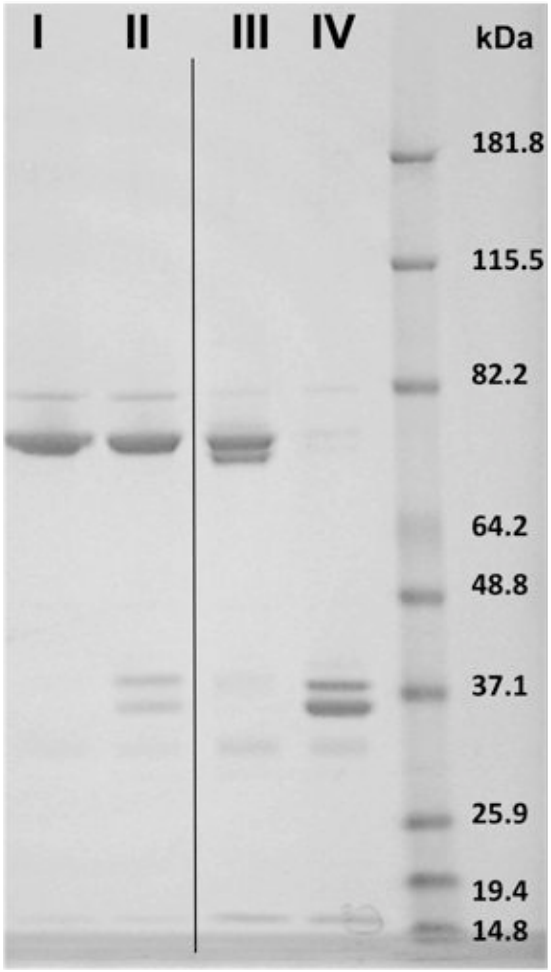

Figure 2.6 Improvement by construct modification

SDS-PAGE analysis with equal ratios of thrombin to fusion proteins. Lane I, mECFP-Th-mCit w/o DTT; II, mECFP-Th-mCit w/ DTT; III, mECFP-G_4STh-mCit w/o DTT; IV, mECFP-G_4STh-mCit w/ DTT. With the same ratio of thrombin to protein (0.01 U/μg), construct modification resulted in more efficient cleavage.

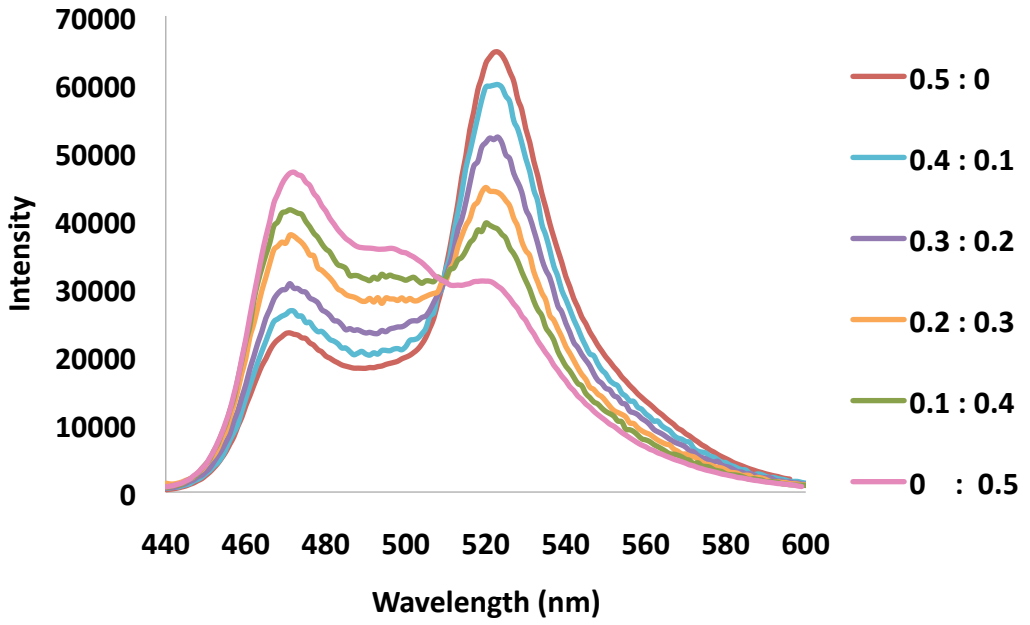

Figure 2.7 Emission spectra of nicked probe through titration of reduced to oxidized DTT.

Nicked and disulfide-bonded probe emissions were scanned at 435 nm CFP excitation with mixed forms of oxidized and reduced DTT. Legends indicate the concentrations (mM) of DTT_{ox} : DTT_{red} buffers with reciprocally varied concentrations from 0 to 0.5 mM in 0.1 mM increments (total 0.5 mM).

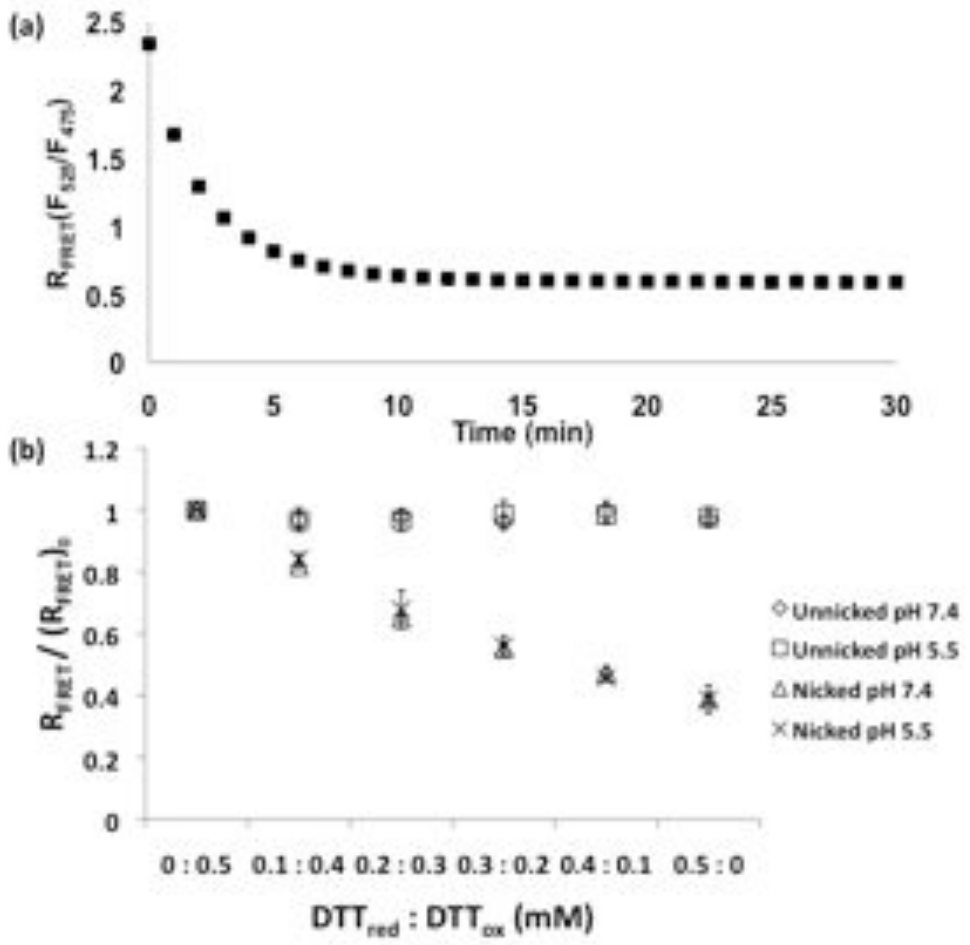

Figure 2.8. R_{FRET} of liposome-encapsulated probe as a function of time (a) and ratios of reduced to oxidized DTT in different pHs (b).

(a) Fluorescence kinetics of disulfide reduction using fluorescence spectroscopy. Fluorescence emission started to be scanned (at 435 nm CFP excitation) immediately after adding reducing agent. (b) Redox equilibria of liposome-encapsulated unnicked (upper data points) and nicked probes (lower) at pH 7.4 and 5.5 and against the DTT_{red}: DTT_{ox} ratios indicated on the x-axis. Liposome-encapsulated probes were diluted in sodium phosphate buffer at the two pH values and incubated 15 min at room temperature, at which point reduction had reached a plateau and fluorescence emission at 525 nm ($mCit_{em}$) and 475 nm ($mECFP_{em}$) were recorded. The R_{FRET} ($mCit_{em}/mECFP_{em}$) values were normalized to that of the initial R_{FRET} measurement, $(R_{FRET})_0$. A higher FRET ratio indicates an oxidizing environment while a lower FRET ratio indicates a reducing environment. Error bars represent standard deviations from the mean, based on triplicates.

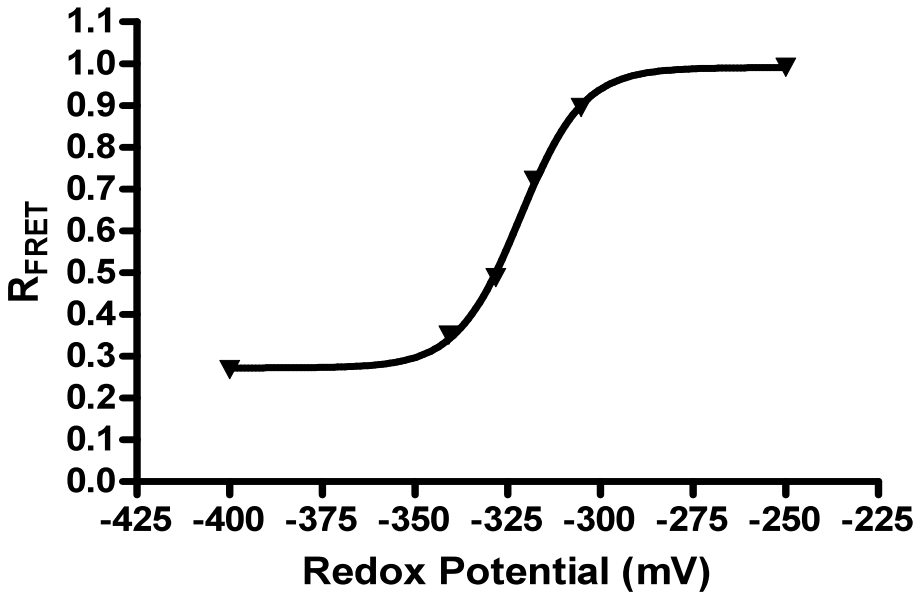

Figure 2.9. Standard redox titration curve.

Redox potential values were obtained by fitting the data to a titration curve following the Nernst equation using the plot of the R_{FRET} for liposome-encapsulation nicked probes versus the ratio of molar concentrations of DTT_{red} to DTT_{ox}.

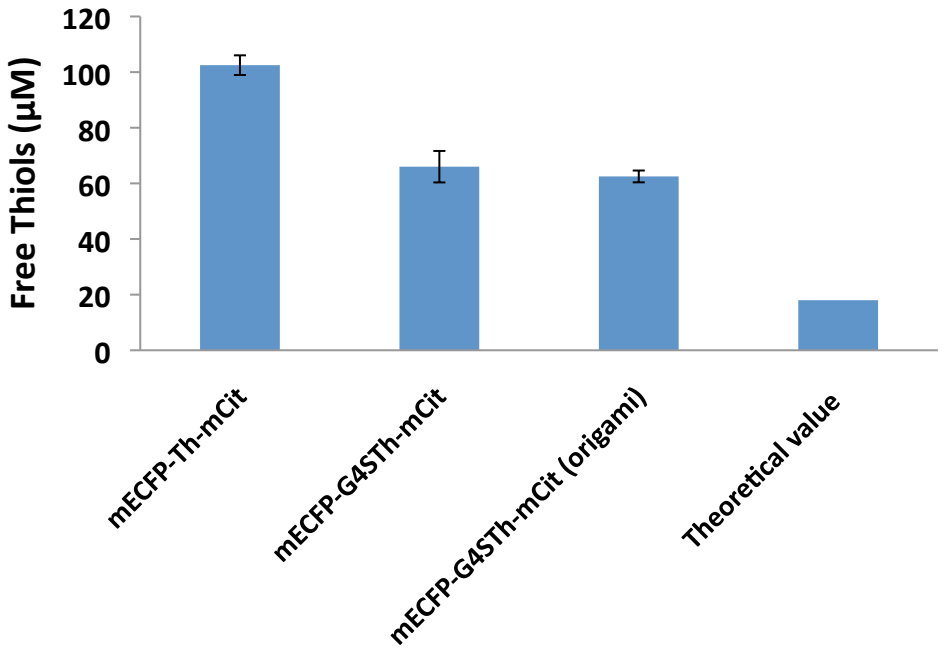

Figure 2.10 Comparison of free thiols using Ellman's assay

Comparison of free thiol concentrations (µM) before and after construct modification by Ellman's assay.

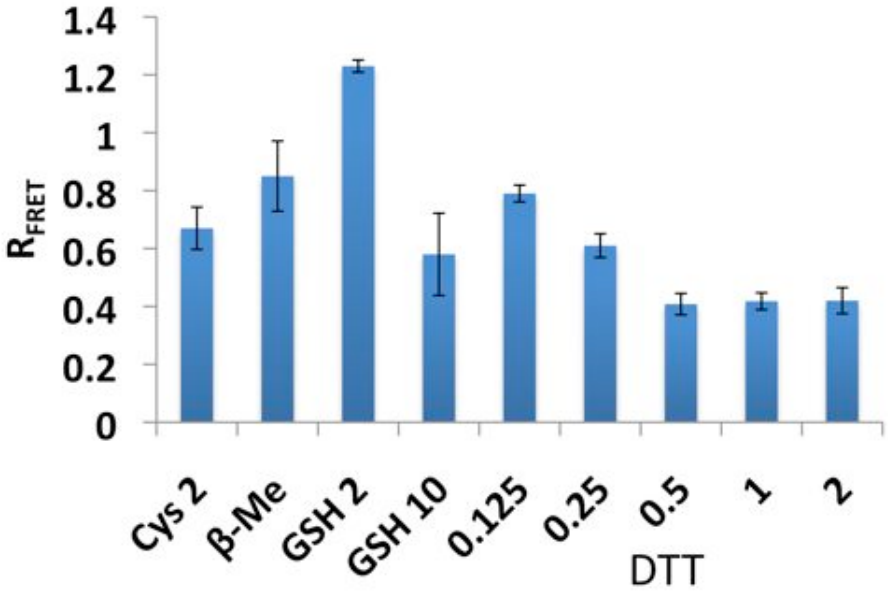

Figure 2.11 Comparison of reducing efficiencies of various reductants

R_{FRET} (defined as a the ratio of fluorescence from emission at 520 nm versus 475 nm and normalized to the untreated case) treated with the indicated concentration of DTT or other reductants. Data represent mean +/- SD from three independent experiments.

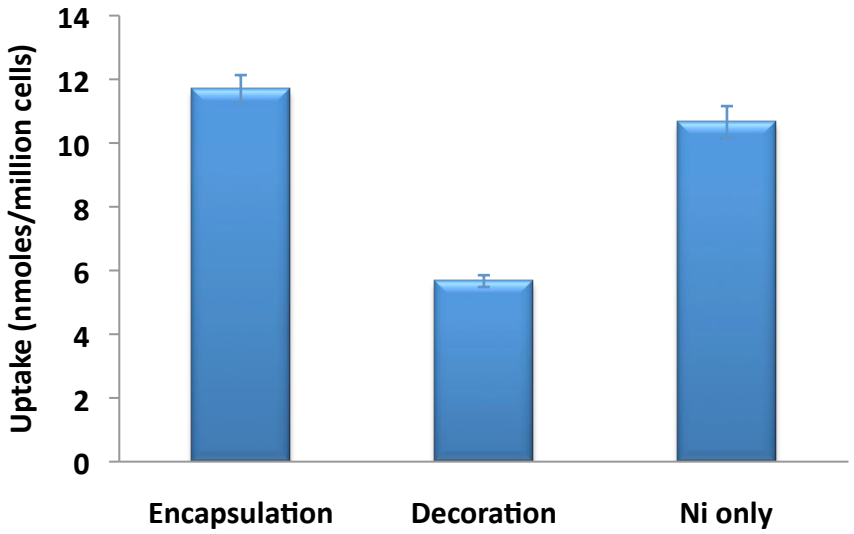

Figure 2.12 Uptake study

Raw cells were cultured in DMEM with 10% FBS and plated at a density of 2.5E06 in 12-well plates 20 h before the experiments. Liposomes were diluted with serum-free media to a concentration of 0.2 mM and 1.0 ml was added to each well. After 4 h incubation at 37^{o}C, cells were washed with PBS and treated with PBS containing 3 mM EDTA at room temp for 5 min and adjusted to the concentration of 1.0E06 cells in 100 uL of PBS buffer.

REFERENCES

1. Sevier, C.S. and C.A. Kaiser, *Formation and transfer of disulphide bonds in living cells.* Nat Rev Mol Cell Biol, 2002. **3**(11): p. 836-47.

2. Saito, G., J.A. Swanson, and K.D. Lee, *Drug delivery strategy utilizing conjugation via reversible disulfide linkages: role and site of cellular reducing activities.* Adv Drug Deliv Rev, 2003. **55**(2): p. 199-215.

3. Pennington, J.D., et al., *Thioredoxifgn and thioredoxin reductase as redox-sensitive molecular targets for cancer therapy.* Curr Pharm Des, 2007. **13**(33): p. 3368-77.

4. Arrigo, A.P., *Gene expression and the thiol redox state.* Free Radic Biol Med, 1999. **27**(9-10): p. 936-44.

5. Bjornberg, O., H. Ostergaard, and J.R. Winther, *Measuring intracellular redox conditions using GFP-based sensors.* Antioxid Redox Signal, 2006. **8**(3-4): p. 354-61.

6. Giepmans, B.N., et al., *The fluorescent toolbox for assessing protein location and function.* Science, 2006. **312**(5771): p. 217-24.

7. Tsien, R.Y., *The green fluorescent protein.* Annu Rev Biochem, 1998. **67**: p. 509-44.

8. Lohman, J.R. and S.J. Remington, *Development of a family of redox-sensitive green fluorescent protein indicators for use in relatively oxidizing subcellular environments.* Biochemistry, 2008. **47**(33): p. 8678-88.

9. Pollok, B.A. and R. Heim, *Using GFP in FRET-based applications.* Trends Cell Biol, 1999. **9**(2): p. 57-60.

10. Takanishi, C.L., et al., *GFP-based FRET analysis in live cells.* Brain Res, 2006. **1091**(1): p. 132-9.

11. Cannon, M.B. and S.J. Remington, *Re-engineering redox-sensitive green fluorescent protein for improved response rate.* Protein Sci, 2006. **15**(1): p. 45-57.

12. Hanson, G.T., et al., *Investigating mitochondrial redox potential with redox-sensitive green fluorescent protein indicators.* J Biol Chem, 2004. **279**(13): p. 13044-53.

13. Dooley, C.T., et al., *Imaging dynamic redox changes in mammalian cells with green fluorescent protein indicators.* J Biol Chem, 2004. **279**(21): p. 22284-93.

14. Gutscher, M., et al., *Real-time imaging of the intracellular glutathione redox potential.* Nat Methods, 2008. **5**(6): p. 553-9.

15. Vogel, S.S., C. Thaler, and S.V. Koushik, *Fanciful FRET.* Sci STKE, 2006. **2006**(331): p. re2.

16. Selvin, P.R., *Fluorescence resonance energy transfer.* Methods Enzymol, 1995. **246**: p. 300-34.

17. Lakowicz, J.R., *Principles of fluorescence spectroscopy*. 3rd ed. 2006, New York: Springer. xxvi, 954 p.

18. Griesbeck, O., et al., *Reducing the environmental sensitivity of yellow fluorescent protein. Mechanism and applications.* J Biol Chem, 2001. **276**(31): p. 29188-94.

19. Chiu, J., et al., *Site-directed, Ligase-Independent Mutagenesis (SLIM): a single-tube methodology approaching 100% efficiency in 4 h.* Nucleic Acids Res, 2004. **32**(21): p. e174.

20. Chiu, J., et al., *Site-directed, Ligase-Independent Mutagenesis (SLIM) for highly efficient mutagenesis of plasmids greater than 8kb.* J Microbiol Methods, 2008. **73**(2): p. 195-8.

21. Zhang, B., *Design of FRET-based GFP probes for detection of protease inhibitors.* Biochem Biophys Res Commun, 2004. **323**(2): p. 674-8.

22. Mandal, M., et al., *Delivery of macromolecules into cytosol using liposomes containing hemolysin.* Methods Enzymol, 2003. **372**: p. 319-39.

23. Szajewski, R.P. and G.M. Whitesides, *Rate constants and equilibrium constants for thiol-disulfide interchange reactions involving oxidized glutathione.* J. Am. Chem. Soc., 1980. **102**: p. 2011-2026.

24. Shaner, N.C., P.A. Steinbach, and R.Y. Tsien, *A guide to choosing fluorescent proteins.* Nat Methods, 2005. **2**(12): p. 905-9.

25. Meyer, A.J. and T.P. Dick, *Fluorescent protein-based redox probes.* Antioxid Redox Signal. **13**(5): p. 621-50.

26. Meyer, A.J., *The integration of glutathione homeostasis and redox signaling.* J Plant Physiol, 2008. **165**(13): p. 1390-403.

27. Tait, A.R. and S.K. Straus, *Overexpression and purification of U24 from human herpesvirus type-6 in E. coli: unconventional use of oxidizing environments with a maltose binding protein-hexahistine dual tag to enhance membrane protein yield.* Microb Cell Fact. **10**: p. 51.

28. Yang, F., L.G. Moss, and G.N. Phillips, Jr., *The molecular structure of green fluorescent protein.* Nat Biotechnol, 1996. **14**(10): p. 1246-51.

29. Hermanson, G.T., *Bioconjugate techniques*. 1996, San Diego: Academic press.

CHAPTER III

LIVE-CELL FRET IMAGING TO MONITOR REDOX POTENTIALS AND CELLULAR REDOX FACTORS IN THE ENDOCYTIC PATHWAY IN MACROPHAGES

SUMMARY

Redox changes were successfully monitored by FRET microscopy of liposome-encapsulated probes in a cell-free system as well as in the endocytic pathway. Live-cell FRET microscopy revealed that disulfide bond reduction began in the early endosome and continued throughout endolysosomal maturation. Phagocyte oxidase activity slowed reduction in endocytic compartments. In contrast, expression of GILT accelerated reduction, indicating regulation of reduction in endocytic compartments and demonstrating the potential utility of this reporter for the design of targeted delivery systems.

INTRODUCTION

Live-cell imaging currently offers the best possible solution when redox measurements are required at the level of organelles [1, 2]. More recently, several studies have attempted to gather functional information from dynamic imaging of redox processes at sites of endocytosis [3, 4]. Even so, quantitative live-cell imaging in the endocytic pathway is technically challenging due to a lack of redox sensors in terms of not only pH-sensitivity but also dynamics. Endocytosis is an uptake mechanism of material into a cell by an invagination of the plasma membrane and its internalization in a membrane-bounded vesicle [5]. In the endocytic pathway molecules are ingested in vesicles derived from the plasma membrane and delivered to early endosomes and then via late endosomes to lysosomes. The dynamic network of routes that lead inward to lysosomes from the cell surface start with the process of endocytosis, which begin as early endosomes that are slightly acidic (pH 6.2-6.5) due to ATP-dependent proton pumps, then becomes more acidified and matures to a late endosome (pH 5-6), and finally merges into the lysosome, with an estimated pH in the range of 4-5 [6]. Two main types of endocytosis are distinguished on the basis of the size of the endocytic vesicles formed: pinocytosis (‘cellular drinking’), which involves the ingestion of fluid and solutes via small vesicles (≤150 nm in diameter), and phagocytosis (‘cellular eating’), which involves the ingestion of large particles, such as microorganisms or cell debris, via large vesicles called phagosomes (generally >250 nm in diameter) [5]. Specifically, endocytosis can be divided into more categories such as clathrin-mediated endocytosis, caveolar-mediated endocytosis, macropinocytosis, and phagocytosis. There are two theories regarding the development of the endolysosomal pathway: the ‘maturation model’

suggests that each organelle along the endocytic pathway is a transient, but distinct, compartment that matures into the next organelle along the pathway. In the 'pre-existing compartment model', the early and late endosomes are considered to be stable specialized compartments linked by vesicular traffic [7]. For the purpose of this study, we define endocytosis as the internalization of extracellular components resulting from invaginations along the plasma membrane in the maturation model [8].

The NADPH oxidase flavocytochrome b558, an integral membrane-bound heterodimer, is composed of a glycosylated 91-kDa glygoprotein, $gp91^{phox}$, and a nonglycosylated 22-kDa subunit ($p22^{phox}$). The NADPH oxidase components include flavocytochrome b558 and three cytosolic regulatory proteins ($p40^{phox}$, $p47^{phox}$, and $p67^{phox}$) and a small GTP-binding protein RAC, which are translocated to the plasma membrane during activation [9]. Cell activation by microorganisms or inflammatory mediators initiates at least three biochemical triggers (phosphorylation, lipid metabolism and guanine-nucleotide exchange on RAC) that together result in membrane translocation and assembly of active enzyme complexes, as summarized in Fig. 3.1. The enzyme activity of $gp91^{phox}$ is regulated by the assembly of these regulatory subunits with $gp91^{phox}$ to form an active complex, generating large quantities of superoxide ion (O_2^-), the precursor of hydrogen peroxide, by electron transfer from NADPH to molecular oxygen (O_2), with the secondary production of other ROS [10]. Using immunofluorescent staining of $gp91^{phox}$ and $p22^{phox}$, Casbon et al. demonstrated that flavocytochrome b was found in the Rab11-positive recycling endocytic compartment, as well as in Rab5-positive early endosomes and the plasma membrane [11]. Activation of macrophages generates ROS and RNS primarily mediated by IFN-γ but can be modulated by other

factors such as lipopolysaccharide (LPS) or cytokines, whereas IL-10 down-modulates activation [12]. The enhanced ability to kill microorganisms is largely a result of increased macrophage production of superoxide, nitric oxide, and their derivatives [13].

As discussed in Chapter I, GILT is the first identified and characterized redox enzyme in the endosomal compartments and plays a role in disulfide reduction, shown using a GILT "knock-out" mouse [14]. In this chapter, we address the possible GILT-dependent mechanisms involved in regulation of redox levels in the endocytic pathway using GILT-/- bone marrow-derived macrophages (BMMs). For an artificial redox environment, both genetic and chemical approaches were used to investigate several key cellular factors that would modulate redox potential in the endocytic pathway.

MATERIALS AND METHODS

Cell culture

All tissue culture media and reagents were purchased from Invitrogen (Carlsbad, CA), and all cells were maintained and experimental incubations were conducted in a humidified incubator at 37°C and 5% CO_2. BMMs were obtained from femurs and tibiae of female C57BL/6 mice (Jackson Laboratory, Bar Harbor, ME) in BMM media (DMEM supplemented with 20% HI-FBS, 30% L-cell conditioned media, 2 mM glutamine, 100 μg/mL streptomycin, 100 U/mL penicillin and 55 μM β-mercaptoethanol) as described previously by Swanson [15]. BMMs were harvested on day six of culture and frozen in liquid nitrogen until the experiment. For experiments, BMMs were plated onto 35 mm glass-bottomed dishes (MatTek, Ashland, MA) in complete DMEM (10% HI-FBS, 100 μg/mL streptomycin and 100 U/mL penicillin) one day prior to the experiment. All animal experiments were in accordance with and approved by the University of Michigan's Committee on the Use and Care of Animals (UCUCA).

FRET microscopy

The procedure using FRET microscopy imaging is illustrated in Fig. 3.5. Briefly, BMMs were plated at a concentration of 10^4 cells/mL onto 35 mm glass-bottomed dishes (MatTek, Ashland, MA) one day prior to incubation with liposomes for 30 min on ice. Cells were washed several times with cold Ringer's buffer (RB, 155 mM NaCl, 5 mM KCl, 2 mM $CaCl_2$, 1 mM $MgCl_2$, 2 mM NaH_2PO_4, 10 mM HEPES, and 10 mM glucose, pH 7.2), followed by addition of buffer warmed to 37 °C immediately before imaging.

Live-cell FRET imaging was performed using an Olympus IX70 inverted microscope with a 100× oil immersion objective, excitation and emission filters in filter wheels (Filter Set Chroma 86006-spr), a temperature-controlled stage, shutters for both phase-contrast and epifluorescence and a cooled digital charge-coupled camera (Cool Snap HQ2, Photometrics). The source of epifluorescent light was a mercury arc lamp (X-Cite series 120, Chroma). The component images consisted of epifluorescence filter combinations for CFP (I_D: excitation 435 nm; emmission 490 nm), Cit (I_A: excitation 505 nm; emission 540 nm), and FRET (I_F: excitation 435 nm; emission 540 nm), as well as phase-contrast images. Coefficients for image processing were determined from COS-7 cells expressing acceptor only (α), donor only (β), and a linked chimera (γ, ξ) after masking to remove some of the background by selecting only interested pixel intensities for analysis. FRET ratios (R_{FRET}) were calculated by dividing I_F (excitation 435 nm, emission 540 nm) by I_D (excitation 435 nm, emission 490 nm), both background-subtracted. The FRET microscope was calibrated using FRET parameters by correcting for shade and bias offset for control of variations in excitation intensity across the field of view that differ between illumination conditions and camera bias. Image acquisition and processing were performed using MetaMorph software version 7.7 (Molecular Devices, Sunnyvale, CA). A region of interest was traced as a circle large enough to include liposome-containing vesicles and transferred to the corresponding fluorescent images, and the average intensity from selected regions was measured with MetaMorph.

Redox kinetics under the microscope

Liposomes (0.3 μmole) were transferred onto a glass-bottomed dish on ice and washed with RB, followed by addition of redox buffers immediately before imaging. Images were collected at 1-min intervals for titration of FRET-reporters in redox buffers using FRET microscopy.

Liposome preparation

Texas Red-1,2-dihexadecanoyl-sn-glycero-3-phosphoethanolamine (TR-DHPE, Molecular Probes, Eugene, OR) was incorporated at 0.5 mol % to label the membranes of pH-sensitive liposomes composed of PE:CHEMS in a 2:1 molar ratio, made by a thin lipid film hydration and freeze/thaw method for uptake by BMMs [16]. Liposomes were extruded through 0.6 μm Whatman Nuclepore polycarbonate filters (GE Healthcare) for the preparation of a defined-size distribution and improved fluorescence signals.

Photobleaching study

Images were collected with liposomes in a cell-free system to test acceptor photobleaching; an exposure time of 200 ms and the use of a neutral density filter (ND-0.6, 25% transmission) were found to be optimal to minimize photobleaching. To correct for the acceptor photobleaching, we multiplied R_{FRET} by the correction factor I_A^0 / I_A^T, where I_A^0 = fluorescence of mCit at time zero and I_A^T = fluorescence of mCit at a given time point [17].

Endolysosomal markers

BMM were transfected using a mouse macrophage Nucleofector kit (Amaxa Biosystems) with 5 μg of plasmid encoding mCherry-Rab5a [18], a fluorescent protein marker of early endosomes. After transfection, cells were transferred to MatTek dishes and incubated in DMEM overnight. To label lysosomes, BMMs were incubated with Texas Red dextran (TRD), MW 10,000 (Molecular Probes) at 0.5 mg/ml in DMEM for 60 min at 37 °C, washed with RB, and incubated in RB for 60 min at 37 °C. For the overall analysis of fluorophore distributions, the average integrated intensities of the mCherry-Rab5a and TRD emission were divided by each of maximum fluorescence and plotted with the R_{FRET} from nicked probes against time.

Cellular redox factors

BMM activation was performed by incubation with growth factors and cytokines as previously described [19]. Briefly, media containing 100 U/mL IFN-γ (R&D Systems, Minneapolis, MN), 100 ng/mL LPS (List Biological, Campbell, CA) and 5 μg/mL anti-IL-10 (R&D Systems) was added to BMMs that had adhered to glass-bottom dishes. Cells were incubated for 16-24 hours and washed with RB and then replaced with activation media containing 5 μg/mL anti-IL-10 and 5 ng/ml IL-6 (Calbiochem, San Diego, CA) for the duration of the experiment. The $gp91^{phox}$-/- mice, which are unable to generate superoxide, were purchased from the Jackson Laboratory. GILT-/- BMMs were kindly provided by Dr. Peter Cresswell (Yale University, New Haven, CT). pH manipulation was performed by increasing endolysosomal pH with 0.5 μM bafilomycin

A1 (Sigma-Aldrich, St. Louis, MO) added to cells in RB 30 min prior to the incubation with liposomes and throughout the experiment. Fluorescent images of liposome-encapsulated HPTS (8-hydroxypyrene-1,3,6-trisulfonic acid trisodium salt, Invitrogen), a pH-sensitive, water-soluble fluorescent dye, were acquired using 405 nm and 440 nm excitation, and 535 nm emission filters.

RESULTS AND DISCUSSION

Image acquisition and processing

FRET parameters (α, β, γ, and ξ) were obtained to calibrate objective, excitation and emission filters, and camera since images contain contaminating signals from camera background noise and uneven illumination (Fig. 3.2). The level of background signal was determined by capturing images without a coverslip mounted on the stage and these values were subtracted from all experimental and calibration images. Shading correction was performed by collecting images of an even layer of fluorophore sandwiched between two coverslips and images were normalized for illumination levels. Experimental images were analyzed by Matlab-based FRET calculator (available from the Center for Live Cell Imaging at the University of Michigan) after shading correction and bias offset using calibration constants [20]. The R_{FRET} was determined by dividing I_F by I_D to obtain the average intensity from the region tool used to draw a circle and adjust it around the liposome.

Redox kinetics and titration with FRET microscopy

In order to examine redox kinetics and sensitivity of liposomes, fluorescence from unnicked vs nicked liposome-encapsulated probe particles were monitored by collecting images in various concentrations of DTT redox buffers via a cell-free system (Fig. 3.3). Pseudo-color ratiometric images of the liposomes at indicated time points and DTT redox concentrations (mM) showed the fully oxidized or fully reduced images based on the color bar in which the red range indicated a high R_{FRET} and the blue range indicated a low

R_{FRET} (Fig. 3.3a). The R_{FRET} from nicked probes started to decrease within 15 min as a result of reducing conditions, yet remained constant at the highest DTT_{ox} concentrations (Fig. 3.3b). The averages of all the data points that were taken at the plateau level from the kinetics (Fig. 3.3b) were plotted against DTT redox buffers (Fig. 3.3c); the R_{FRET} of unnicked probes remained constant regardless of the redox potential, while the R_{FRET} of nicked probes decreased with increasing reduction potential.

Photobleaching correction and image resolution

Photobleaching is the photochemical destruction of a fluorophore that leads to a steady decrease in fluorescence intensity over time [21]. Because mCit is less photostable than mECFP [22], a decrease in the R_{FRET} independent of disulfide reduction was observed (Fig. 3.4a, diamonds). To compensate for this effect, the FRET ratio was rectified by the correction factor I_A^0 / I_A^T [17]. After photobleaching correction during timelapse FRET imaging, the corrected data (squares) demonstrated improvement over the data before correction (diamonds). To optimize resolution, the mean liposome fluorescence intensities were compared after extruding liposomes through filter membranes having different pore sizes. The overall fluorescence signal increased by ~30% when the 0.6 μm extrusion filter membrane was used compared to 0.2 μm (Fig. 3.4b). To track the particle, liposomal membranes were labeled with TR-DHPE (illustrated in Fig. 3.5), which is bright enough to track the particle to ensure but has little-to-no spectral overlap with the probe (TRD_{ex} = 560, TRD_{em} = 645 nm) [23]. With the use of TR-DHPE, cellular uptake of liposomes can be efficiently demonstrated to efficiently identify phase-

contrast and TRD, thus allowing the probes to be easily monitored during morphological transitions such as membrane ruffling (Fig 3.6).

Time course of disulfide reduction in BMMs

Redox changes in the endocytic pathway were monitored by live-cell FRET microscopy of internalized liposome-encapsulated probes. Fig. 3.7a shows the average R_{FRET} of probes from 15 different cells, each normalized to the initial time point. Upon internalization of the control (unnicked) probe, R_{FRET} remained constant while the R_{FRET} from nicked probes decreased over time. The secondary axis shows the corresponding redox potential obtained from a standard titration curve in Fig. 2.9. This result suggested that the disulfide bond was cleaved within the endocytic pathway following internalization of the probes. Fig. 3.7f shows unnormalized values of R_{FRET}, and the number of cells (frequency) were plotted against R_{FRET} at time 0, $(R_{FRET})_0$, to illustrate the cell-to-cell variability of R_{FRET} at the initial time point (Fig. 3.7g).

Quantitative analysis of fluorophore distribution correlated with endolysosomal markers

To determine the time course and spatial localization of disulfide reduction during endolysosomal maturation, an early endosomal marker, mCherry-Rab5a, and an extracellularly applied lysosomal marker, TRD, were used (Figs. 3.7b, c). Rab5a is a small GTPase localized to early endosomes and endosomal membranes [18]. TRD is a fluid-phase endocytosis marker that accumulates within lysosomes [24]. Multispectral fluorescent images were obtained and overlaid onto corresponding phase-contrast images. Squares overlaid in the left panel indicate the co-localized area that is enlarged in the

right panel resulting line-scanned images through the center of the early endosome and corresponding quantitative analysis of fluorophore distribution along the line was plotted in the bottom (Fig. 3.7d). The highest mCit fluorescence value is between the two peaks of Rab5a-associated fluorescence, indicating that the liposome was located inside of the endosome. The internalized probe signal, which co-localized with Rab5a-associated fluorescence, increased rapidly and reached a maximum within 10 min after endocytosis (Fig. 3.7e). This was followed by an increase in its colocalization with TRD fluorescence, which reached its highest value after 20 min. This window serves as a visual guide, indicating that within the dynamic range of endolysosomal localization, the decrease in the R_{FRET} corresponded to the time between the appearance of mCherry-Rab5a and TRD, suggesting that disulfide reduction began in the early endosome and continued throughout endolysosomal maturation.

Cellular redox factors modulating the reduction processes in the endosomal pathway

We then investigated several key cellular factors that would modulate redox potential in the endocytic pathway, using both genetic and chemical approaches. First, ROS, generated via NADPH oxidase activity, would regulate the oxidative state of the endosomes in macrophages and thus regulate reduction dynamics [25]. To determine the effect of ROS, macrophages were activated with growth factors and cytokines overnight to produce more ROS with the assumption that this treatment would mimic conditions in which the redox potential of the endocytic pathway would be most heavily skewed

towards oxidation. Morphological changes accompanied macrophage activation, most of which were generally larger than nonactivated macrophages and had phase-dense spherical granules (Fig. 3.8). Time-lapse video revealed active ruffling and the occasional formation of macropinosomes. R_{FRET} in activated wild-type macrophages decreased following endocytosis, although not as rapidly as in non-activated wild-type macrophages, demonstrating that increased ROS conditions inhibited reduction (Fig. 3.9). The R_{FRET} from control (unnicked) probes remained constant regardless of the activation conditions. $gp91^{phox}$ is a 91 kDa heme-binding glycoprotein subunit of the NADPH oxidase complex, which is essential for the generation of ROS [26]. The physiological significance of phagosomal NADPH oxidase has been illustrated by the inability of $gp91^{phox}$-/- macrophages to generate superoxide [27], and by the enhanced LLO-dependent escape of *L. monocytogenes* in the $gp91^{phox}$-/- macrophages [28]. R_{FRET} from $gp91^{phox}$-/- macrophages decreased rapidly, with a significantly shorter half-time compared to that of wild-type macrophages (7.3 min vs. 9.0 min, $p<0.05$). The FRET signal decreased more slowly in activated $gp91^{phox}$-/- macrophages, although not as slowly as activated wild-type macrophages. These results demonstrate that the oxidation level in the endolysosomal pathway controls disulfide bond reduction dynamics, primarily by $gp91^{phox}$-dependent ROS production.

GILT catalyzes disulfide reduction, with maximal reductase activity at acidic pH [29]. R_{FRET} decreased in GILT-/- macrophages more slowly than in wild-type macrophages (Fig. 3.10), suggesting that the endolysosomal redox environment was less reducing due to the absence of GILT. R_{FRET} of the unnicked control probes remained constant regardless of the presence of GILT.

Lastly, when macrophages were treated with the proton ATPase inhibitor bafilomycin A1 a decrease in R_{FRET} was detected, but no significant difference was discerned between bafilomycin A1-treated and non-treated cells in terms of half-time of reduction. Overall, R_{FRET} decayed to a greater extent with a significantly lower R_{FRET} plateau value (Fig. 3.11a). We also observed a marked overall acceleration of reduction with ammonium chloride, with a corresponding elevation of vacuolar pH (inset), as determined by measuring the ratio of the pH-sensitive fluorescence dye HPTS emission at 535 nm produced at two excitation wavelengths, 440 nm and 405 nm ($HPTS_{440}$ / $HPTS_{405}$) [30]. The top row images with bright fluorescence at ex 405 nm and dim fluorescence at 440 nm indicated low pH, whereas the bottom row images with bright fluorescence at ex 440 nm and dim fluorescence at ex 405 nm indicated higher pH ($HPTS_{440}$ / $HPTS_{405}$ = 0.97 vs 1.62, Fig. 3.11b).

In this chapter, we have demonstrated that reduction of disulfide bonds begins in the early endosome and continues throughout endolysosomal maturation. Activation of macrophages typically leads to the generation of reactive nitrogen intermediates (RNI) such as nitric oxide and peroxynitrite, and ROI (H_2O_2, superoxide and hydroxyl free radicals) [31]. Macrophages stimulated by cytokines or growth factors have also been shown to inhibit endosomal escape of *L. monocytogenes* from phagosomes; this increase in their microbicidal activity is partially due to the generation of ROI by the NADPH oxidase complex [28]. Compared with non-activated wild-type macrophages, activated wild-type macrophages exhibited a slower reduction process along the endocytic pathway, while non-activated $gp91^{phox}$-/- macrophages exhibited faster reduction. Taken together, these observations indicate that decreased levels of oxidative enzymes promote faster

kinetics of disulfide reduction during endocytosis via attenuation of ROI production. It is plausible that activation of $gp91^{phox}$-/- macrophages could lead to compensation for the loss of $gp91^{phox}$-/- by, for example, up-regulating other oxidase components that contribute to the RNI-mediated oxidation, based on the observation that both ROI and RNI are involved in the listericidal capacity of activated macrophages [32]. In addition, coexpression of $gp91^{phox}$ and $p22^{phox}$ were required to support superoxide generation based on the cell-free NADPH oxidase assay, indicating that the functional assembly of the subunits is required for the active enzyme complex [26]. Consistent with this idea, another cellular factor investigated for its effects on redox dynamics in the endocytic compartment was GILT, which has been identified as a significant host component of infection by *L. monocytogenes* [33]. The N-terminal cysteine in the active-site motif of GILT has been proposed to initiate nucleophilic attack on disulfides, resulting in their reduction and thereby assisting in the unfolding of protein antigens for presentation in the context of MHC class II molecules [14, 34, 35]. Although reduction of disulfide bonds is chemically favored and the thiol reductase family is optimally efficient at neutral pH [36], key structural features of GILT provide it with both stability and activity under acidic conditions. Indeed, it was shown that macrophages lacking GILT were greatly hindered in their ability to reduce the probe (Fig. 3.10), confirming that GILT activity is a determinant of endocytic redox potential.

The pH-independence of the FRET probe enabled us to investigate the role of acidification in disulfide bond reduction dynamics in the endocytic compartments. Based on several lines of reasoning, including (i) the inhibition of *Listeria* phagosomal escape at basic pH [30], (ii) the low-pH maximal reductase activity of GILT [14], and (iii) the

increased susceptibility of disulfide bonds to enzymatic cleavage under acidic conditions during antigen unfolding in antigen-presenting cells [37], it was anticipated that increasing the endosomal pH would slow reduction dynamics in endocytic pathway even though Rybicka et al. found that NADPH oxidase activity controls the level of phagosomal proteolysis in macrophages in a manner that is independent of lumenal pH [25]. Our results with bafilomycin A1, however, showed a somewhat higher reduction rate and a slightly greater extent of reduction with inhibition of the acidification of endosomes. Similar trends were obtained in cells in which endosomal pH was elevated by ammonium chloride treatment. This apparent paradox is potentially due to the presence of cellular reducing factors that may still function in an unacidified endocytic compartment, or to the fact that disulfide reduction and exchange reactions are electrochemically favored at neutral pH. During this process, denaturation and unfolding of the antigens are facilitated by the acidic environment of endocytic compartments [37]. However, disulfide bonds are not susceptible to lysosomal proteolysis and remain chemically stable in the acidic environment; they must be cleaved instead by redox-involved processes [38].

Based on the findings presented in this chapter, it seems plausible that redox environments would be controlled by several cellular redox factors. Further investigation into redox modulation by inhibiting PDI, or by delivering ROS inhibitors such as superoxide dismutase, an antioxidant enzyme that catalyzes the reaction of the superoxide anion to hydrogen peroxide [39], or by delivering sulfhydryl-blocking agents (e.g., DTNB) that have been shown to prevent diphtheria toxin cytotoxicity [40], will provide useful information for elucidating key biochemical redox regulators.

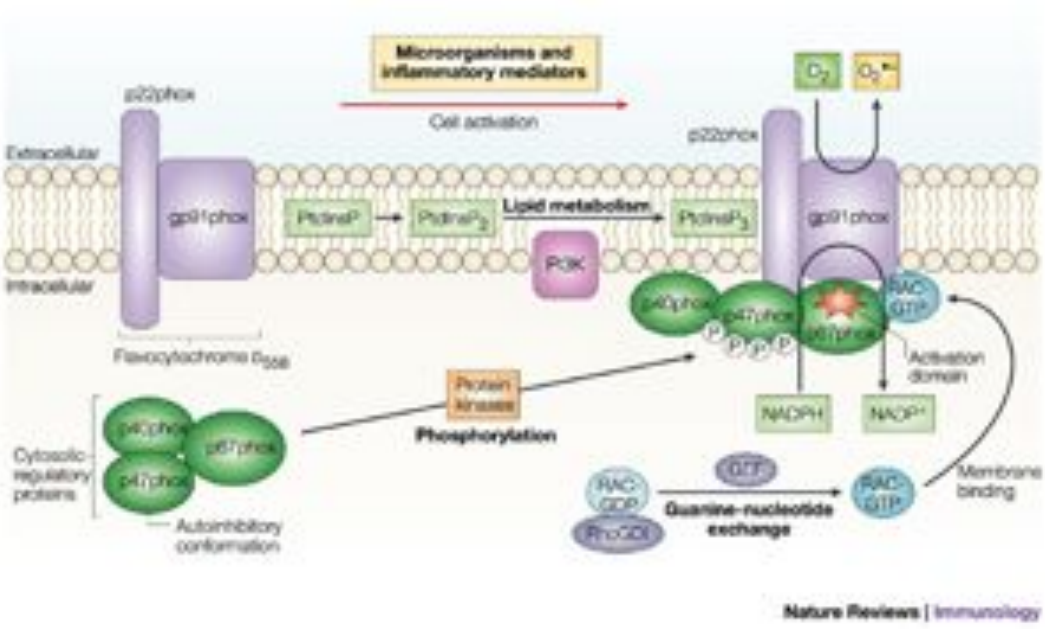

Figure 3.1 Activation of ROS generation by assembly of NADPH regulatory proteins

Figure adapted from Lambeth [9].

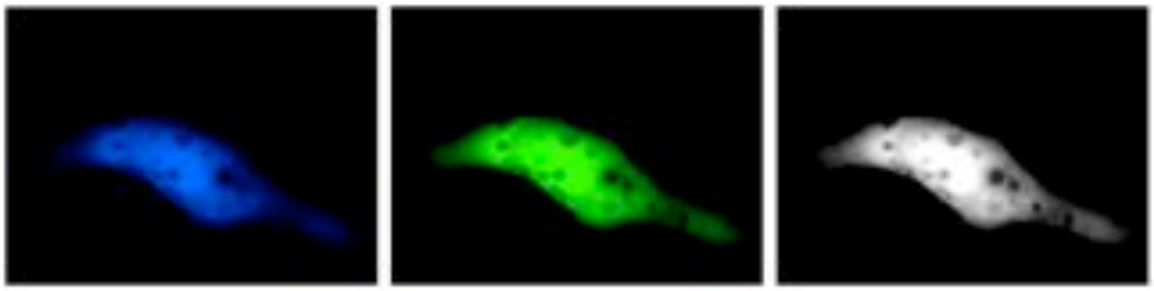

Alpha	0.150028	Acceptor only cell
Beta	0.917306	Donor only cell
Gamma	0.166539	Linked probe cell
Xi	0.333498	

Figure 3.2 Cos-7 cells transfection for calibration constants

Calibration constants were acquired from COS-7 cells transfected with CFP, Cit, and linked construct to calibrate FRET microscopy.

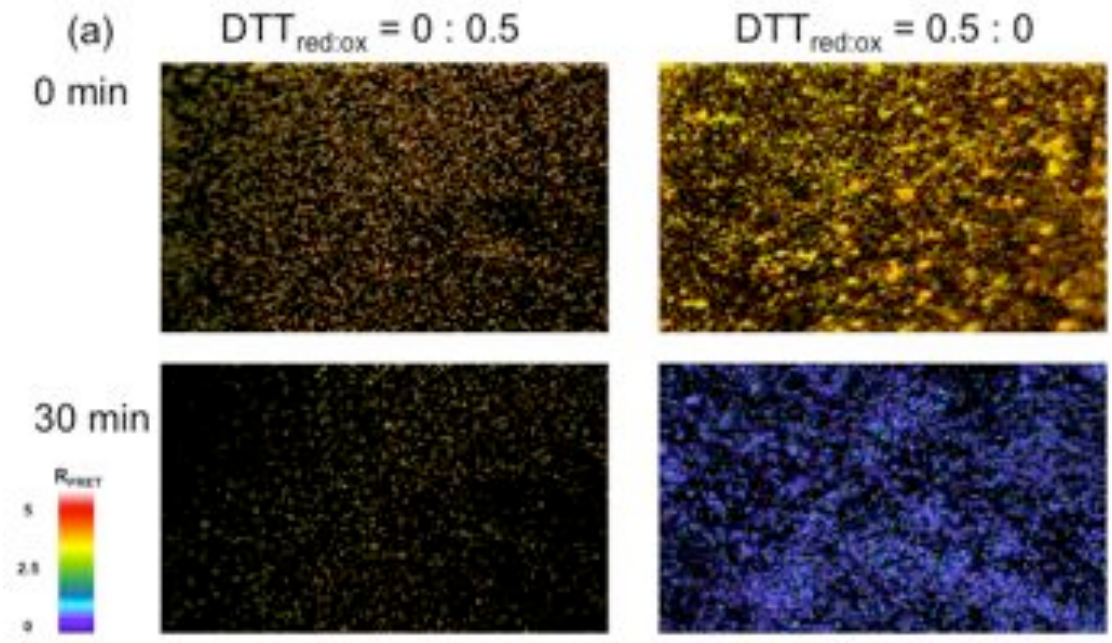

Figure 3.3 Redox titration from liposome-encapsulation probes using FRET microscopy in cell-free system

(a) Representative results of R_{FRET} image from liposome-encapsulation nicked probes. The top row images were taken at time 0 and the bottom row images after 30 min. Pseudo-color ratiometric images indicate different oxidized/reduced states. Color bar indicates the R_{FRET} in the ratio images. (b) Kinetics of redox titration from nicked probes using DTT redox buffers. All of the R_{FRET} values were normalized to that of the initial R_{FRET} measurement. (c) Redox equilibria of unnicked (diamond) and nicked (square) at pH 7.4 against the DTT_{red} : DTT_{ox} (mM) ratios indicated on the x-axis.

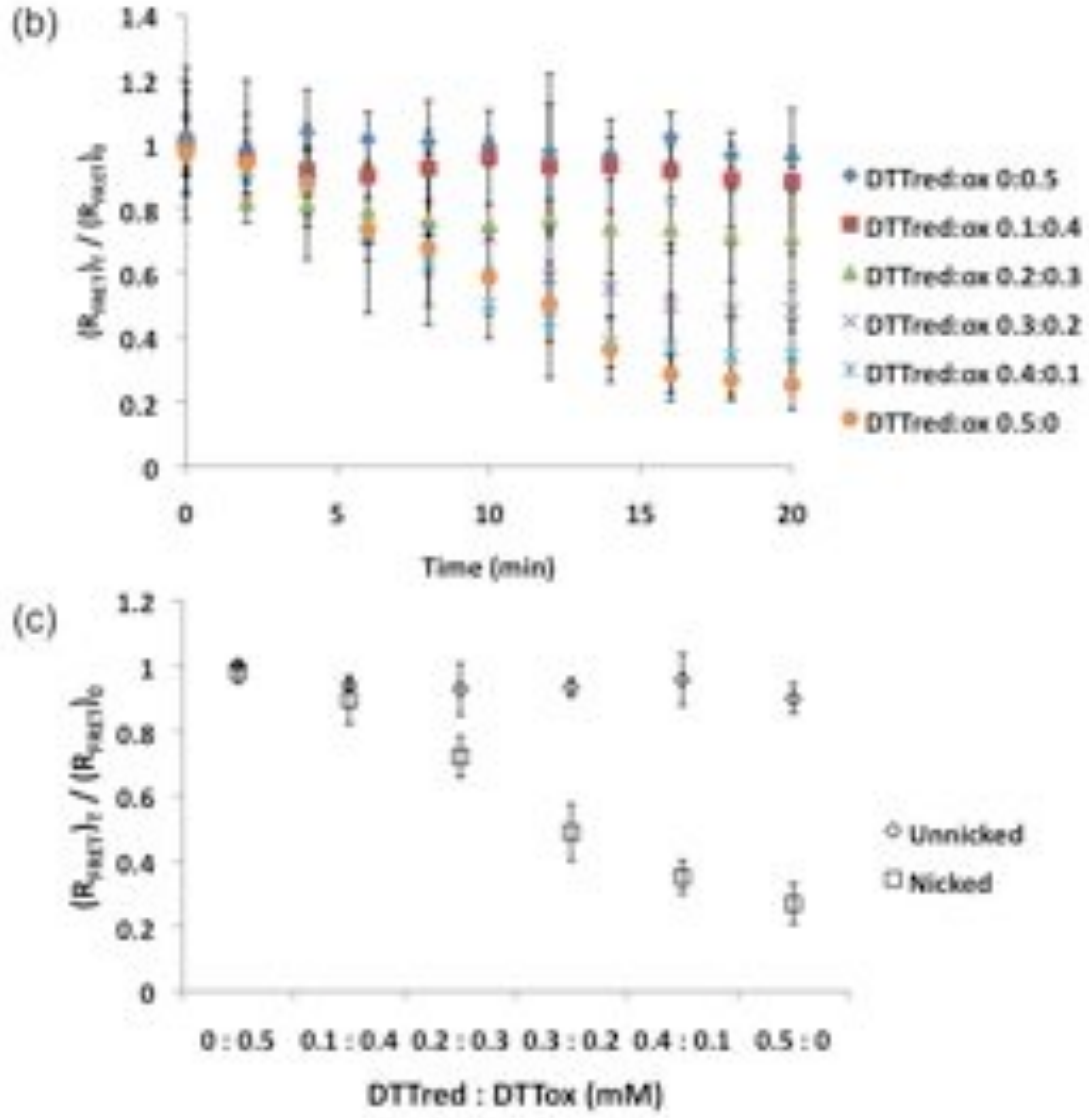
(b)
1.4
1.2
1
0.8
0.6
0.4
0.2
0
0
5
10
15
20
Time (min)
DTTred:ox 0:0.5
DTTred:ox 0.1:0.4
DTTred:ox 0.2:0.3
DTTred:ox 0.3:0.2
DTTred:ox 0.4:0.1
DTTred:ox 0.5:0
(c)
1.2
1
0.8
0.6
0.4
0.2
0
0 : 0.5
0.1 : 0.4
0.2 : 0.3
0.3 : 0.2
0.4 : 0.1
0.5 : 0
DTTred : DTTox (mM)
Unnicked
Nicked

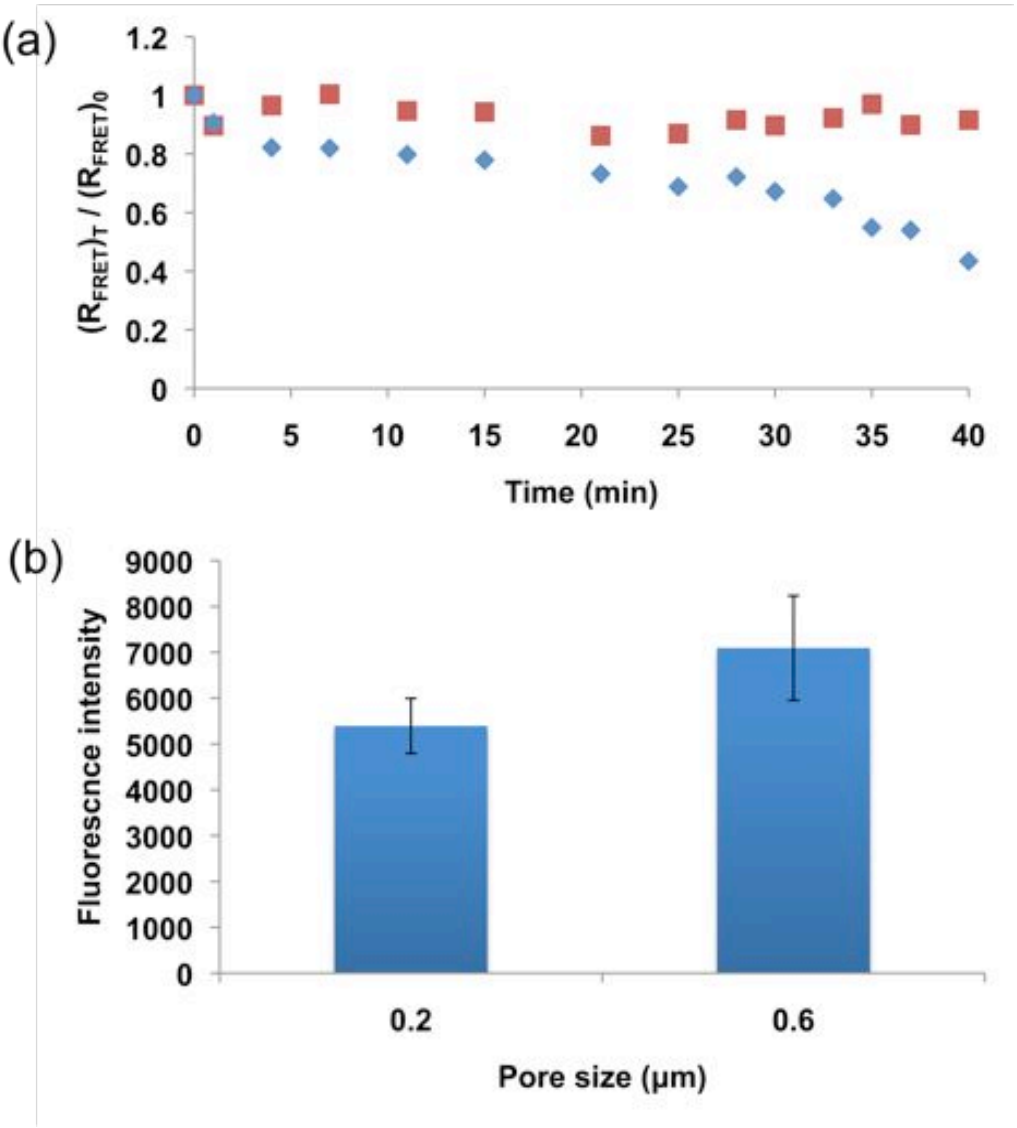

Figure 3.4 Photobleaching correction and improved fluorescence signal (cell-free system).

(a) R_{FRET} with unnicked probes after photobleaching correction. The diamonds represent the original data and the squares represent the corrected data after photobleaching correction. (b) Each assay contained 0.3 μmol of liposomes on glass-bottom dishes in Ringer's buffer. Extrusion of the liposomes through 0.6 μm filters resulted in a 30% increase in fluorescence signal compared with that after extrusion through 0.2 μm.

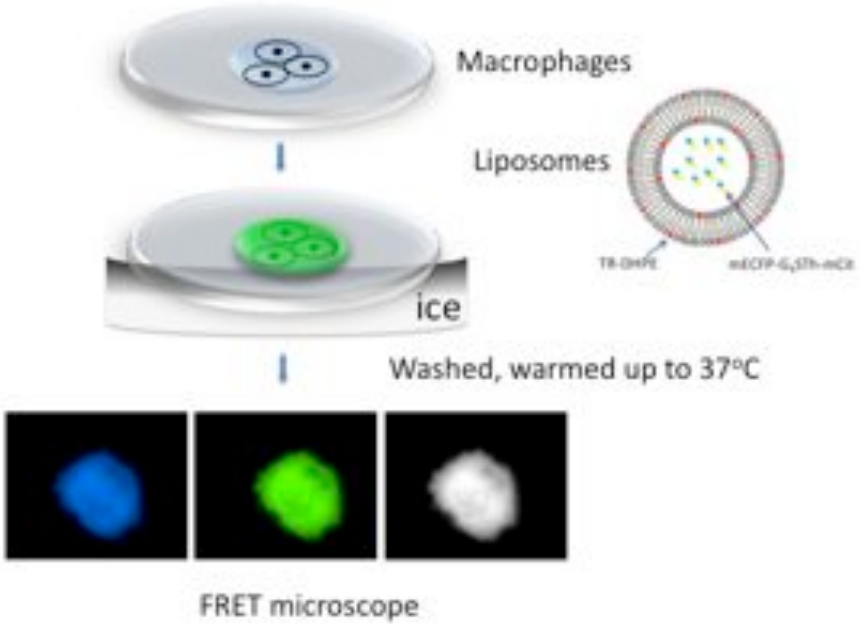

Figure 3.5 Summary of method used to perform FRET microscopy imaging.

BMMs were plated to 35 mm glass bottom dishes one day before the experiment, then incubated with liposomes for 30 min on ice. After that, cells were washed several times with a cold RB and a 37 °C warm RB was added immediately before starting the imaging. Images were collected using different filters for CFP, citrine, FRET (representative images on the bottom) and texas red channel for some cases.

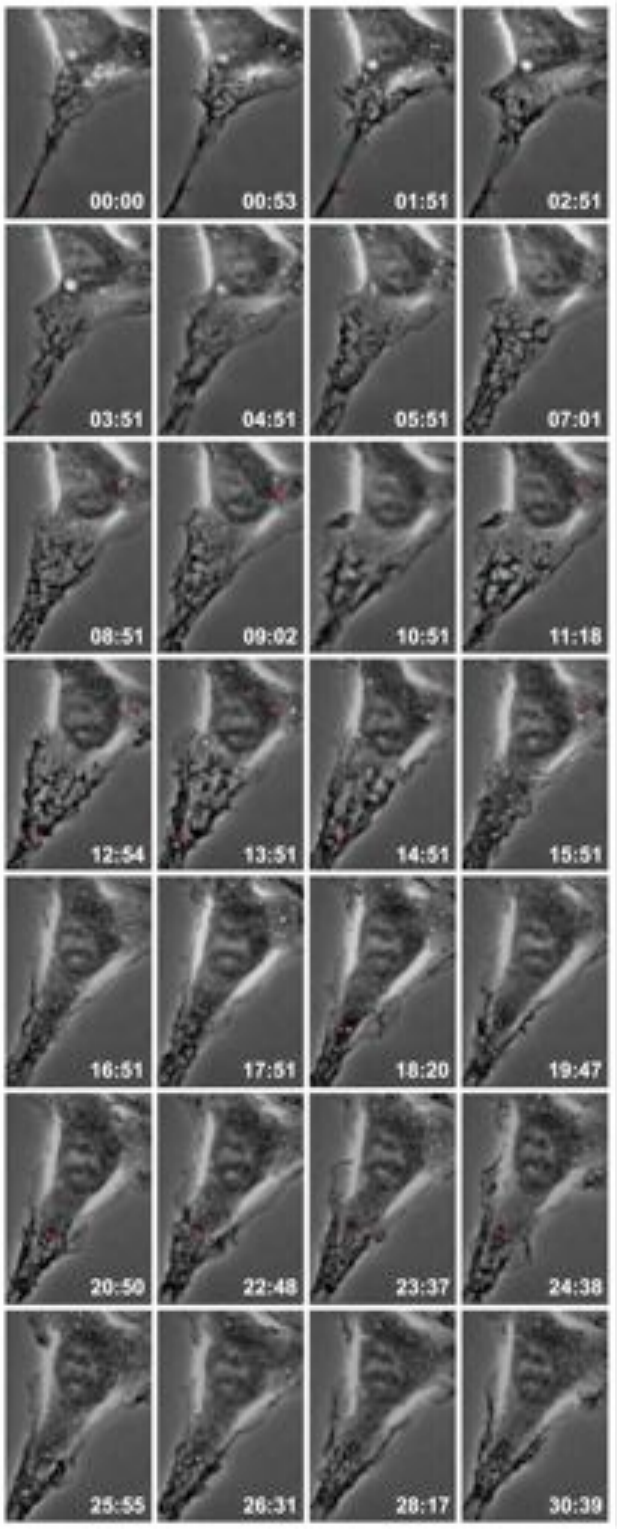

Figure 3.6 Time course images in BMM using TRD-labeled liposome.

Time series of overlaid images with TRD and phase-contrast channel after uptake of TRD-labeled liposome encapsulated probes (red dots). Each panel contains component overlaid images at indicated time point, separated from the adjacent images by time.

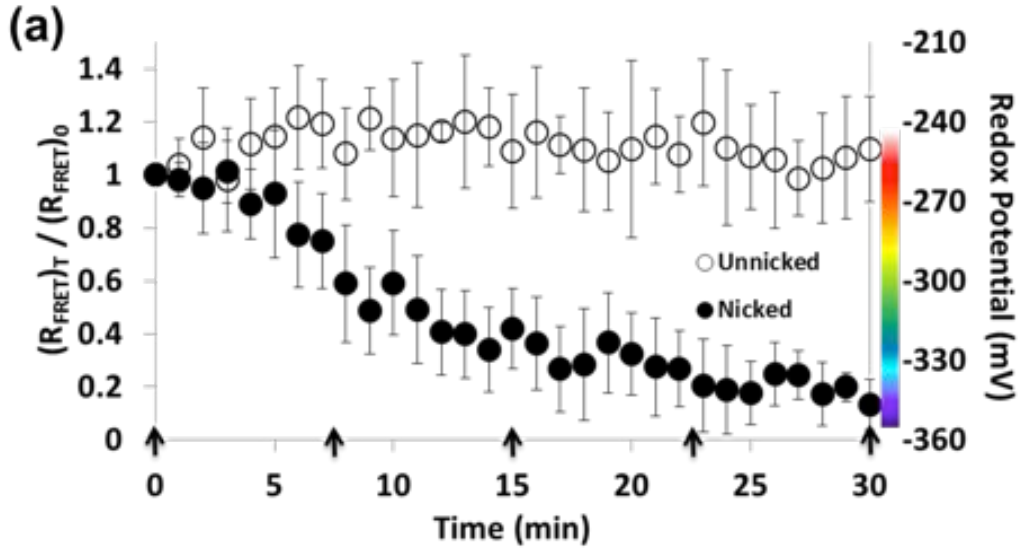

Figure 3.7 Time course of R_{FRET} and redox potentials and quantitative analysis of fluorophore distributions correlated with endolysosomal markers.

(a) Each data point represents the average of the FRET ratios ± SD from independent experiments using liposomes with unnicked (open circles) vs nicked (closed circles) probes in BMMs that were normalized to the initial time point and plotted versus time (n=15), and the secondary y-axis shows corresponding redox potentials obtained from a titration curve in Fig. 2.9. Times at which each image was taken are indicated by arrows in the x-axis. (b,c) Representative microscopy data using mCherry-Rab5a as an early endosomal marker and TRD to label lysosomes. Images of fluorescence from markers at marked time points (first row). Probes encapsulated in liposomes are shown as green dots in phase-mCit overlaid images (second row). The bottom row displays pseudocolor R_{FRET} in magnified areas indicated by squares above. Scale bar = 2 μm. (d) For direct colocalization of fluorophores, overlaid images of liposome- and Rab5a-positive endosomes were line-scanned along the x-axis through the center of the endosome. (e) Data points of relative fluorescence were obtained from manually selected portions of the regions of corresponding images from phase-mCit overlaid images (n≥3). (f) Replotted from Fig 3.7a with unnormalized values of R_{FRET}, and (g) the number of cells (frequency) were plotted against R_{FRET} at time 0, $(R_{FRET})_0$, to illustrate the cell-to-cell variability of R_{FRET} is displayed in the histogram for comparison to the data that were normalized to initial time point.

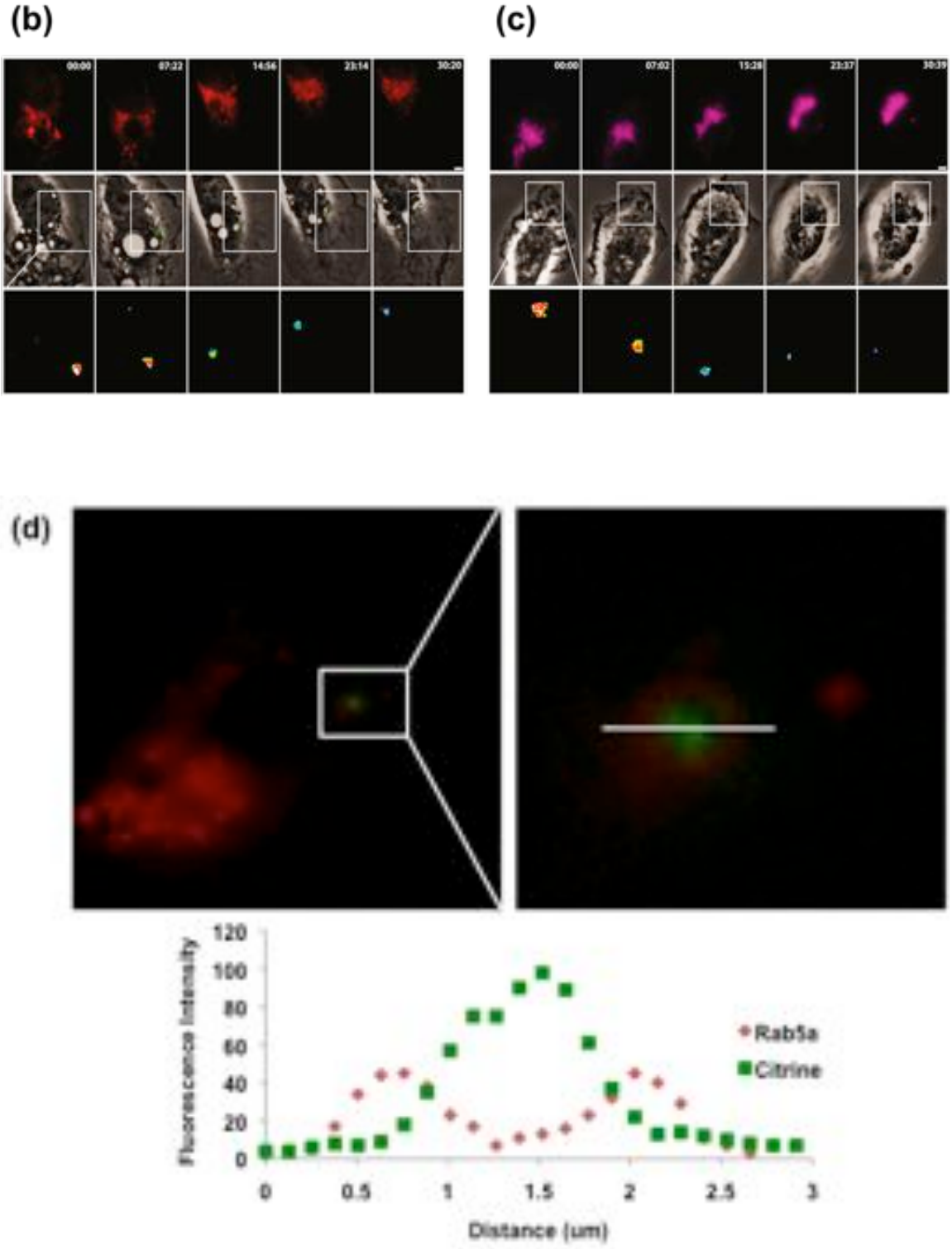
(b)
(c)
(d)
Fluorescence Intensity
120
100
80
60
40
20
0
0
0.5
1
1.5
2
2.5
3
Distance (um)
Rab5a
Citrine

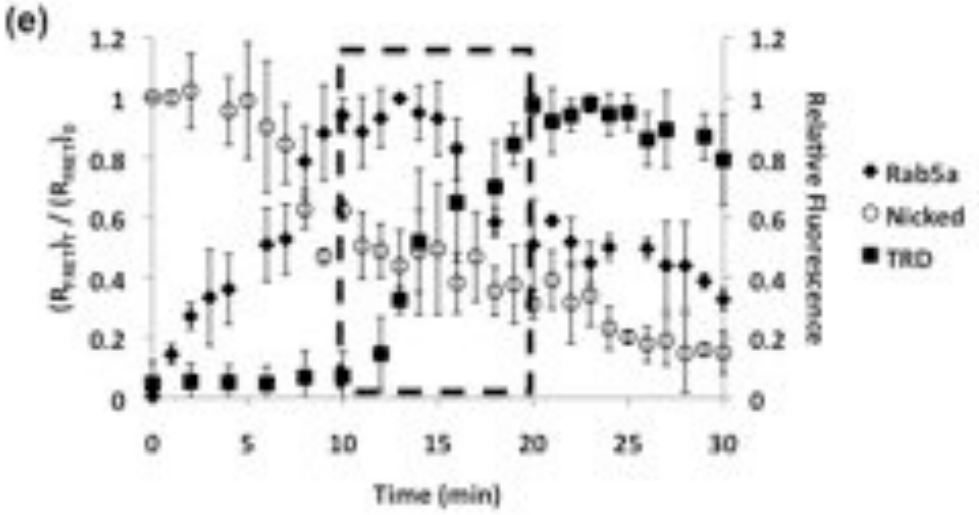
(e)
1.2
1
0.8
0.6
0.4
0.2
0
0
5
10
15
20
25
30
Time (min)
Relative Fluorescence
Rab5a
Nicked
TRD

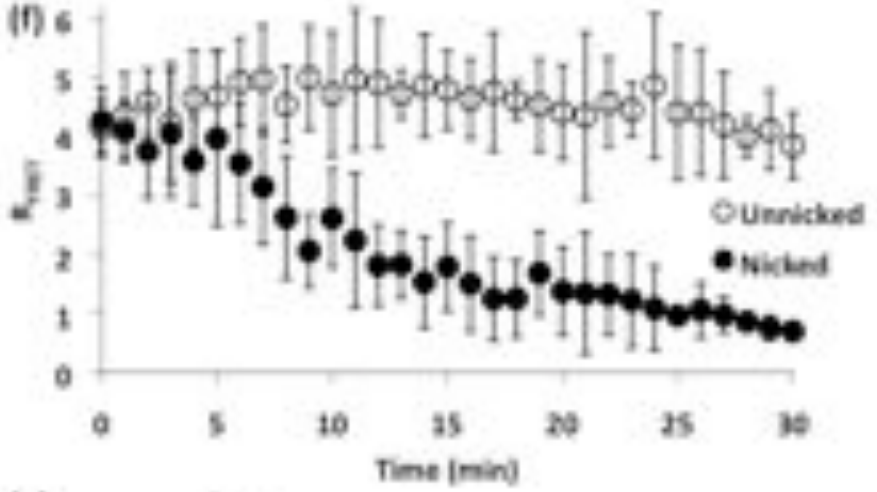
(f)
6
5
4
3
2
1
0
0
5
10
15
20
25
30
Time (min)
Unnicked
Nicked

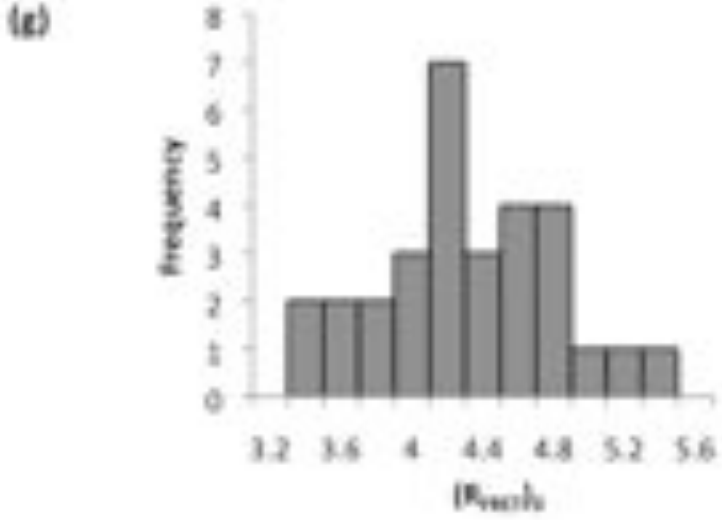
(g)
8
7
6
5
4
3
2
1
0
Frequency
3.2
3.6
4
4.4
4.8
5.2
5.6

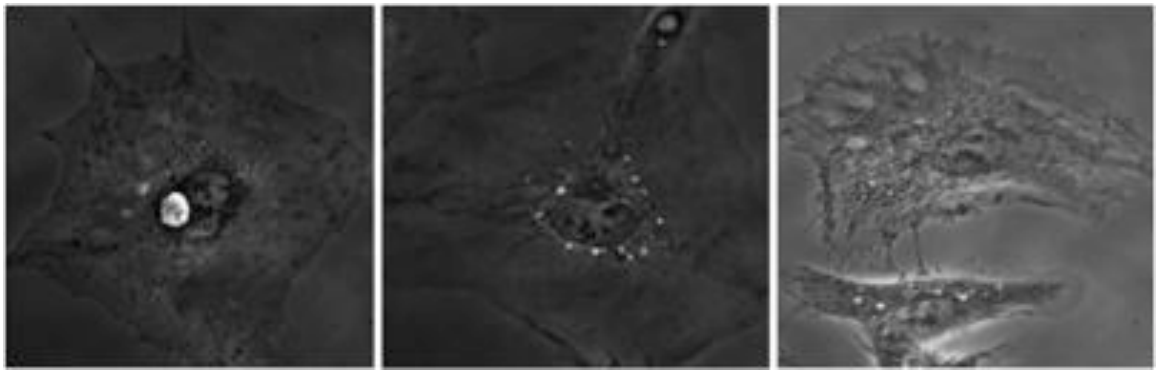

Figure 3.8 Morphological changes accompanying macrophage activation.

Representative phase-contrast images for BMM activated with growth factors and cytokines.

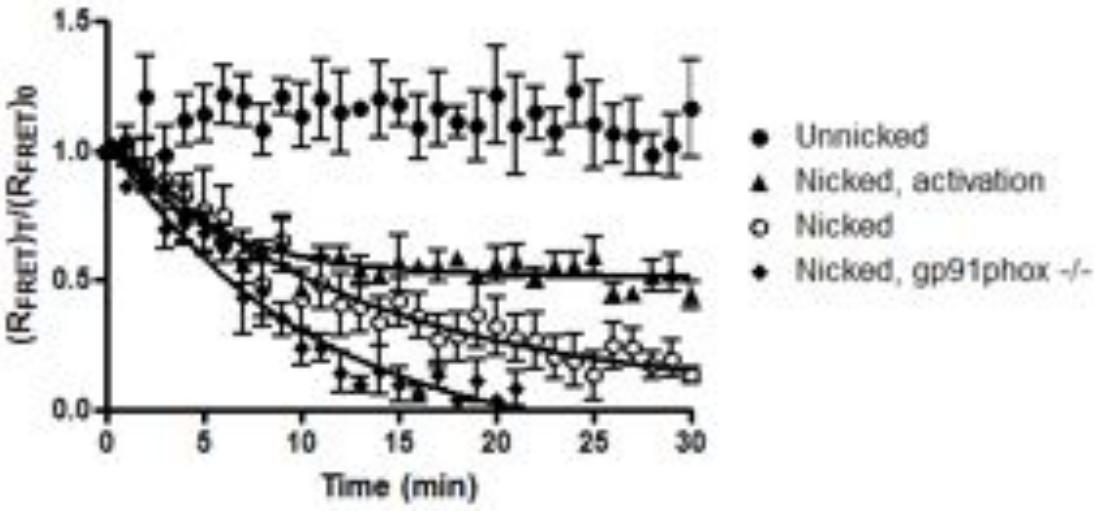

Figure 3.9 Effects of oxidation level on redox environment in the endocytic pathway.

The closed circles show the R_{FRET} from unnicked probes with activated wild-type macrophages and non-activated $gp91^{phox}$-/- macrophages, and the open circles show nicked probes with non-activated wild-type macrophages. The triangles and the diamonds represent the R_{FRET} from encapsulated nicked probes using activated wild-type macrophages and non-activated $gp91^{phox}$-/-, respectively ($n \geq 5$).

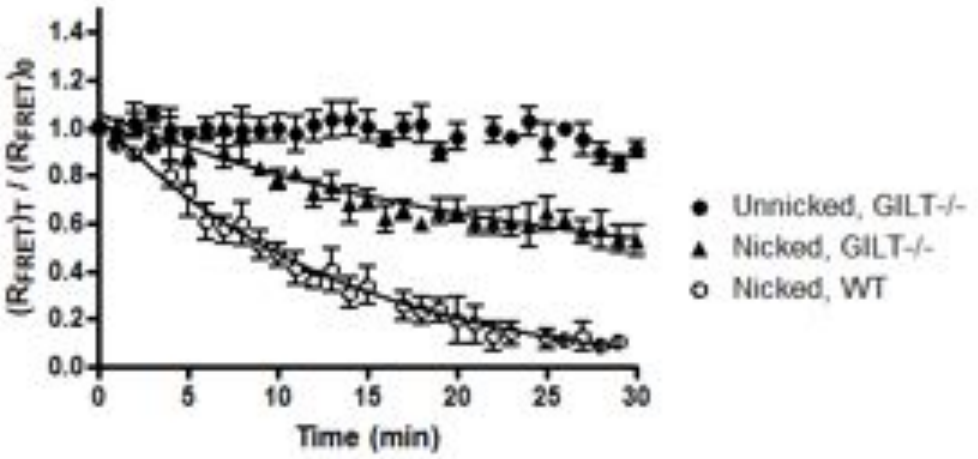

Figure 3.10 Reduction of FRET-based redox probe is attenuated in GILT-/- macrophages.

The closed circles show the R_{FRET} from unnicked probes with GILT-/- macrophages and the triangles and the open circles represent the R_{FRET} from encapsulated nicked probes using GILT-/- and wild-type macrophages, respectively (n≥5).

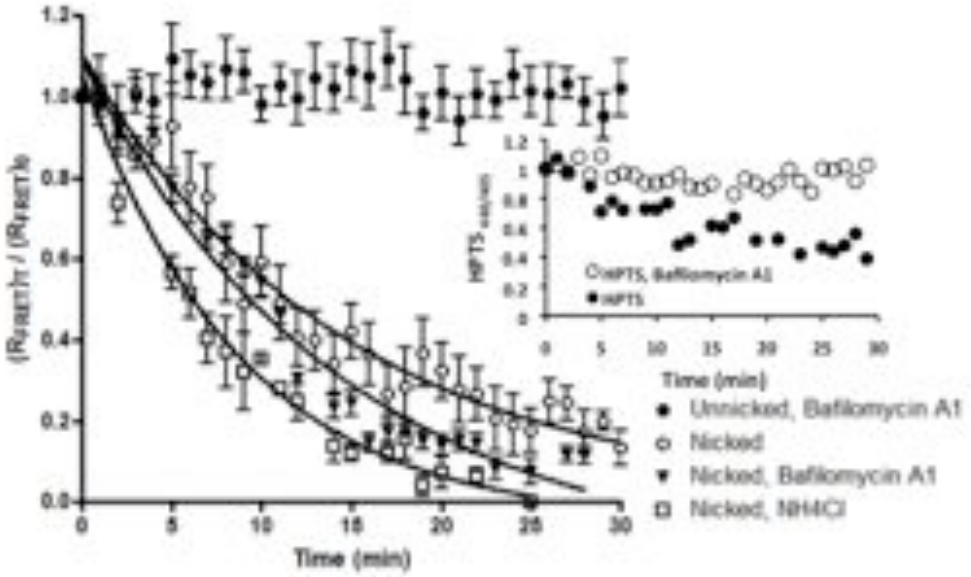

Figure 3.11 Effects of pH modulation on redox changes in BMMs.

(a) Fluorescent images of liposomes with encapsulated HPTS in vacuoles were taken at ex 405 nm and ex 440 nm, and em 535 nm. The ratio of fluorescence, $HPTS_{440}$ / $HPTS_{405}$, from these two images indicated the pH of the vacuolar environment (inset). The ratio of HPTS and the R_{FRET} from unnicked probes were plotted against time with and without bafilomycin A1 or ammonium chloride treatment. (b) BMM images after incubation with HPTS at indicated excitation wavelength in the presence and absence of bafilomycin A1. Scale bar = 10 μm.

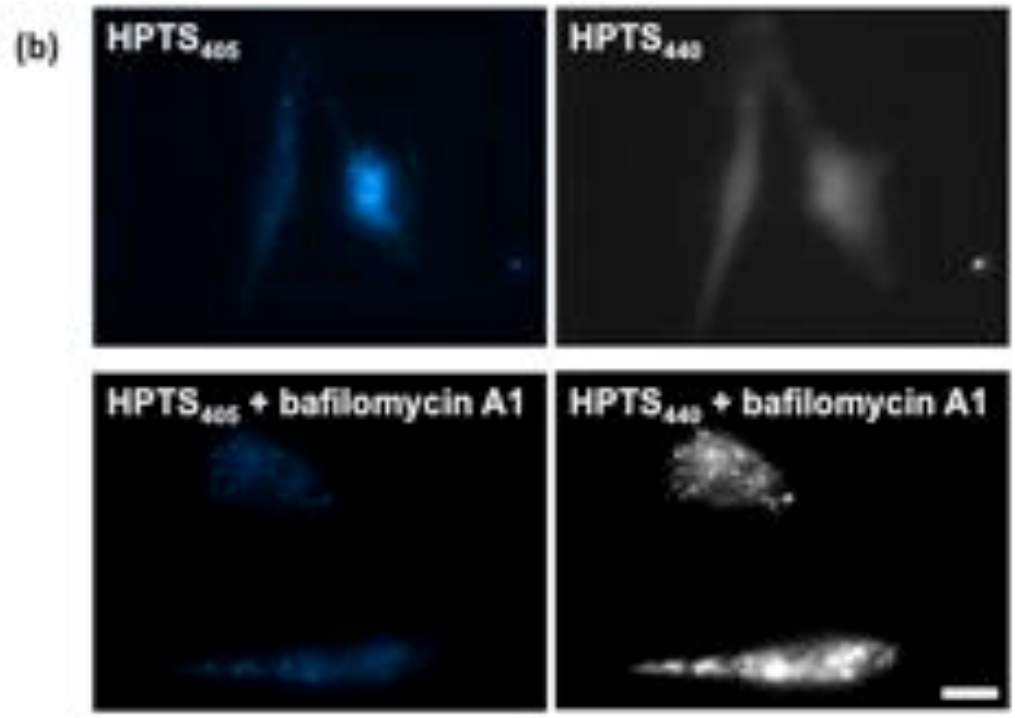
(b)
HPTS405
HPTS440
HPTS405 + bafilomycin A1
HPTS440 + bafilomycin A1

REFERENCES

1. Meyer, A.J. and T.P. Dick, *Fluorescent protein-based redox probes.* Antioxid Redox Signal. **13**(5): p. 621-50.

2. Gutscher, M., et al., *Real-time imaging of the intracellular glutathione redox potential.* Nat Methods, 2008. **5**(6): p. 553-9.

3. Yang, J., et al., *Evaluation of disulfide reduction during receptor-mediated endocytosis by using FRET imaging.* Proc Natl Acad Sci U S A, 2006. **103**(37): p. 13872-7.

4. Austin, C.D., et al., *Oxidizing potential of endosomes and lysosomes limits intracellular cleavage of disulfide-based antibody-drug conjugates.* Proc Natl Acad Sci U S A, 2005. **102**(50): p. 17987-92.

5. Bruce Alberts, D.B., Julian Lewis, Martin Raff, Keith Roberts, James Watson, *Molecular biology of the cell*. 3rd ed. 1994, New York: Garland Science.

6. Tjelle, T.E., et al., *Isolation and characterization of early endosomes, late endosomes and terminal lysosomes: their role in protein degradation.* J Cell Sci, 1996. **109 (Pt 12)**: p. 2905-14.

7. Pillay, C.S., E. Elliott, and C. Dennison, *Endolysosomal proteolysis and its regulation.* Biochem J, 2002. **363**(Pt 3): p. 417-29.

8. Provoda, C.J. and K.D. Lee, *Bacterial pore-forming hemolysins and their use in the cytosolic delivery of macromolecules.* Adv Drug Deliv Rev, 2000. **41**(2): p. 209-21.

9. Lambeth, J.D., *NOX enzymes and the biology of reactive oxygen.* Nat Rev Immunol, 2004. **4**(3): p. 181-9.

10. Nauseef, W.M., *Assembly of the phagocyte NADPH oxidase.* Histochem Cell Biol, 2004. **122**(4): p. 277-91.

11. Casbon, A.J., et al., *Macrophage NADPH oxidase flavocytochrome B localizes to the plasma membrane and Rab11-positive recycling endosomes.* J Immunol, 2009. **182**(4): p. 2325-39.

12. Racoosin, E.L. and J.A. Swanson, *Macrophage colony-stimulating factor (rM-CSF) stimulates pinocytosis in bone marrow-derived macrophages.* J Exp Med, 1989. **170**(5): p. 1635-48.

13. MacMicking, J., Q.W. Xie, and C. Nathan, *Nitric oxide and macrophage function.* Annu Rev Immunol, 1997. **15**: p. 323-50.

14. Phan, U.T., B. Arunachalam, and P. Cresswell, *Gamma-interferon-inducible lysosomal thiol reductase (GILT). Maturation, activity, and mechanism of action.* J Biol Chem, 2000. **275**(34): p. 25907-14.

15. Swanson, J.A., *Phorbol esters stimulate macropinocytosis and solute flow through macrophages.* J Cell Sci, 1989. **94 (Pt 1)**: p. 135-42.

16. Mandal, M., et al., *Delivery of macromolecules into cytosol using liposomes containing hemolysin.* Methods Enzymol, 2003. **372**: p. 319-39.

17. Palmer, A.E. and R.Y. Tsien, *Measuring calcium signaling using genetically targetable fluorescent indicators.* Nat Protoc, 2006. **1**(3): p. 1057-65.

18. Feliciano, W.D., et al., *Coordination of the Rab5 cycle on macropinosomes.* Traffic. **12**(12): p. 1911-22.

19. Myers, J.T. and J.A. Swanson, *Calcium spikes in activated macrophages during Fcgamma receptor-mediated phagocytosis.* J Leukoc Biol, 2002. **72**(4): p. 677-84.

20. Hoppe, A., K. Christensen, and J.A. Swanson, *Fluorescence resonance energy transfer-based stoichiometry in living cells.* Biophys J, 2002. **83**(6): p. 3652-64.

21. Seward, H.E. and C.R. Bagshaw, *The photochemistry of fluorescent proteins: implications for their biological applications.* Chem Soc Rev, 2009. **38**(10): p. 2842-51.

22. Shaner, N.C., P.A. Steinbach, and R.Y. Tsien, *A guide to choosing fluorescent proteins.* Nat Methods, 2005. **2**(12): p. 905-9.

23. Gao, X., et al., *In vivo molecular and cellular imaging with quantum dots.* Curr Opin Biotechnol, 2005. **16**(1): p. 63-72.

24. Ramoino, P., et al., *Fluid phase and receptor-mediated endocytosis in Paramecium primaurelia by fluorescence confocal laser scanning microscopy.* Eur Biophys J, 2001. **30**(5): p. 305-12.

25. Rybicka, J.M., et al., *NADPH oxidase activity controls phagosomal proteolysis in macrophages through modulation of the lumenal redox environment of phagosomes.* Proc Natl Acad Sci U S A. **107**(23): p. 10496-501.

26. Yu, L., et al., *Gp91(phox) is the heme binding subunit of the superoxide-generating NADPH oxidase.* Proc Natl Acad Sci U S A, 1998. **95**(14): p. 7993-8.

27. Gao, X.P., et al., *Role of NADPH oxidase in the mechanism of lung neutrophil sequestration and microvessel injury induced by Gram-negative sepsis: studies in p47phox-/- and gp91phox-/- mice.* J Immunol, 2002. **168**(8): p. 3974-82.

28. Myers, J.T., A.W. Tsang, and J.A. Swanson, *Localized reactive oxygen and nitrogen intermediates inhibit escape of Listeria monocytogenes from vacuoles in activated macrophages.* J Immunol, 2003. **171**(10): p. 5447-53.
29. Arunachalam, B., et al., *Enzymatic reduction of disulfide bonds in lysosomes: characterization of a gamma-interferon-inducible lysosomal thiol reductase (GILT).* Proc Natl Acad Sci U S A, 2000. **97**(2): p. 745-50.

30. Beauregard, K.E., et al., *pH-dependent perforation of macrophage phagosomes by listeriolysin O from Listeria monocytogenes.* J Exp Med, 1997. **186**(7): p. 1159-63.
31. Burke, B. and C.E. Lewis, *The macrophage*. 2nd ed. 2002, Oxford ; New York: Oxford University Press. xxvii, 647 p.325-6.

32. Ohya, S., et al., *The contributions of reactive oxygen intermediates and reactive nitrogen intermediates to listericidal mechanisms differ in macrophages activated pre- and postinfection.* Infect Immun, 1998. **66**(9): p. 4043-9.

33. Singh, R., A. Jamieson, and P. Cresswell, *GILT is a critical host factor for Listeria monocytogenes infection.* Nature, 2008. **455**(7217): p. 1244-7.

34. Singh, R. and P. Cresswell, *Defective cross-presentation of viral antigens in GILT-free mice.* Science. **328**(5984): p. 1394-8.

35. Phan, U.T., M. Maric, and P. Cresswell, *Disulfide reduction in major histocompatibility complex class II-restricted antigen processing by interferon-gamma-inducible lysosomal thiol reductase.* Methods Enzymol, 2002. **348**: p. 43-8.

36. Feener, E.P., W.C. Shen, and H.J. Ryser, *Cleavage of disulfide bonds in endocytosed macromolecules. A processing not associated with lysosomes or endosomes.* J Biol Chem, 1990. **265**(31): p. 18780-5.

37. Collins, D.S., E.R. Unanue, and C.V. Harding, *Reduction of disulfide bonds within lysosomes is a key step in antigen processing.* J Immunol, 1991. **147**(12): p. 4054-9.

38. Jensen, P.E., *Reduction of disulfide bonds during antigen processing: evidence from a thiol-dependent insulin determinant.* J Exp Med, 1991. **174**(5): p. 1121-30.

39. Lee, S. and N. Murthy, *Targeted delivery of catalase and superoxide dismutase to macrophages using folate*. Biochem Biophys Res Commun, 2007. 360(1): p. 275-9.

40. Ryser, H.J., R. Mandel, and F. Ghani, *Cell surface sulfhydryls are required for the cytotoxicity of diphtheria toxin but not of ricin in Chinese hamster ovary cells.* J Biol Chem, 1991. **266**(28): p. 18439-42.

CHAPTER IV

CELL TYPE-DEPENDENT REDUCTION PROCESSES IN THE ENDOSOMAL PATHWAY

SUMMARY

In Chapter III, the redox potential along the endocytic pathway was estimated to be considerably reducing, with a range between -300 and -340 mV, as revealed by FRET microscopy using liposome-encapsulated redox-sensitive fusion proteins in BMMs. We wanted to extend the range of cell types to compare FRET signals across PC-3, BT-549, fibroblast, and bone marrow dendritic cells (BMDCs) to draw conclusions about the redox potential in the endocytic pathways. We found that the redox-sensitive reporter used to monitor reducing environments in the endocytic pathway could be taken up by all cell types tested and live-tracked via FRET microscope. We also found that all of the endosomes have reducing potential; however, the kinetics of disulfide reduction varied depending on the cell types and macrophages had the most reducing environment of all the cells tested. Although the results are consistent with unnicked probes in that the rates and extents of disulfide reduction did not change much, their subsequent events of nicked probes differed depending on the cell types. Specifically, disulfide reduction in cancer cells showed a slower rate and extent, while that in fibroblasts was faster than cancer cells but not as fast as BMDCs. These findings may have useful implications for disulfide

conjugated macromolecular therapeutics across different types of cells. This study will provide information that can be used to investigate the impact of novel treatments as well as inform the design of targeted pharmaceutical agents that rely on disulfide bonds.

INTRODUCTION

Through the observation of the redox states in BMMs, endosomal compartments are likely to be reducing; however, it has not been well studied whether the relative contribution from different types of cells could be similar to or different from redox potentials in the endocytic pathway [1]. As previously explained in Chapter I, regulation of redox is critical to the maintenance and function of many cellular processes, varying with proliferation and differentiation and is also related to diversity of cell type specificity [2]. Thus, cellular redox biology is inseparable from variations of cell types.

Antigen Presenting Cells (APCs)

APCs can be divided into two groups: professional or non-professional. Professional APCs include macrophages, B cells, and dendritic cells, all of which are efficient at internalizing antigen, either by phagocytosis or by receptor-mediated endocytosis [3]. The T cell recognizes and interacts with peptides derived from degraded protein antigens and molecules of the major histocompatibility complex (MHC) on the plasma membrane of APCs. If endogenous antigens, they tend to be presented in the context of MHC class I molecules, which stimulate a subpopulation of T cells (CD8+ cells) that can become killer or cytotoxic T lymphocytes (CTL) [4]. Exogenous antigens can be presented in the context of MHC class II antigens, which stimulate T-helper cells (CD4+ cells), and those T cells are activated by an additional co-stimulatory signals [5]. Expression of co-stimulatory molecules distinguishes professional and non-professional APCs. A non-professional APC does not constitutively express the MHC class

molecules required for interaction with T cells; these are expressed only upon stimulation of the non-professional APC by certain cytokines, such as IFN-γ [6]. Non-professional APCs include fibroblasts (skin), thymic epithelial cells, thyroid epithelial cells, glial cells (brain), pancreatic beta cells and vascular endothelial cells [3]. Since B cells, each of which express and secrete a specific antibody, are the least efficient professional APCs for most other antigens [7], DCs were included and fibroblasts were chosen due to their interesting redox features for comparison of redox regulation in different cell types.

Dendritic Cells (DCs)

DCs, the most efficient and exhibiting the broadest range of antigen presentation, play a key role in the immune system as major professional APCs. It has been reported that DC redox equilibrium influences their ability to induce T cell activation and regulation that could affect the outcome of the immune response during systemic diseases and aging [8]. T lymphocyte proliferation and activation require a reducing microenvironment in the immune response that is provided by DCs. During T cell activation, secretion of glutathione and accumulation of cysteine by DCs result in a reducing extracellular environment that changes the redox-sensitive proteins, which might be critical for signaling in the immune synapse and DC-T cell interaction [9].

Fibroblasts

The variation in extracellular Cys/CySS redox state has been demonstrated to regulate the mechanisms and functional consequences of redox changes [10]. In human gut epithelial (Caco-2) cells and normal human retinal pigment epithelial (hRPE) cells, cell proliferation was greater at a more reduced redox state [11]. Furthermore, buthionine sulfoximine, an inhibitor of GSH synthesis, induced a less reducing redox state and decreased proliferation [12]. On the other hand, a lung fibroblast model showed that oxidized Cys/CySS redox potential values stimulate fibroblast proliferation and matrix expression [13]. These results suggest that extracellular Cys/CySS redox-dependent cell proliferation is cell type-specific and is mediated by intracellular kinase activation. The cell type specificity may reflect differences in cell responses to physiologic conditions, wherein fibroblasts respond to proliferate for tissue repair following immune cell-induced oxidative conditions, while reducing conditions are most stimulatory to other cells [12]. In fibroblasts, a lysosomal transport system is highly specific for the amino acid cysteine [14]. This cysteine-specific transport route may play an important role in supporting lysosomal proteolysis by providing thiols for the lysosomal thiol-dependent proteases and by reducing protein disulfide bridges, thereby allowing proteins to unfold, which can facilitate their degradation. In contrast to many of the previously characterized lysosomal transport systems, this system appears to function for net delivery of its substrate into the lysosomal compartment rather than to serve for exodus of the products of lysosomal hydrolysis [14]. Therefore, the intracellular location of cysteine transport activity highly correlates with cell type specificity. Furthermore, GILT, also referred to as IP-30, was found to be inducible by IFN-γ in human monocytes, fibroblasts, endothelial cells, and

keratinocytes [15]. GILT deficiency in fibroblasts leads to decreased levels of reduced glutathione and an increased GSSG/GSH ratio [16]. Hastings et al. showed how the induction level of GILT varied depending on the IFN-γ that enhances the resistance of cells such as macrophages, endothelial cells, and fibroblasts by inducing MHC class II antigens [17].

Cancer redox metabolism

Persistent oxidative stress, a main feature of cancer cells when compared to normal cells, results from high levels of reactive oxygen species (ROS), since cancer cells have an abnormal redox balance involving down-regulation of antioxidant enzymes and impaired mitochondrial function [18]. It is reported that ROS-mediated oxidative stress (either by environmental carginogenesis or by mitochondrial metabolism) and genomic instability compliant with cancer progression play a major role in the development of breast, prostate, pancreatic and colon cancer [19]. NADPH oxidase systems associated with ROS generation contribute to the causation and pathogenesis of prostate cancer [20, 21]. Carcinoma cell oxidative stress can be induced either by thymidine phosphorylase, an enzyme that is overexpressed in the majority of breast cancer cells, or lactoperoxidase, an enzyme that is involved breast-specific metabolism of oestrogenic hormones [22].

There have been many attempts to determine intracellular redox state depending on their differentiation and pathophysiology; however, knowledge concerning cell type variations in redox potentials along the endocytic pathway still remains elusive. Through

the observation of the redox states using redox-sensitive fusion proteins, endosomal compartments can be elucidated by different cell types. In this chapter, we sought to address this issue by first investigating APCs and cancer cell lines to compare FRET signals using a well-established live cell imaging.

MATERIALS AND METHODS

Cancer cell culture

Cancer cells were purchased from ATCC and cell culture media were purchased from GIBCO. All cells were maintained at 37^{o}C in 90% humidity with 5 % CO2. BT-549 cells were maintained in RPMI-1640 medium supplemented with 10 % HI-FBS. PC-3 cells were grown in DMEM medium with 10% FBS and BT-549 cells were grown in DMEM media with 10% FBS on T75cm^2 flasks (DB Falcon). BT-549 and PC-3 cells were plated in glass-bottomed dishes at a density in 25,000 cells/well. For imaging with BT-549 and PC-3 cells, media were replaced with RB immediately prior to adding liposomes.

Fibroblast Culture

Fibroblast cells were obtained from C57BL/6 mice by the procedure described by Seluanov et al. [23] using skin specimens from the underarm area. Using two scalpels, the tissue fragment was cut by pulling apart, not separated into pieces but stretched thinly. The tissue was transferred into a sterile beaker with a stirring bar and incubated in DMEM with 1 mg/ml collagenase IV (Invitrogen) at 37 °C for 60-90 min. After tissue fragments were centrifuged, the supernatant was carefully decanted and the pellet was vigorously resuspended with DMEM media to plate tissue culture-treated dish. On day 7, the tissue pieces were transferred to a new plate for an additional 7 days. By day 14 all viable fibroblasts had exited the tissue fragments and cells were harvested to plate them on a new plate in EMEM with 15% FBS, 100 units/mL penicillin, 1 mM sodium pyruvate,

1X non-essential amino acids, and sodium pyruvate for supporting growth of fibroblasts only.

Generation of Dendritic Cells from Bone Marrow of mouse

With minor modifications from previous method [24, 25], BMDCs were obtained from 7 week old female C57BL/6 mice. The femurs and tibias were removed and transferred into a dish of RPMI-1640 after cleaning off all tissues. Both epiphyses were cut with scissors and the bone marrow was washed out using RPMI-1640 with a sterile syringe, repeated until the bone was clean. The cells were centrifuged and the pellets were resuspended with ACK lysis buffer (Invitrogen) incubated 5 min at room temperature. Dendritic cell media was prepared with RPMI-1640 supplemented with 10% FBS, 100 μg/mL streptomycin, 100 units/mL penicillin, 1 mM sodium pyruvate, 2 mM glutamine, 50 μM β-mercaptoethanol, 10 ng/mL granulocyte-macrophage colony-stimulating factor (GM-CSF, Peprotech), and 10 ng/ml interleukin-4 (IL-4, Peprotech). After red blood cells were removed, cells were spun down, resuspended in dendritic cell media and plated $1x10^7$ cells per dish. The cultured cells were washed and replenished with fresh media every two days. On day 6, loosely adherent aggregates were removed by pipetting, centrifuged and plated in $1x10^7$ cells per dish. During 24-48 hrs following transfer, mature BMDCs were released then collected by gently swirling the dish.

Liposome preparation

For liposome preparation, probes were encapsulated inside pH-sensitive liposomes composed of PE:CHEMS in a 2:1 molar ratio, by a thin lipid film hydration and freeze/thaw method [26]. Liposomes were extruded through reduced pore size of membrane filters (0.2 μm) for efficient uptake [27] and unencapsulated probes were removed from liposomes by size-exclusion chromatography using a 1 x 25 cm Sepharose CL-4B column (GE Healthcare).

Quantitation of Lysosome markers

To label lysosomes, BT-549, PC-3, fibroblasts, BMDCs were incubated with TRD (5 mg/ml; Molecular Probes, Inc., Eugene, OR) in medium for 60 min at 37 ^{o}C. Cells were washed three times with RB and incubated in warm RB without TRD for another 60 min. Liposomes were then incubated with cells on ice for 30 min to bind cell membranes without endocytosis. Cells were washed three times with cold RB and warm RB was added immediately before imaging.

Statistical analysis

Data were compared by the Tukey honestly significant difference (HSD) test as Post-ANOVA Comparisons. A p-value less than 0.05 was considered statistically significant.

RESULTS

Morphology of cells

Harvested BMDCs and fibroblasts were plated onto glass-bottom dishes to confirm their morphology under microscope. In many BMDCs, branched dendrites and spikes in the dendritic tree were observed and all fibroblasts were highly branched and extended spread by connective tissue stretch (Fig. 4.1). BT-549 and PC-3 cells were maintained by spread shape as morphological features.

Comparison of disulfide reduction rate and extent

As previously described, cells were incubated with nicked or unnicked liposomes on ice for 30 min, then washed to remove unbound liposomes. Warm RB was added immediately before starting to collect images on a temperature-controlled stage. To determine whether the intracellular redox environment is varied, and if so, how the cell types affect the disulfide reduction rate, we collected images every 1 min for 50 min and measured the FRET ratio after liposome uptake. Upon internalization of the control unnicked probe, R_{FRET} remained constant regardless of cell type, while the R_{FRET} from nicked probes decreased over time with similar rate and extent both in BT-549 and PC-3 (Fig. 4.2). In fibroblasts, the R_{FRET} decreased slightly faster than in cancer cells, but not as rapidly as in BMDCs (Fig. 4.3). To directly compare the kinetics of disulfide bond reduction, curves were fitted to one-phase exponential decay; the FRET signal from BMMs decreased most rapidly with a significantly shorter half-time (8.96 min, $p<0.05$) and the lowest level of plateau (0.06). BMDCs showed less reducing than macrophages;

however, when compared with the other cell types, BMDCs decayed to a greater extent (0.25) and decreased faster (14.54 min). Both BT-549 and PC-3 had a similar half-life (26.87 and 25 min, respectively) and plateau (0.31 and 0.29, respectively). Fibroblast cells showed unique features of kinetics with relatively rapid decay (16.83 min), but the highest level of plateau (0.40).

Different rates of lysosomal maturation

We then investigated the kinetics of lysosomal maturation to determine whether the disulfide bond is reduced differently when probes are associated with differing degrees of continued interaction with the lysosomal compartment by different cellular processes. We used TRD as a lysosomal marker to determine rates of progression by measuring TRD-associated fluorescence signals that colocalized with liposomes at various time points. For the overall analysis of fluorophore distributions, the average integrated intensities of the TRD emission were normalized by the maximum fluorescence and plotted against time (Fig 4.5). Based on the analysis of fluorophore distribution from endocytic tracer TRD, the progression of lysosomal maturation of BMDCs, fibroblasts, and cancer cells was slower than BMMs. The time required to approach the highest value with TRD fluorescence was 40~45 min for cancer cells and BMDCs, and ~50 min for fibroblasts (Fig 4.6). All liposomes reached maximal TRD labeling for lysosomes later than did BMMs.

DISCUSSION

Although knowledge concerning cell type variations in redox state is currently lacking, one cell type in which redox metabolism has been studied is the fibroblast. For example, primary murine lung fibroblasts were stimulated to proliferate when exposed to oxidized conditions, while reducing conditions are most stimulatory to other cells [12]. More broadly, lysosomal transporters are highly specific for the amino acid cysteine, which may support lysosomal proteolysis by reducing disulfide bonds [14]; perhaps the induction level of GILT is cell lineage-dependent [28]. While these studies contribute to understanding the key elements of redox regulation, direct comparison of redox potential profiles in different cell types is still not well studied. Comparison of the intracellular reducing environment between B cell lymphoma and macrophage hybridoma cell lines was revealed to be similar based on the intracellular levels of cysteine and glutathione [29]; however, conventional methods that were employed might lead to loss of cell integrity during intracellular thiol assays. To overcome these limitations, we have established a non-disruptive real-time imaging to determine redox comparison after uptake of the liposome-encapsulated redox-sensitive probes in whole live cells. To investigate the feasibility of this approach, we monitored the reduction mechanism of probes by measuring FRET signals along the endocytic pathway. The rationale for this strategy was that if we could observe differential redox rates in these cell lines, then this approach could likely be extended to include a more complete library from different tissue sources.

Based on the redox standard curve in Fig. 2.9, BMMs have the most reducing potential with a midpoint potential of -323 mV, while cancer cells have the most

oxidizing potential of approximately -314 mV, and fibroblasts and BMDCs have a midpoint potential of -317 mV and -320mV, respectively. All cells appeared to have slower reduction rates than BMMs; only BMDCs decreased significantly faster in the endocytic pathway compared with fibroblasts and cancer cells. Previous studies showed that BMMs overall presented liposomal antigen more efficiently than BMDCs, suggesting that efficiency of LLO-mediated endosomal escape, which may relate to regulation of the unique Cys of LLO by redox potential, could vary in different cell types [24]. Similar reduction kinetics were observed for BT-549 and PC-3, which could be explained by high levels of ROS arising from redox metabolism of cancer cells. To verify whether this progress through endolysosomal pathway can be conferred to macrophages, we incubated TRD with other cell types and compared the lysosomal maturation rate by macrophages. There was a possibility that the differences in disulfide reduction could be due to different fates in the endocytic process or retention of liposome uptake, while the endocytic uptake of conventional liposomes by macrophages is very rapid [30, 31]. The timing of association and dissociation of phagosomes might be displayed differently, whereas macrophages have invariant feature of maturation [32]. The maturation pathway followed by fibroblast phagosomes showed distinct kinetics that are not defined as much as macrophages by the sequential appearance of TRD (Fig. 4.5). In contrast to TRD fluorescence accumulated in macrophages or in the perinuclear region of BMDCs, fibroblasts have TRD-positive lysosomes seen as discrete granules along the extensive cell spreading all around the periphery area (Fig 4.7). The reason for this discrepancy is that loading or chase time might not be long enough for internalized TRD to accumulate in fibroblast lysosomes. Each glass-bottomed dish containing different cell types was

incubated with TRD in DMEM for 1 h, and incubated in RB for another 1 h to redistribute TRD into lysosomes. However, Nazarian et al. reported that fibroblasts were incubated for 16 h at 37°C in medium containing 5 mg/ml TRD followed by 4 h chase period in medium [33], or cultured with TRD in DMEM with 1 mg/ml BSA for 4 h at 37°C and then incubated in normal medium for 20 h without TRD [34]. Alternatively, we could compare the rate of acidification using fluorescein isothiocyanate (FITC) dextran, a pH-sensitive dye, to obtain measurements of pH based on calibration of fluorescence ratio vs pH [35] since maturation of the phagosome was accompanied by luminal acidification [36]. Even though it is evident that the progression is slower, we speculate that the overall higher level of disulfide reduction by BMMs compared to other cell types is not simply due to a faster progression to lysosomes. Gursel et al. and Stier et al. similarly reported that BMMs had a greater uptake in liposomal antigen as well as efficiency of liposomal presentation than BMDCs [24, 37]. Although it is not well defined, the composition of cholesterol of the endolysosomal compartment could vary depending on cell type [38], which may affect redox potential [39] identified by NADPH oxidase redox signaling which is organized by cholesterol-enriched microdomains. Furthermore, the slowest disulfide to be reduced in PC-3 could be supported by data from higher degrees of ROS generation in the PC-3 cells than other cancer cell lines [20]. These observations imply that cell type-dependent variations in the disulfide reduction mechanism of endocytosed macromolecules could derive from a number of factors. Overall, BMMs reduced disulfide bonds faster than other cell types, and the trend was also observed by the lysosomal markers. These results combined together suggest that endosomal compartments may be more reduced in BMMs than in BMDCs, while cancer

cells exhibit somewhat oxidizing potential, and further implicated differential redox environmental activity and varying efficiency of redox enzymes in different cell types.

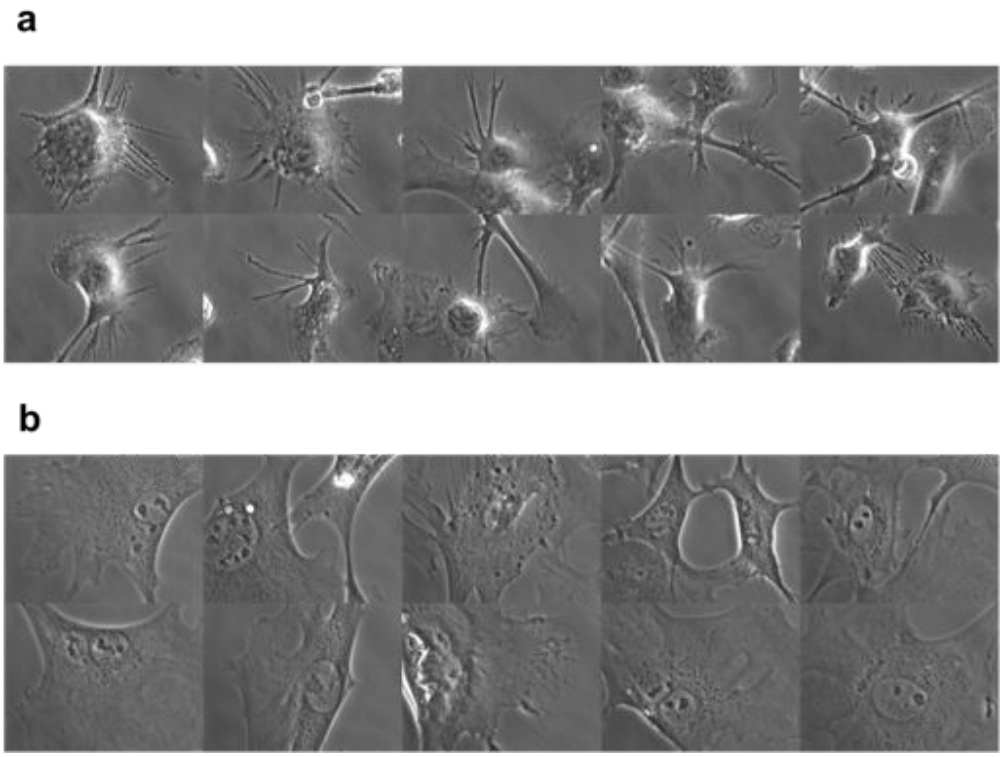

Figure 4.1 Representative morphology of BMDCs (a) and fibroblasts (b).

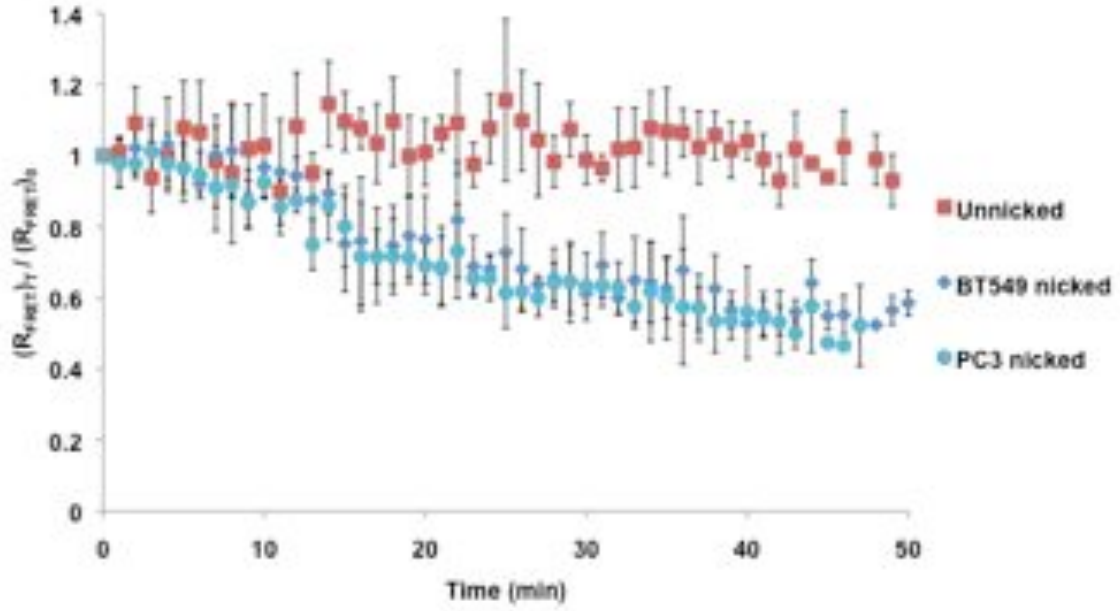

Figure 4.2 Time course of R_{FRET} in cancer cells

Liposome-encapsulated unnicked probes with average of BT-549 and PC-3 (squares) vs nicked probes in BT-549 (diamonds) and PC-3 (circles).

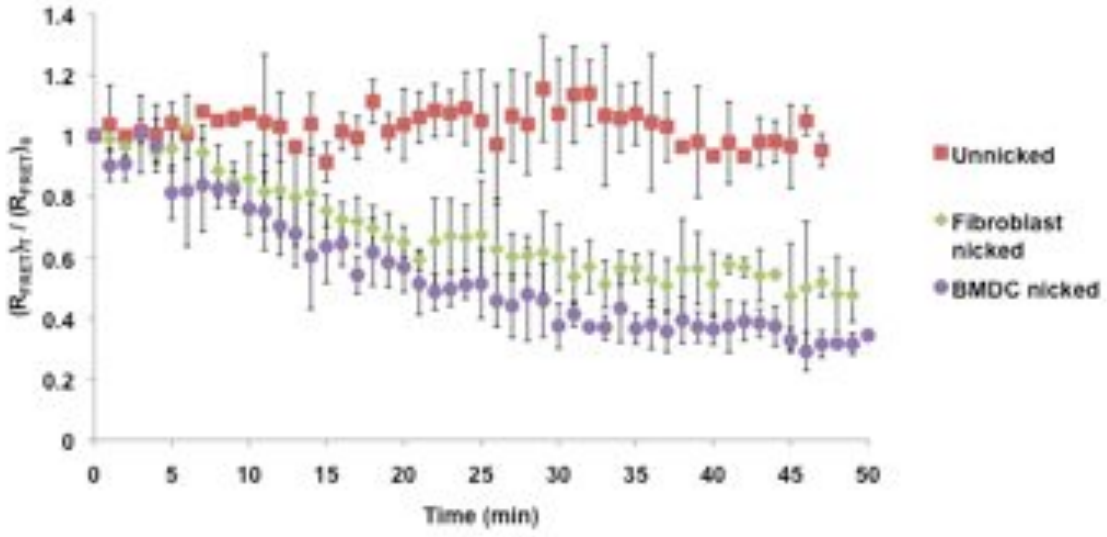

Figure 4.3 Time course of R_{FRET} in fibroblasts and BMDC

Liposome-encapsulated unnicked probes with average of fibroblasts and BMDCs (squares) vs nicked probes in fibroblasts (diamonds) and BMDCs (circles).

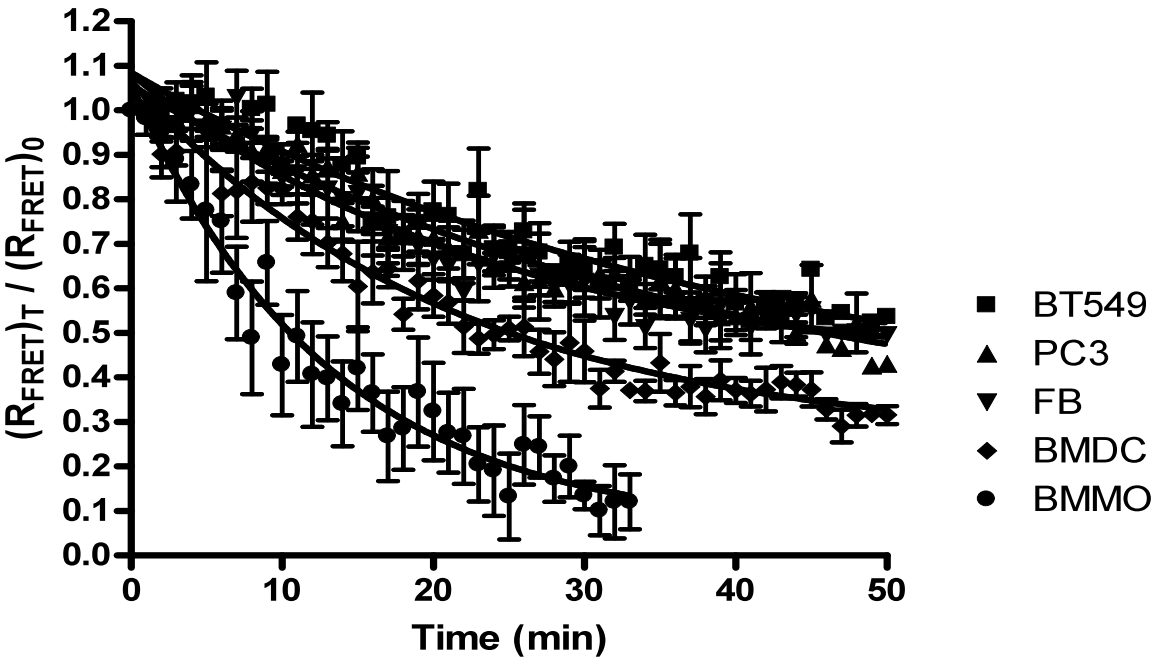

One phase exponential decay	BT549	PC3	FB	BMDC	BMMO
SPAN	0.776	0.7712	0.6783	0.8125	1.004
K	0.0258	0.02772	0.04118	0.04767	0.07736
PLATEAU (extent)	0.3089	0.2885	0.4045	0.2535	0.05607
Half-time (rate)	26.87	25	16.83	14.54	8.96

Figure 4.4 Comparison of disulfide reduction in different cell types.

From the top, the R_{FRET} curve is from BT-549, PC-3, fibroblast, BMDC, and BMM on the bottom. These values were obtained following the equation by Curve fitting in one-phase exponential decay: $Y = Span \times e^{-Kx} + Plateau$, Half-time = 0.69/K

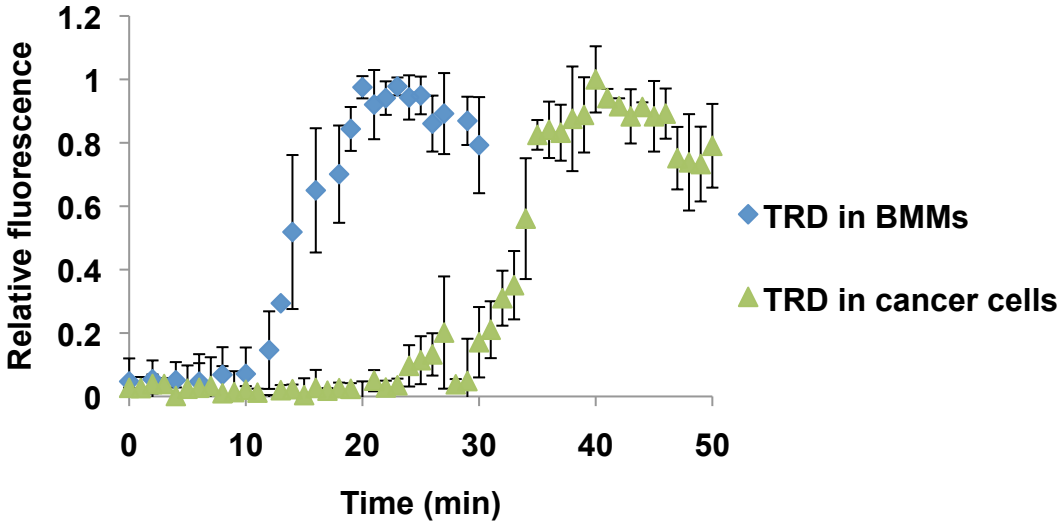

Figure 4.5 Kinetics of vesicular trafficking with TRD in cancer cells.

Data points of relative fluorescence were obtained from TRD-associated fluorescence in BMMs vs cancer cells from corresponding fluorescence images of liposome.

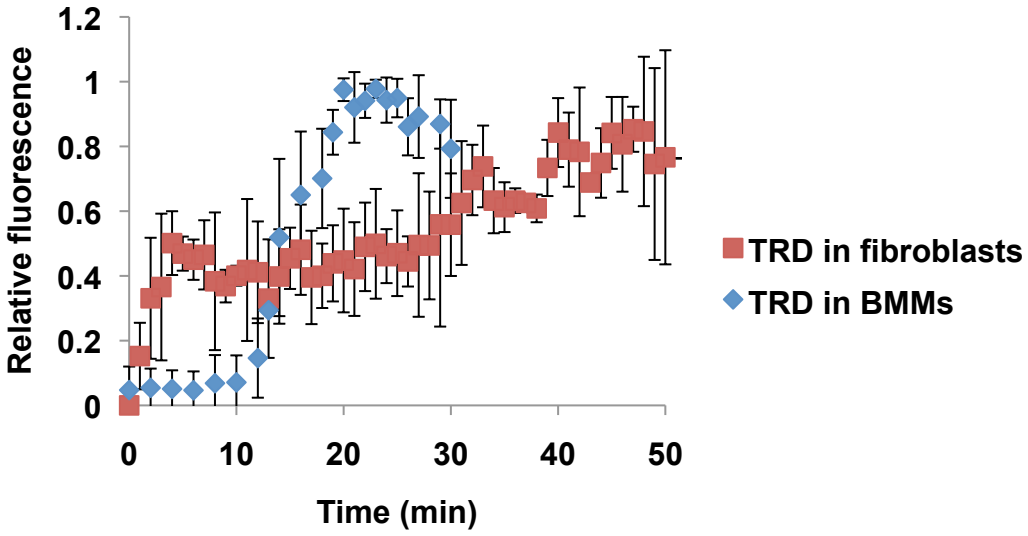

Figure 4.6 Kinetics of vesicular trafficking with TRD in fibroblasts.

Data points of relative fluorescence were obtained from TRD-associated fluorescence in BMMs vs fibroblasts from corresponding fluorescence images of liposome.

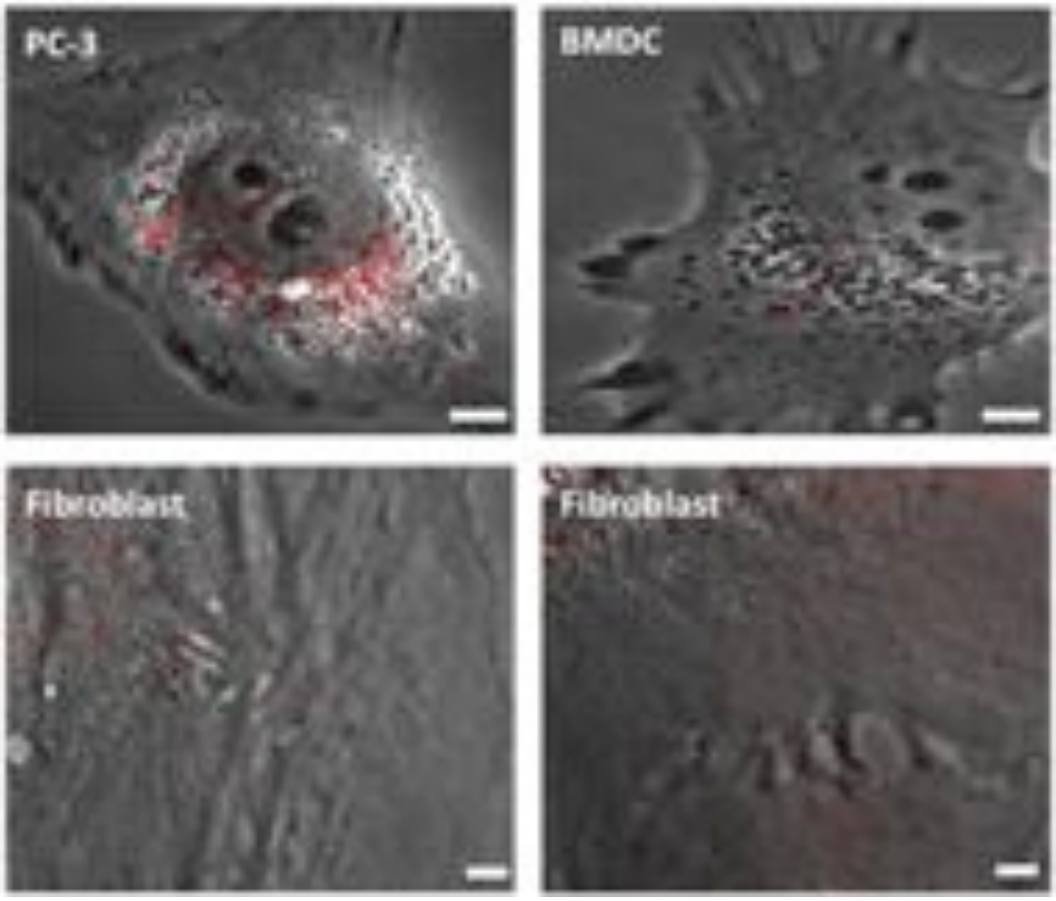

Figure 4.7 Representative microscopy images using TRD to label lysosomes.

Overlaid images of phase-contrast and TRD-associated fluorescence (red): in contrast to TRD fluorescence accumulated in the perinuclear region of PC3 or dendritic cell (top images), fibroblasts (bottom images) have TRD-positive lysosomes as discrete granules along the extensive cell spreading all around the periphery area. Scale bar = 5 μm.

REFERENCES

1. Go, Y.M. and D.P. Jones, *Redox clamp model for study of extracellular thiols and disulfides in redox signaling.* Methods Enzymol. **474**: p. 165-79.

2. Go, Y.M. and D.P. Jones, *Redox compartmentalization in eukaryotic cells.* Biochim Biophys Acta, 2008. **1780**(11): p. 1273-90.

3. Fry, M., *Essential biochemistry for medicine*, Chichester, Wiley-Blackwell.

4. Rock, K.L. and A.L. Goldberg, *Degradation of cell proteins and the generation of MHC class I-presented peptides.* Annu Rev Immunol, 1999. **17**: p. 739-79.

5. Germain, R.N., *MHC-dependent antigen processing and peptide presentation: providing ligands for T lymphocyte activation.* Cell, 1994. **76**(2): p. 287-99.

6. Nickoloff, B.J. and L.A. Turka, *Immunological functions of non-professional antigen-presenting cells: new insights from studies of T-cell interactions with keratinocytes.* Immunol Today, 1994. **15**(10): p. 464-9.

7. Kakiuchi, T., R.W. Chesnut, and H.M. Grey, *B cells as antigen-presenting cells: the requirement for B cell activation.* J Immunol, 1983. **131**(1): p. 109-14.

8. Angelini, G., et al., *Antigen-presenting dendritic cells provide the reducing extracellular microenvironment required for T lymphocyte activation.* Proc Natl Acad Sci U S A, 2002. **99**(3): p. 1491-6.

9. Yan, Z., et al., *Extracellular redox modulation by regulatory T cells.* Nat Chem Biol, 2009. **5**(10): p. 721-3.

10. Nkabyo, Y.S., et al., *Extracellular cysteine/cystine redox regulates the p44/p42 MAPK pathway by metalloproteinase-dependent epidermal growth factor receptor signaling.* Am J Physiol Gastrointest Liver Physiol, 2005. **289**(1): p. G70-8.

11. Jiang, S., et al., *Oxidant-induced apoptosis in human retinal pigment epithelial cells: dependence on extracellular redox state.* Invest Ophthalmol Vis Sci, 2005. **46**(3): p. 1054-61.

12. Hutter, D.E., B.G. Till, and J.J. Greene, *Redox state changes in density-dependent regulation of proliferation.* Exp Cell Res, 1997. **232**(2): p. 435-8.

13. Ramirez, A., et al., *Extracellular cysteine/cystine redox potential controls lung fibroblast proliferation and matrix expression through upregulation of transforming growth factor-beta.* Am J Physiol Lung Cell Mol Physiol, 2007. **293**(4): p. L972-81.

14. Pisoni, R.L., et al., *A cysteine-specific lysosomal transport system provides a major route for the delivery of thiol to human fibroblast lysosomes: possible role in supporting lysosomal proteolysis.* J Cell Biol, 1990. **110**(2): p. 327-35.

15. Luster, A.D., et al., *Molecular and biochemical characterization of a novel gamma-interferon-inducible protein.* J Biol Chem, 1988. **263**(24): p. 12036-43.

16. Chiang, H.S. and M. Maric, *Lysosomal thiol reductase negatively regulates autophagy by altering glutathione synthesis and oxidation.* Free Radic Biol Med. **51**(3): p. 688-99.

17. Hastings, K.T. and P. Cresswell, *Disulfide reduction in the endocytic pathway: immunological functions of gamma-interferon-inducible lysosomal thiol reductase.* Antioxid Redox Signal. **15**(3): p. 657-68.

18. Warburg, O., *On respiratory impairment in cancer cells.* Science, 1956. **124**(3215): p. 269-70.

19. Acharya, A., et al., *Redox regulation in cancer: a double-edged sword with therapeutic potential.* Oxid Med Cell Longev. **3**(1): p. 23-34.

20. Kumar, B., et al., *Oxidative stress is inherent in prostate cancer cells and is required for aggressive phenotype.* Cancer Res, 2008. **68**(6): p. 1777-85.

21. Nyska, A., A. Dayan, and R.R. Maronpot, *New tools in therapeutic research--prostatic cancer and models.* Toxicol Pathol, 2002. **30**(2): p. 283-7.

22. Brown, N.S. and R. Bicknell, *Hypoxia and oxidative stress in breast cancer. Oxidative stress: its effects on the growth, metastatic potential and response to therapy of breast cancer.* Breast Cancer Res, 2001. **3**(5): p. 323-7.

23. Seluanov, A., A. Vaidya, and V. Gorbunova, *Establishing primary adult fibroblast cultures from rodents.* J Vis Exp, (44).

24. Stier, E.M., M. Mandal, and K.D. Lee, *Differential cytosolic delivery and presentation of antigen by listeriolysin O-liposomes to macrophages and dendritic cells.* Mol Pharm, 2005. **2**(1): p. 74-82.

25. Inaba, K., et al., *Generation of large numbers of dendritic cells from mouse bone marrow cultures supplemented with granulocyte/macrophage colony-stimulating factor.* J Exp Med, 1992. **176**(6): p. 1693-702.

26. Mandal, M., et al., *Delivery of macromolecules into cytosol using liposomes containing hemolysin.* Methods Enzymol, 2003. **372**: p. 319-39.

27. He, C., et al., *Effects of particle size and surface charge on cellular uptake and biodistribution of polymeric nanoparticles.* Biomaterials. **31**(13): p. 3657-66.

28. Luster, A.D. and J.V. Ravetch, *Biochemical characterization of a gamma interferon-inducible cytokine (IP-10).* J Exp Med, 1987. **166**(4): p. 1084-97.

29. Gainey, D., S. Short, and K.L. McCoy, *Intracellular location of cysteine transport activity correlates with productive processing of antigen disulfide.* J Cell Physiol, 1996. **168**(2): p. 248-54.

30. Oh, Y.K. and J.A. Swanson, *Different fates of phagocytosed particles after delivery into macrophage lysosomes.* J Cell Biol, 1996. **132**(4): p. 585-93.

31. Miller, C.R., et al., *Liposome-cell interactions in vitro: effect of liposome surface charge on the binding and endocytosis of conventional and sterically stabilized liposomes.* Biochemistry, 1998. **37**(37): p. 12875-83.

32. Henry, R.M., et al., *The uniformity of phagosome maturation in macrophages.* J Cell Biol, 2004. **164**(2): p. 185-94.

33. Nazarian, R., J.M. Falcon-Perez, and E.C. Dell'Angelica, *Biogenesis of lysosome-related organelles complex 3 (BLOC-3): a complex containing the Hermansky-Pudlak syndrome (HPS) proteins HPS1 and HPS4.* Proc Natl Acad Sci U S A, 2003. **100**(15): p. 8770-5.

34. Kuronita, T., et al., *A role for the lysosomal membrane protein LGP85 in the biogenesis and maintenance of endosomal and lysosomal morphology.* J Cell Sci, 2002. **115**(Pt 21): p. 4117-31.

35. Rivero, F. and M. Maniak, *Quantitative and microscopic methods for studying the endocytic pathway.* Methods Mol Biol, 2006. **346**: p. 423-38.

36. Downey, G.P., et al., *Phagosomal maturation, acidification, and inhibition of bacterial growth in nonphagocytic cells transfected with FcgammaRIIA receptors.* J Biol Chem, 1999. **274**(40): p. 28436-44.

37. Gursel, I., et al., *Sterically stabilized cationic liposomes improve the uptake and immunostimulatory activity of CpG oligonucleotides.* J Immunol, 2001. **167**(6): p. 3324-8.

38. Sobo, K., et al., *Late endosomal cholesterol accumulation leads to impaired intra-endosomal trafficking.* PLoS One, 2007. **2**(9): p. e851.

39. Vilhardt, F. and B. van Deurs, *The phagocyte NADPH oxidase depends on cholesterol-enriched membrane microdomains for assembly.* EMBO J, 2004. **23**(4): p. 739-48.

CHAPTER V

CONCLUSIONS AND FUTURE DIRECTIONS

A number of biosensors have recently emerged that have contributed to the understanding of cellular redox dynamics [1-5]. Despite the gains made in imaging probe design, however, particular aspects of the redox network remain elusive. We designed a genetically encoded redox-sensitive fusion protein, consisting of mECFP and mCit joined by an intervening disulfide-bonded and protease-sensitive linker, to monitor disulfide reduction and measure redox potentials in the endosomal compartments. To our knowledge, we report the first real-time imaging of redox biosensor within the endosome and lysosome in live whole cells using FRET microscopy. There have been some attempts to determine endosomal redox activity, and FRET-based folate-conjugate compounds have been used to monitor receptor-mediated endocytosis [6]. However, synthetically conjugated molecules have often been used in redox measurements unsuccessfully due to their heterogeneous nature, and furthermore, there are only limited numbers of receptor-ligand complexes in receptor-mediated endocytosis compared to non-specific macropinocytosis, which will be encountered general endocytic pathway. Therefore, a homogeneous application of genetically encoded endogenous probes to monitor the cellular thiol-disulfide redox state is important to address this issue. Methods

for in vivo monitoring of redox changes in different cellular compartments have been developed in recent years; however, these sensors are limited to reducing compartments, and are not suited for acidic environments due to pH sensitivity [5, 7]. Currently available redox biosensors mostly employ single GFP variants such as roGFPs [3]. In a FRET-based biosensor, a redox event induces a conformational change in the linker, altering the distance between the FRET donor-acceptor pair, which in turn results in a change in FRET efficiency as measured by changes in the emission spectra profiles. This specific and discriminatory feature of FRET is one of the driving motives behind our development, rather than relying only on changes in the fluorescent intensity of a single component. To address some of challenges in arriving at a quantitative description of the kinetics and dynamics of redox components, a FRET-based approach was implemented to achieve maximum sensitivity within the physiological redox range after construct modification using SLIM PCR [8]. By improving the yield of disulfide formation (sensitivity) and decreasing the ratios of thrombin to proteins (specificity), site-specific modification was shown to be successful in which the linker region is easily accessible to thrombin by reducing steric hindrance, confirmed by Ellman's assay and SDS-PAGE. A distinct advantage of our approach is its modular and ratiometric characteristics, such that the dynamic range between the fully oxidized and fully reduced forms of the probe corresponded to a 5-fold range in spectroscopic signal when measured ratiometrically, which led to improved discrimination of the redox states in complex biological specimens. The ratiometric response was of paramount importance for dealing with variable expression levels, source intensity, detector sensitivities, and sample concentrations. Although fluorescent proteins can be inherently quenched by pH

sensitivity and photobleaching [9], the pH-independence of the R_{FRET} enabled us to investigate disulfide reduction dynamics in the endocytic compartments and photobleaching correction led us to overcome a steady decrease in R_{FRET} resulting from acceptor photobleaching. To improve the signal-to-noise ratio, Cerulean (a cyan derivative) [10] or Venus (yellow derivative) [11] were substituted for mECFP or mCit by site-directed mutagenesis (Fig. 5.1a). This FRET pair, Cerulean-Venus, has both high a donor quantum yield and a large acceptor extinction coefficient, demonstrating significantly increased contrast as well as an improved signal-to-noise ratio [12]. Nevertheless, 24% of R_{FRET} was diminished after the mutations (Fig. 5.1b). An increase in Főrster distance (calculated 4.9 vs 5.4 nm) is one possible reason for the change in FRET efficiency [13], or alternatively an incorrect dipole-dipole interaction. Given that the inherent sensitivity of FRET measurements is dependent on distance and orientation, the precise control over changes in energy transfer could be challenging. However, the use of genetic engineering shows enormous potential, which is relatively straightforward and allows targeting to most cellular compartments by fusion with organelle-specific peptides [9].

Liposome-encapsulated probes were also shown to be well-suited for measuring redox conditions in the endocytic pathway due to the propensity of cells to endocytose lipidic particles [28]. The high sensitivity and temporal resolution provided by ratiometric imaging of individual phagosomes indicated that some aspects of a redox environment were monitored in real time along the endocytic pathway. Quantitative analysis of single phagocytic events in live cells revealed details in redox dynamics that would be missed in fixed cells or isolated phagosomes. Furthermore, real-time imaging of redox dynamics

using exogenously applied probes provides major obvious advantages compared to static measurements using endogenously expressed roGFPs (such as via transfection) as it allows direct delivery to and monitoring of the endolysosomal pathway. Relative fluorescence from mCherry-Rab5a-positive endosomes or TRD-associated lysosomes was also used to quantify the dynamics of markers. Through the concomitant use of colocalized endolysosomal markers, we have demonstrated that reduction of disulfide bonds begins in the early endosome and continues throughout endolysosomal maturation. To investigate cellular factors that modulate the reduction processes, both genetic and chemical approaches were used in order to mimic conditions in which the endocytic pathway would be most heavily skewed towards either an oxidizing potential or reducing potential. Decreased levels of oxidative enzymes ($gp91^{phox}$) promote faster kinetics via attenuation of ROI production, while increased ROS conditions inhibited reduction. Macrophages lacking GILT were greatly hindered in their ability to reduce the probe, confirming that GILT activity is indeed a determinant of endocytic redox potential. GILT, which is a critical factor for disulfide reduction for antigen presentation [14] and LLO [15], is constitutively expressed in most APCs, including monocytes/macrophages, B cells, BMDCs, and some fibroblasts [16, 17]. The induction level of GILT may be varied in different cell types depending on the level of IFN-γ, [18]; therefore careful attention would be required for the choice of target cell associated with disulfide-based drug delivery systems.

LLO has been utilized in drug delivery systems that mimic the *Listeria* invasion to deliver exogenous macromolecules into the cytosol. Previous studies in our laboratory have demonstrated enhanced gene expression and delivery using the endosomolytic pore-

forming protein, LLO, conjugated with polycation or encapsulated in liposomes [19-22], which is supportive indirect evidence for reducing activity along the endocytic pathway. However, the regulatory mechanisms and key elements of LLO activity are still not completely understood. For example, while it is known that oxidation of the single cysteine of LLO with a sufficiently bulky molecule results in the reduction or elimination LLO's activity, the redox potential required for reducing that disulfide in the endosome is not known. Whereas it has been reported that disulfide reduction facilitates lysosomal proteolysis, which in turn is promoted by the import of cysteine mediated by the cysteine-specific lysosomal transport system [31], studies on the rate of degradation vs reduction/activation are currently lacking. Our study has the potential to provide insights as to how the unique cysteine of LLO is reduced in the endocytic pathway to activate LLO and how that is regulated and related to delivery strategies. This study will be important for the rational design of LLO-mediated delivery and macromolecule/delivery system conjugates and complexes that are modulated by redox potential gradients, as well as for the clarification of the *Listeria* invasion mechanism.

To further investigate redox activity in the endocytic pathway, we sought to compare the intrinsic redox potential of different kinds of cells. The selected cells included BMDCs as one of the major APCs, and fibroblasts, as their redox-dependent cellular processes have been previously elucidated, and cancer cells are frequently under persistent oxidative stress. The sensitivity of ratiometric FRET microscopy detected the redox potential during the gradual maturation of endosomal compartments, creating complete spatiotemporal profiles of each cell type. All of the endosomal compartments tested have reducing potential; however, the extent and rate of disulfide reduction varied

depending on the cell type. BMMs have the most reducing potential, while cancer cells have the most oxidizing potential. BMMs, as compared with BMDCs, are more efficient in acquiring liposomal antigen as well as in overall presentation of liposomal antigen to T lymphocytes [23], probably BMMs could reduce antigenic disulfide bond more efficiently before antigen processing and presentation as estimated by more reducing midpoint potential in BMMs than BMDCs. Cell type-dependent variations in the disulfide reduction mechanism of endocytosed macromolecules could derive from a number of factors, including kinetics of vesicular trafficking by different rates of maturation, induction levels of GILT [24] and expression levels of surface PDI [25], location of cysteine transporters in lysosomes [26], and cell proliferation and differentiation [27, 28].

Future studies could use endolysosomal enzyme-cleavable redox probes by replacing the thrombin cleavable site with a cathepsin D-cleavable site (LVEL|FVLS), as a more straightforward design to monitor disulfide reduction in the endocytic pathway (Fig. 5.2). Since cathepsin D (CD) is an endopeptidase that is almost exclusively expressed in the endocytic pathway, it would not have to be cleaved prior to incubation with cells [29, 30]. Endosomolytic LLO could also be incorporated either by using a labeled fusion protein or by co-encapsulation inside liposomes to directly report on the redox state of LLO, as well as investigate the rational design of LLO-mediated macromolecular delivery modulated by redox potentials. It is also plausible that whole living animals could be monitored in order to determine the localization and kinetics of *in vivo* redox imaging by incorporation of luciferin injected into luciferase-transgenic mice.

This study *in toto* underlines the importance of directly monitoring the spatiotemporal dynamics of the reduction-oxidation homeostasis in the endocytic pathway and elucidating the key biochemical redox regulators. To our knowledge, this is the first study using redox biosensors that have been used to monitor and compare reduction profiles of endocytic pathways in live cells. The control of the reduction of disulfide bonds in the endocytosed macromolecules would depend on cell types and their differentiation and pathophysiology. Further investigation in other cell types in various physiological states will provide critical information that can be used to investigate the impact of novel treatments as well as informing the design of targeted pharmaceutical agents that rely on disulfide bonds.

Figure 5.1 Peptide sequence and emission spectra of Cerulen-G_4STh-Venus.

(a) Cerulean and Venus were substituted for mECFP and mCit by site-directed mutagenesis. Amino acids in bold characters correspond to the expressed part of cloning vector backbone pET-29b, underlined amino acids to protein tag, Strep-tag and His-tag, and dotted underline to a linker containing thrombin recognition sequence and two cysteines plus spacer. Mutants are colored as blue (mECFP to Cerulean : S72A, Y145A, H148D) and yellow (mCit to Venus : F46L, F64L, M69Q, M153T, V163A, S175G). (b) Comparison of emission profile between mECFP-G_4STh-mCit vs Cerulen-G_4STh-Venus.

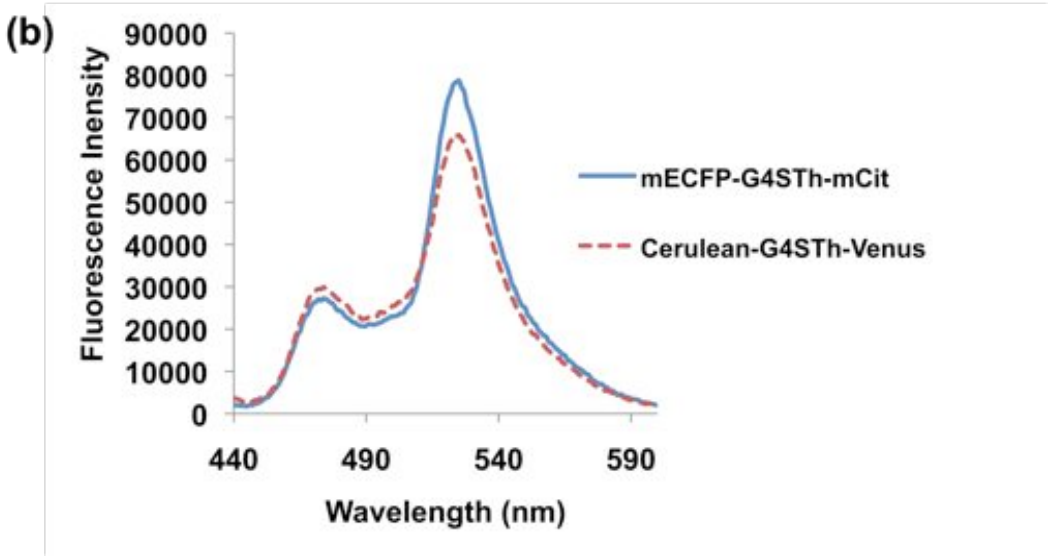
(b)
Fluorescence Inensity
90000
80000
70000
60000
50000
40000
30000
20000
10000
0
440
490
540
590
Wavelength (nm)
mECFP-G4STh-mCit
Cerulean-G4STh-Venus

Figure 5.2 Peptide sequence of mECFP-CD-mCit.

Amino acids in bold characters correspond to expressed part of cloning vector backbone pET-29b, underlined amino acids to protein tag, Strep-tag and His-tag, and dotted underline to a linker containing CD cleavable sequence and two cysteines plus spacer.

REFERENCES

1. Bjornberg, O., H. Ostergaard, and J.R. Winther, *Measuring intracellular redox conditions using GFP-based sensors.* Antioxid Redox Signal, 2006. **8**(3-4): p. 354-61.

2. Meyer, A.J. and T.P. Dick, *Fluorescent protein-based redox probes.* Antioxid Redox Signal. **13**(5): p. 621-50.

3. Cannon, M.B. and S. James Remington, *Redox-sensitive green fluorescent protein: probes for dynamic intracellular redox responses. A review.* Methods Mol Biol, 2009. **476**: p. 50-64.

4. Gutscher, M., et al., *Real-time imaging of the intracellular glutathione redox potential.* Nat Methods, 2008. **5**(6): p. 553-9.

5. Hanson, G.T., et al., *Investigating mitochondrial redox potential with redox-sensitive green fluorescent protein indicators.* J Biol Chem, 2004. **279**(13): p. 13044-53.

6. Yang, J., et al., *Evaluation of disulfide reduction during receptor-mediated endocytosis by using FRET imaging.* Proc Natl Acad Sci U S A, 2006. **103**(37): p. 13872-7.

7. Dooley, C.T., et al., *Imaging dynamic redox changes in mammalian cells with green fluorescent protein indicators.* J Biol Chem, 2004. **279**(21): p. 22284-93.

8. Chiu, J., et al., *Site-directed, Ligase-Independent Mutagenesis (SLIM): a single-tube methodology approaching 100% efficiency in 4 h.* Nucleic Acids Res, 2004. **32**(21): p. e174.

9. Ibraheem, A. and R.E. Campbell, *Designs and applications of fluorescent protein-based biosensors.* Curr Opin Chem Biol. **14**(1): p. 30-6.

10. Rizzo, M.A., et al., *An improved cyan fluorescent protein variant useful for FRET.* Nat Biotechnol, 2004. **22**(4): p. 445-9.

11. Nagai, T., et al., *A variant of yellow fluorescent protein with fast and efficient maturation for cell-biological applications.* Nat Biotechnol, 2002. **20**(1): p. 87-90.

12. Rizzo, M.A. and D.W. Piston, *High-contrast imaging of fluorescent protein FRET by fluorescence polarization microscopy.* Biophys J, 2005. **88**(2): p. L14-6.

13. Vogel, S.S., C. Thaler, and S.V. Koushik, *Fanciful FRET.* Sci STKE, 2006. **2006**(331): p. re2.

14. Maric, M., et al., *Defective antigen processing in GILT-free mice.* Science, 2001. **294**(5545): p. 1361-5.

15. Singh, R., A. Jamieson, and P. Cresswell, *GILT is a critical host factor for Listeria monocytogenes infection.* Nature, 2008. **455**(7217): p. 1244-7.

16. Arunachalam, B., et al., *Enzymatic reduction of disulfide bonds in lysosomes: characterization of a gamma-interferon-inducible lysosomal thiol reductase (GILT).* Proc Natl Acad Sci U S A, 2000. **97**(2): p. 745-50.

17. Bogunovic, B., et al., *An unexpected functional link between lysosomal thiol reductase and mitochondrial manganese superoxide dismutase.* J Biol Chem, 2008. **283**(14): p. 8855-62.

18. Luster, A.D., et al., *Molecular and biochemical characterization of a novel gamma-interferon-inducible protein.* J Biol Chem, 1988. **263**(24): p. 12036-43.

19. Saito, G., G.L. Amidon, and K.D. Lee, *Enhanced cytosolic delivery of plasmid DNA by a sulfhydryl-activatable listeriolysin O/protamine conjugate utilizing cellular reducing potential.* Gene Ther, 2003. **10**(1): p. 72-83.

20. Choi, S. and K.D. Lee, *Enhanced gene delivery using disulfide-crosslinked low molecular weight polyethylenimine with listeriolysin o-polyethylenimine disulfide conjugate.* J Control Release, 2008. **131**(1): p. 70-6.

21. Sun, X., C. Provoda, and K.D. Lee, *Enhanced in vivo gene expression mediated by listeriolysin O incorporated anionic LPDII: Its utility in cytotoxic T lymphocyte-inducing DNA vaccine.* J Control Release. **148**(2): p. 219-25.

22. Lorenzi, G.L. and K.D. Lee, *Enhanced plasmid DNA delivery using anionic LPDII by listeriolysin O incorporation.* J Gene Med, 2005. **7**(8): p. 1077-85.

23. Stier, E.M., M. Mandal, and K.D. Lee, *Differential cytosolic delivery and presentation of antigen by listeriolysin O-liposomes to macrophages and dendritic cells.* Mol Pharm, 2005. **2**(1): p. 74-82.

24. Luster, A.D. and J.V. Ravetch, *Biochemical characterization of a gamma interferon-inducible cytokine (IP-10).* J Exp Med, 1987. **166**(4): p. 1084-97.

25. Jiang, X.M., et al., *Redox control of exofacial protein thiols/disulfides by protein disulfide isomerase.* J Biol Chem, 1999. **274**(4): p. 2416-23.

26. Pisoni, R.L., et al., *A cysteine-specific lysosomal transport system provides a major route for the delivery of thiol to human fibroblast lysosomes: possible role in supporting lysosomal proteolysis.* J Cell Biol, 1990. **110**(2): p. 327-35.

27. Nkabyo, Y.S., et al., *Glutathione and thioredoxin redox during differentiation in human colon epithelial (Caco-2) cells.* Am J Physiol Gastrointest Liver Physiol, 2002. **283**(6): p. G1352-9.

28. Ramirez, A., et al., *Extracellular cysteine/cystine redox potential controls lung fibroblast proliferation and matrix expression through upregulation of transforming growth factor-beta.* Am J Physiol Lung Cell Mol Physiol, 2007. **293**(4): p. L972-81.

29. Minarowska, A., et al., *Human cathepsin D.* Folia Histochem Cytobiol, 2008. **46**(1): p. 23-38.

30. Blum, J.S., M.L. Fiani, and P.D. Stahl, *Localization of cathepsin D in endosomes: characterization and biological importance.* Adv Exp Med Biol, 1991. **306**: p. 281-7.

31. Pisoni, R.L., et al., *A cysteine-specific lysosomal transport system provides a major route for the delivery of thiol to human fibroblast lysosomes: possible role in supporting lysosomal proteolysis.* J Cell Biol, 1990. 110(2): p. 327-35.